*Journal of the*
# OPTICAL SOCIETY *of* AMERICA

VOLUME 31 MARCH, 1941 NUMBER 3

## Final Measurements of the Velocity of Light

WILMER C. ANDERSON*
*Cruft Laboratory, Harvard University, Cambridge, Massachusetts*
(Received December 19, 1940)

Improvements in the apparatus formerly used include the use of an eleven-stage electron multiplier tube, the control of the transmitter frequency by the laboratory standard, the substitution of a 1000-watt water-cooled mercury arc for the light source, a new type of Kerr cell, changes in the mirror supports and base line measurements, and the use of an automatic recorder. The apparatus has been completely rebuilt and converted to a.c. operation. The optical system has been changed to permit simpler measurements of the path difference, and electrical circuits have been devised to smooth out the fluctuations due to voltage variations and other causes.

Group velocity is discussed as a correction factor in this and previous measurements. The correction is shown to amount to as much as 7 km/sec. in some cases. Electron transit time is shown to be a limiting factor for this method of measuring the velocity of light. The final result of 2895 observations is given as 299,776±14 km/sec. This includes a group velocity correction and should not be compared with previous results without taking this into consideration. The conclusion is reached that the velocity of light is a constant as nearly as we can measure it at present.

### INTRODUCTION

A SUMMARY of previous terrestrial measurements of the velocity of light and a brief discussion of the accuracy and method for each has been given by de Bray[1] and Mittelstaedt.[2] From this analysis, certain determinations were selected as presumably more reliable than others and a plot of these values against the mean time of their determinations suggested a possible linear decrease with time or a periodic function of time.[3] Birge and others[4] have discussed these apparent variations and their theoretical significance.

If, however, these various values obtained by direct measurement, as well as two obtained by indirect means, are plotted as lines instead of points, the length of each line representing the experimental error involved in each case, a graph as shown in Fig. 1 results. Under these conditions there will appear little reason for trying to find

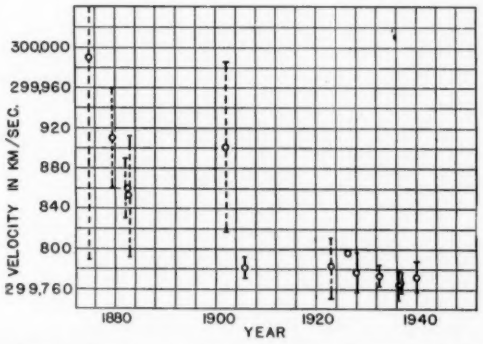


FIG. 1. Plot showing the principal measurements of the velocity of light by direct and indirect methods since 1870.

* Now with American Research Company, Beaumont, Texas.

[1] M. E. J. G. de Bray, Nature **120**, 602 (1927).
[2] O. Mittelstaedt, Physik. Zeits. **30**, 165 (1929).
[3] M. E. J. G. de Bray, Nature **133**, 464 (1934); F. K. Edmondson, Nature **133**, 759 (1934).
[4] R. T. Birge, Nature **134**, 771 (1934); Rev. Mod. Phys. 1, 1 (1929); D. C. Miller, Rev. Mod. Phys. **5**, 3 (1933).



BOSTON UNIVERSITY
COLLEGE OF LIBERAL ARTS
LIBRARY

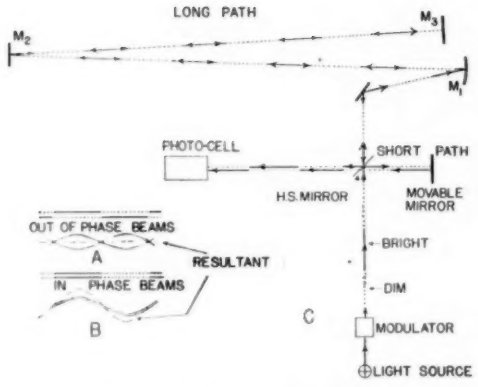


FIG. 2. Schematic diagram of the present method for measuring the velocity of light.

a variation of the same order of magnitude as the errors of measurement. Also the fact that the six most accurate determinations, including direct and indirect methods, and covering a period of 30 years, agree much more closely than is to be expected upon the basis of the periodic variations of Edmondson, or the linear variations of de Bray, seems to indicate that the variations in early measurements were due to experimental error rather than natural causes. Furthermore, it will be noticed that the short period variations found by Pease and Pearson[5] also were based upon statistical means and the actual spread of values is so great in comparison with the variations that an attempt to show periodicity seems somewhat unwarranted under the circumstances. Until sufficient evidence is forthcoming, i.e., until readings are sufficiently accurate, without statistical manipulation, to show variations in the velocity with time, it would appear somewhat anticipatory to assume, on data insufficiently accurate, that there are such. It was the purpose of the present assembly to attempt to settle this question one way or the other without too much dependence upon human observation and statistical manipulation.

### A brief review of the method

The present arrangement[6] is best discussed with the aid of Fig. 2. A light beam is passed through a modulator where it is made to vary sinusoidally in intensity about some steady value. From the modulator the beam passes through a half-silvered mirror, a portion being reflected from the surface over to a movable mirror. From this mirror the beam is returned, passing through the half-silvered mirror to a photoelectric cell. The other portion of the original beam transmitted by the half-silvered mirror passes over the much longer path ($M_1M_2M_3$), and is returned along the same path, being reflected this time from the half-silvered mirror over to the same photoelectric cell. A tuned circuit converts these photoelectric currents into voltages which are amplified and recorded. It can be shown that the resultant voltage is dependent upon the phase relation of the original light modulations and this voltage will be either a maximum when the beams are in phase, or a minimum when one beam is an odd number of half-cycles behind the other. By noting the path difference for a given minimum position, the velocity of light is readily computed by the relation:

$$c = 2fs/n, \tag{1}$$

where $n$ = the number of half-cycles phase difference, $s$ = the optical path difference between the two light beams, $f$ = the frequency of modulation of the beams, and $c$ = the velocity of light.

## APPARATUS

### The transmitter

The light source formerly used was a 500-watt Pointolite. This was replaced by a 500-watt special projection lamp having an overlapping double row of filaments and later by a 1000-watt air-cooled lamp of the same type. The latter has a commercial rating of 27,000 lumens.

Since April of this year (1940) measurements have been made with a type H6 mercury vapor lamp. This is a high pressure, water-cooled capillary with a rating of 1000 watts and 65,000 lumens output. When this lamp was used it was unnecessary to use the 60-cycle modulation on the Kerr cell to obtain an audible component in the beam,[6] since the light has a decided 120-cycle modulation. Only the steady biasing voltage and the radiofrequency voltage were necessary.

The light is modulated by a water-cooled Kerr

[5] Michelson, Pease and Pearson, Astrophys. J. **82**, 26 (1935).
[6] Cf. W. C. Anderson, Rev. Sci. Inst. **8**, 239 (1937).

cell (see Fig. 3) similar to the ones previously used. The present cell has glass-sealed end plates and vertical cooling jacket to eliminate air bubbles when the cell is being filled. A polished ground-glass stopcock requiring no lubricant permits draining and refilling of the cell without removing its water and electrical connections. The entire cell is of Pyrex glass and was annealed for several hours in a furnace to eliminate strains. The electrodes are of polished nickel and were inserted after the end plates were sealed on to prevent oxidation. Very pure nitrobenzene is used for the liquid dielectric. A motor driven glass propeller circulates the liquid through the cell proper and the water jacket for cooling purposes.

The cell is operated with a biasing voltage of 5000 to 10,000 volts and about 90 watts of radiofrequency energy. From rough current measurements and reactance calculations this means that the radiofrequency voltage across the cell is about 1000 volts.

The radiofrequency voltage applied to the cell for modulation purposes is obtained from a power amplifier having an output of about 90 watts at a frequency of 19.2 megacycles. The driving voltage for the power tubes is secured by an arrangement as follows:

Voltage from the 50-kilocycle standard frequency generator of the laboratory, designed by Professor G. W. Pierce,[7] is amplified and then piped to the room housing the velocity of light apparatus. Here it is again amplified at 50 kilocycles and then used to drive a system of tuned radiofrequency amplifiers and doubling stages. After passing through eleven such stages, eight acting as doublers or triplers and three as straight amplifiers, the 19.2-megacycle driving voltage for the power tubes emerges.

The radiofrequency voltage is supplied to the Kerr cell by means of loosely coupling the coil of the cell tank circuit to the output coil of the power amplifier. Tuning of the Kerr cell circuit is accomplished by varying the position of a clip on the coil, and noting the illumination produced in a small neon bulb near the Kerr cell terminals.

[7] Cf. G. W. Pierce, Proc. Am. Acad. Arts Sci. **10**, 271 (1925); see also Proc. I. R. E. **16**, 1072 (1928).

**The receiver and associated apparatus**

The receiving system has been greatly improved over the one previously used. The various units with one or two exceptions have all been converted to permit operation from the regular alternating-current power lines instead of from batteries as formerly. It has always been a rather difficult problem to prevent interference from the stray radiation of the radiofrequency transmitter, only a few feet away. When the same alternating-current power lines are used for both the transmitter and the very sensitive receiving system, the problem becomes even more acute. In the past[6] a low-frequency component has been added to the light beam modulation to distinguish it from the unmodulated radiofrequency fields of the transmitter.

In the present arrangement, the power lines enter the shielded receiving system at only one point. Additional parallel lines are furnished the other units by means of shielded leads taken from an internal connection to this line. A four-section filter consisting of radiofrequency chokes in each

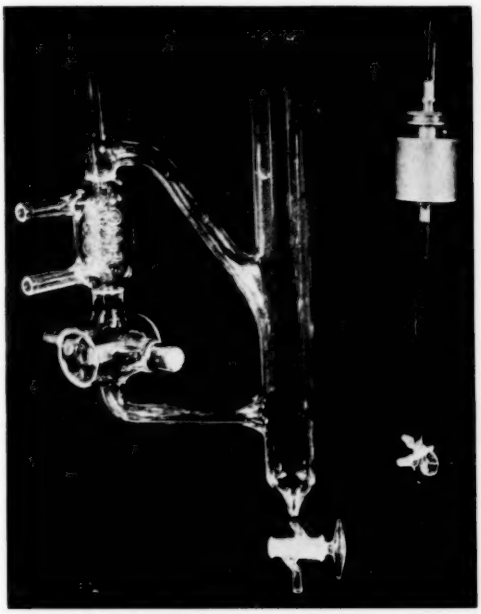

FIG. 3. Glass-sealed Kerr cell with stopcock for draining and refilling without removal from the apparatus. The water-cooling jacket and glass screw pump are similar to those previously used for this purpose.

line and condensers across the line is employed on the leads coming from the outside power lines, and similar two-section filters are used on all the secondary shielded leads to the other units. All power supplies, for both the transmitter and the receiver, are regulated to diminish voltage fluctuations.

The photoelectric cell formerly used has been replaced by a photosensitive electron multiplier tube of eleven stages. With 100 volts per stage the present tube has a sensitivity of about 2 amperes per lumen, compared with 30 microamperes per lumen for the ordinary vacuum photoelectric cell. This arrangement has the very desirable advantage of amplifying the light signal without doing likewise for the stray radio-frequency voltages picked up from the transmitter. Such is not the case for the stages following, but the light signal is given such an impetus by the multiplier tube that the gain in the following amplifier can be reduced to levels sufficiently low to practically eliminate the effect of any stray radiation.

The electrical circuit for a five-stage multiplier tube and the acorn pentode preamplifier stage is shown in Fig. 4. The five-stage tube was used in preliminary work and has since been supplanted by the eleven-stage one, but the circuit is very similar. The points marked *A* and *B* are connected to the input terminals of a sensitive receiver.

The audiofrequency output voltage of this

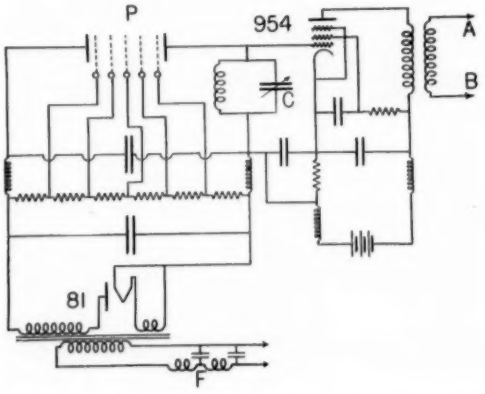


FIG. 4. Electron multiplier tube circuit and acorn pentode used for preamplifier stage. The terminals *AB* were connected to the input of a high gain short wave receiver.

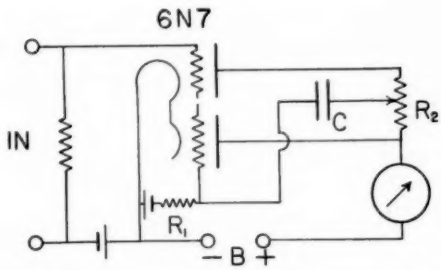


FIG. 5. Schematic diagram of feed-back circuit used for diminishing extraneous fluctuations in the output voltage.

receiver, after rectification, feeds into a circuit as shown in Fig. 5. In this circuit one triode acts as an ordinary direct-current amplifier. Fluctuations due to various causes will then be amplified by this tube as well as the slowly changing signal voltage. To neutralize these fluctuations a voltage from the output of the first tube is then fed back through the resistance-capacity coupling to the second triode. The plate circuits of the two triodes have a common path through the recording meter. It is easily seen that current variations having a period shorter than the $R_1C$ factor of the feed-back circuit will be canceled in that portion of the circuit occupied by the meter. As long as the signal voltage varies slowly in comparison to the extraneous fluctuations and the $R_1C$ factor, the resultant current will show the signal variations with greatly diminished fluctuations. Since the rate of change of the signal voltage is governed by the speed of the movable mirror, it is merely necessary to reduce the speed of the latter until the desired conditions are reached. The actual circuit used is shown in Fig. 6.

A photographic arrangement is employed to eliminate frictional errors usually associated with mechanical ink or waxed paper recorders. At first, lights illuminated the face of the meter (see Fig. 5) and an image of the latter was projected by means of a lens upon a narrow vertical slit. The image of the black meter needle traced a white line upon the paper because of insufficient exposure. The paper motion was governed by the motion of the movable mirror so that horizontal distances upon the record were directly mensurable. A fine vertical wire stretched across the paper holder served to produce a white

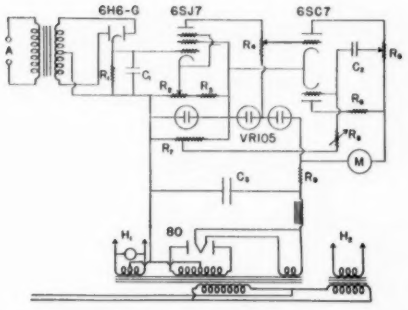


FIG. 6. Actual circuit used for fluctuation elimination.

fiduciary line on all records. Relays and trigger devices automatically limited the distance traversed by the moving mirror and recording arm. This arrangement has now been supplanted by a 35-mm motion picture camera adapted for the purpose. The face of the meter has been blackened and a small polished nickel wire placed beneath and at right angles to the needle and rigidly fastened to the face. When light strikes this surface it gives the equivalent of a narrow slit but with considerably more light than formerly was obtained. This arrangement in a box is placed at one side of the lathe bed. The camera is fastened to the movable mirror and the lens faces the meter face. A flexible bellows joins the two so that no stray light gets in (see Fig. 7). Horizontal as well as vertical motions are thus reduced to a size suitable for a frame $1'' \times \frac{3}{2}''$ on the paper. To determine the amount of reduction produced, the polished wire mentioned above is scratched at centimeter intervals. The motion of the mirror then shows these up as horizontal lines somewhat closer together, depending upon the reduction involved.

**Optical arrangement**

The optical arrangement is shown in Fig. 8. Light from the 1000-watt projection lamp passes through a condensing lens system, a Polaroid polarizer, the Kerr cell, and a second polarizer. At this point a second lens focuses the light upon a circular hole in a metal plate. The hole is traversed by fine cross hairs arranged to divide the opening into quarters. The purpose of the cross hairs will be discussed later.

After passing through the circular opening the beam strikes a half-silvered mirror, $M_6$, and is split. The reflected portion passes through a diaphragm, $D$, and a lens. The lens is placed at a distance equal to its focal length from the circular opening so that the rays emerging from the lens are essentially parallel. Hence the intensity or direction of the reflected light from the mirror, $M_3$, is not altered appreciably when the latter is moved through the necessary range for a reading. The light reflected from the mirror, $M_3$, retraces its path through the lens, and a portion passes through the half-silvered mirror to finally fall upon the photoelectric cell.

The diaphragm is used to match the intensity of the beam traversing the short path, with that of the beam passing over the long path. An exact match is not necessary as shown in a preceding discussion.[6] The more closely they are matched, however, the more accurately the minimum point can be determined.

The portion of the original beam which was transmitted by the half-silvered mirror passes over the path $M_6M_1M_5$.

From $M_5$ the beam is returned over the same path to the half-silvered mirror again. Here a portion is reflected and combines with the other beam arriving from the short arm and the two together enter the photoelectric cell.

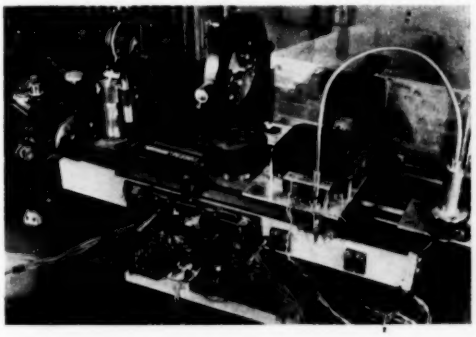

FIG. 7. Automatic recorder used in final phase of the work.

$M_5$ is an 8″ plane mirror. Mirrors $M_1$ and $M_2$ are concave; one is 9″ in diameter and has a focal length of about 5 meters; the other is 8″ in diameter and has a focal length of 2.5 meters. All mirror surfaces are accurate to within one wave-length of light.

The mirrors $M_1$ and $M_2$ are arranged in a dual-mounting assembly, back to back (see Fig. 9),

so that either one can be rotated into proper focusing position with accuracy. The 9″ concave mirror is arranged to produce an image of the circular opening and cross hairs upon the surface of mirror $M_5$ at the end of the long path. The reflected light, in turn, retraces its path and forms an image the same size as the original just in front of the photoelectric cell surface. The image produced by light from the short arm also focuses at the same point and the two cross-hair images can be brought into exact coincidence by slight adjustments. The combined light then enters a very short focus lens and produces practically a point image upon the cathode of the photoelectric cell.

The 8″ concave mirror is arranged to reflect the light directly back over the path $M_2M_6$, without traversing the longer path $M_1M_5$. The focal length has been so chosen that it also produces an image at the same point as the light from the short arm. Thus either concave mirror can be rotated into position readily and adjusted so that the light either traverses the path $M_1M_5M_1M_6$, or the path $M_2M_6$. In order to produce a minimum with the 9″ concave mirror in position at say $M_1$, it is necessary that the path differences be equal to an odd number of half-wave-lengths of the radiofrequency modulation. That is,

$$2S+2x-2y=(2n+1)\lambda/2. \tag{2}$$

With the 8″ concave mirror in position $M_2$, a minimum will be produced at some new position

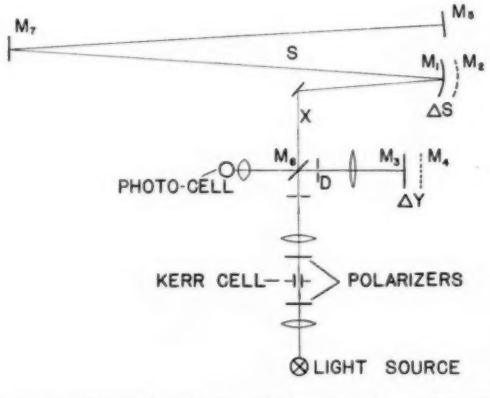


FIG. 8. Schematic diagram of the optical arrangement used for simplifying distance measurements.

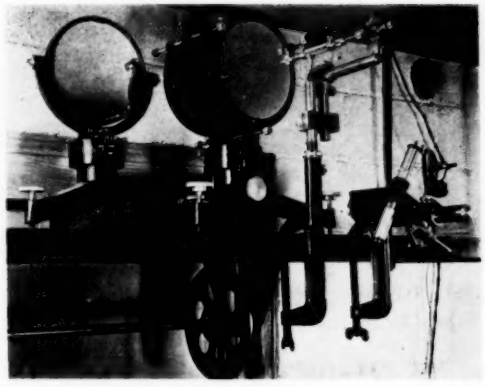

FIG. 9. Dual mounting for the concave mirrors (right) and single mounting for plane mirror (left). The micrometer microscope and special inside micrometer calipers for obtaining the mirror positions with respect to the tape are also shown.

of the lathe mirror, $M_4$. The relation in this case is

$$2x+2\Delta S-2y-2\Delta y=\lambda/2. \tag{3}$$

If we subtract Eq. (3) from (2) we obtain the relation:

$$2S-2\Delta S+2\Delta y=n\lambda, \tag{4}$$

where $n$ is an integer. This means then that it is unnecessary to measure the length of the short path or the distances $x$ and $y$. It is only necessary to know the length of the path $S$, and the short intervals $\Delta S$ and $\Delta y$. The distance measurements are in this way considerably simplified.

## Control devices

The movable mirror is mounted upon a small lathe bed carefully machined to eliminate small surface irregularities. A millimeter-pitch screw is used to drive the mirror assembly. A pulley attached to one end is driven by an induction motor and serves to rotate the screw. A reduction-pulley arrangement enables various speeds of rotation of the screw to be obtained.

In Figs. 7 and 10 is shown the motor control assembly. A Bakelite strip $A$, attached to the moving mirror, tripped switches at either end and in the center of its path. The switches $B$ and C, and relays $D$ and $E$, stopped the motor, turned off the recording lights, $L$, and wound up a new section of film into place. The motor circuit was kept open for a sufficient time, about

20 seconds, to permit these various operations to take place before a relay closed a reversing switch and started the motor rotating in the opposite direction. The necessary lag was introduced by the thermal inertia of the heaters of the rectifiers shown in Fig. 10, which furnished the current to the relay coils $F$ and $G$. Variation of the resistance $R$ permitted control of the amount of thermal lag within certain limits.

The film-winding motor was controlled by means of special unidirectional switches operated by another moving arm mounted directly beneath the camera assembly (see Fig. 8). Single frame winding of the film was accomplished quite accurately by means of gears and a commutating device acting through another relay.

The time and date were automatically placed on each record by means of a special timing circuit and switch. Inside the recorder box directly beneath the recording meter but partitioned from it was a watch with reduced face and hands, and a slip of paper giving other data such as the date, etc. A small flashlight bulb was placed in front of these but shielded so that its direct light would not shine in the camera lens. An overvoltage was applied to the lamp briefly so as to give a "snapshot" of the paper and watch face on the film along with the record.

The greatest difficulty came in making the exposure time short enough "to stop" the motion of the lathe mirror and yet be consistent and automatic. This was finally solved by the use of the circuit shown in Fig. 11. The initiating impulse is caused by the closing of the switch $S$. This operates the relay $K_1$ to break the upper contact and close the lower, permitting the condenser $C$ to discharge through the resistance $R$ and applying a positive potential to the grid of a tube for a certain time interval determined by $RC$. If the tube was previously biased so that insufficient plate current flows through the relay $K_2$ to operate it, then sufficient current will now flow just as long as the above-mentioned voltage applied to the grid of the tube exceeds a certain value.

It will be noticed that once the initiating key $S$ is closed the rest of the operation is automatic. The interval that the relay $K_2$ is closed is determined by $RC$ and not by the length of time $S$ is closed, provided of course $S$ is closed long enough for $C$ to discharge. Thus the switch $S$ can be any slow acting mechanical switch and yet the exposure time can be kept small and varied at will by adjusting the value of $R$.

## Measurements

### Frequency

The period of the radiofrequency modulating voltage was controlled by the primary standard of frequency of the laboratory as discussed earlier in this paper. The standard is a 50-kilocycle piezoelectric oscillator with the necessary temperature controls. It is checked frequently with the standard frequencies sent out from Arlington. A synchronous clock driven by a 1000-cycle subharmonic of the master oscillator is also checked with the national time signals. The error in time was certainly less than one part in a million and conceivably less than one part in eight million from all measurements made upon it.

### Distance

The distance was measured with an invar-steel tape and special end-point apparatus. The tape was supported upon light 10″ pulleys with ball bearings and under a tension of 15 kg. A fine even-depth line was ruled upon each end of the tape. The distance between these lines was determined under the same conditions by the National Bureau of Standards. The error in absolute value was estimated to be less than one part in 210,000.

The distance between the mirrors was referred to the tape as a base line. This was done by

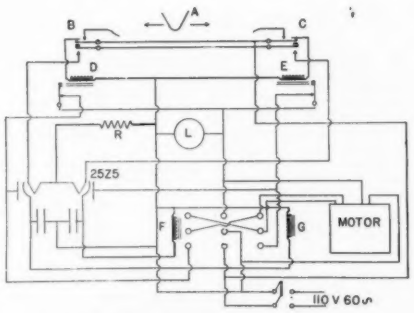


FIG. 10. Automatic motor control circuit for operating the recorder and lathe mirror.

means of a special device shown in Fig. 8. An inside micrometer caliper with calibrated rods was adapted for the purpose.

The micrometer is held so that the fixed end is against the side of an extremely fine bronze wire. The other end of the wire is weighted so that it hangs directly beside the ruled line on the tape. A micrometer microscope is then focused at the junction of the two and is used for measuring the small interval between the tape line and the side of the wire. This distance usually amounts to less than 0.2 mm and was read to 0.001 mm.

The opposite end of the inside micrometer has the movable head and the latter is rotated until it just touches the surface of the mirror at its center. A ratchet head was first employed but it was found that an electrical contact was better. A pair of high resistance headphones is placed in series with the micrometer and the aluminum surface of the mirror. A small alternating-current voltage is then imposed upon the arrangement. Readings can be repeated with this arrangement to better than 0.002 mm.

The tape is supported directly beneath each pair of mirrors and the distance measured as above. Twice the sum of these distances gives the total path length, $S$. The concave mirrors are interchanged and the difference in position measured.

The transference errors thus far have been less than 0.3 mm for the 171-meter interval.

The distance to be used in computation is the interval $S$ plus the corrections $\Delta S$ and $\Delta y$. The interval $\Delta y$ is obtained from measurements of the recorded minimum points for the concave mirrors interchanged. This distance is measured directly from the records with a comparator graduated in 0.01-mm units.

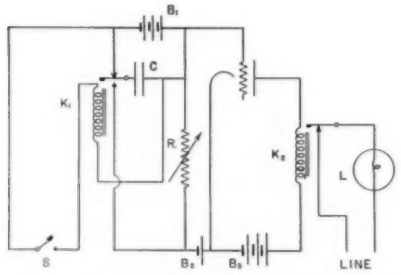


FIG. 11. Timing circuit for incorporating the date and time on a record by means of a brief exposure. The lamp $L$ is flashed for a time interval independent of the length of time that the slowly acting switch $S$ is closed.

### Procedure

The H.R.O. receiver is turned on at least a half-day before readings are to be taken and is usually left on continuously to prevent drift in the superheterodyne component due to a temperature rise. The other components are turned on several hours in advance and allowed to reach temperature equilibrium. This is particularly desirable for the Kerr cell.

With the electrical apparatus in thermal equilibrium, the light beams are made coincident by means of the cross-hair images.

The intensity of the stronger beam is then adjusted by means of the iris diaphragm until it equals that of the weaker beam as shown by the output meter reading.

With the camera loaded with 50 feet of 35-mm. film it is necessary to reload only about once a day. The recording apparatus is entirely automatic.

After a number of records have been taken with the first concave mirror in position, the other is rotated into position and records taken for it. This gives the long and short path intervals. Fig. 12 shows typical records.

### Constant errors

In $A$ of Fig. 13 is shown a cross-sectional view of an ordinary photoelectric cell with cylindrical shell type cathode and concentric wire anode, $E$. If $A$ and $B$ represent the points where the centers of gravity of two beams of light strike the cathode surface, then it is readily seen that the electrons ejected at $A$ and $B$, neglecting initial velocity, will have equal transit times in going from the cathode to the anode.

In case $B$ of Fig. 13, however, we have a different situation. This represents a cross-sectional view of the cathode and first few stages of an electron multiplier tube of the type used in this work. Here it will be seen that if the two centers of gravity of the beams $C$ and $D$ do not coincide, then the electron transit times will in general not be the same for the two beams. Thus if $C$ represents the beam coming from the short arm and $D$ that coming from the long arm of the

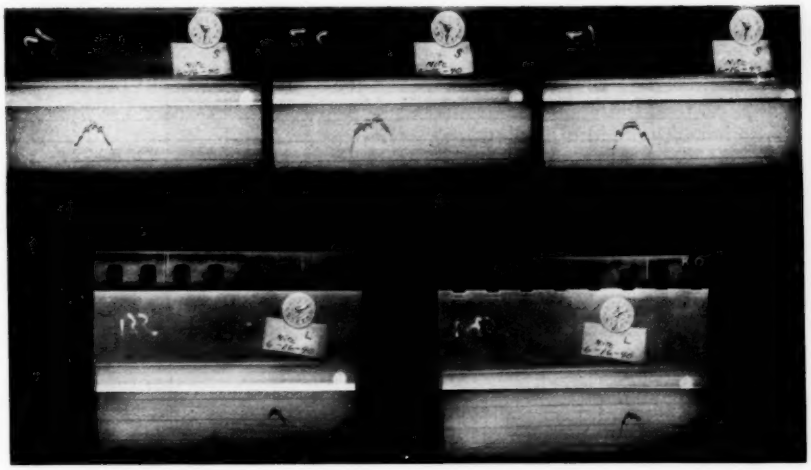

FIG. 12. Prints made from a series of records taken on the night of June 16–17, 1940. The upper ones are for the short path at about 10:30 P.M., while the lower ones are for the long path at about 2:00 A.M., June 17th. The original records are much clearer than these prints might indicate.

apparatus, there will be an *apparent* phase difference between the two *beams* that is due instead to a *real* phase difference between the *electrons* ejected by the two beams.

This factor has given considerable trouble and the variations shown in the results can very well be attributed to shifts in the coincidence of the two beams. This shift can be attributed to thermal expansion of the mirror holders in the long path, and to building vibrations. The former causes slowly changing shifts usually in one direction or the other during a run of several hours. The building vibrations, however, show up as rapid fluctuations and shifts. Even a steady wind can produce observable shifts in the minimum point.

Many different methods and devices have been tried to eliminate or minimize this error. These have included keeping the light beams as nearly coaxial and concentric as possible in the path leading to the photoelectric cell. Many weary hours of adjustment have been expended in this operation. A short focus lens placed next to the cell to reduce the size of the final images upon the cathode surface has also been used. At present the final images covered less than one millimeter and any variation in their coincidence was reduced about tenfold.

Rotating mixing devices have also been tried but usually introduced more error than they eliminated. The final solution in the author's opinion should be one of change in the design of the electron multiplier tube, but this brings up so many new factors that no satisfactory solution has been found to date.

### Group velocity

A source of error apparently overlooked in all absolute determinations of the velocity of light for vacuum has been pointed out by Birge.[8] This is the correction for group velocity, assumed to be negligible by previous observers. Lord Rayleigh[9] and others[10] have discussed the effect of group velocity upon velocity measurements, but except for Michelson's carbon bisulfide measurements no other corrections appear to have been made for this phenomenon.

The expression for the group velocity is ordinarily given as:

$$U = V - \lambda dV/d\lambda$$

and the corresponding expression for the group

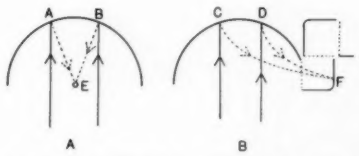


FIG. 13. Diagram showing in exaggerated form the effect of electron transit time on the final results.

[8] Private communication to the author.
[9] Lord Rayleigh, *Collected Papers* (1911), Vol. I, p. 322; Vol. VI, p. 41; Phil. Mag. **22**, 130 (1914).
[10] P. Ehrenfest, Ann. d. Physik **33**, 1571 (1910).

index of refraction is very nearly

$$\mu_g = \mu - \lambda d\mu/d\lambda.$$

Assuming the simple Cauchy expression for the dispersion of light in a medium,

$$\mu = A + B/\lambda^2 + C/\lambda^4,$$

we obtain for the group index,

$$\mu_g = A + 3B/\lambda^2 + 5C/\lambda^4.$$

The *variation* with wave-length for the group index is therefore over three times that for the wave index of refraction.

In the case of glass this correction becomes quite prominent and amounts to over three percent of the total correction. Even in Michelson's mile-long tunnel this factor is present due to the passage of the light back and forth through the window to the tunnel. Thick glass to withstand the pressure without deformation was probably used and amounted to several centimeters both ways.

In Mittelstaedt's experiment there was not only a correction because of the air and glass, but also for the nitrobenzene in the Kerr cells. He states that the change in optical path to vacuum increases the effective length by 21 mm due to lenses, 68 mm due to air, and 12 mm due to the nitrobenzene. If these corrections are in terms of wave velocity, then there will be an additional correction of about 1.8 mm for the glass, 2.4 mm for air, and 1.4 mm for nitrobenzene. The total additional correction to his value for the velocity of light because of group velocity, will then be approximately 6 km/sec. and make his value for $c_0$ approximately 299,784 km/sec. These computations are based upon assumed values as follows:

| | $A$ | $B$ | $C$ | $\lambda$ | $\mu_g$ |
|---|---|---|---|---|---|
| Air | | | | 5500A | 1.0002868 |
| Glass | 1.554 | $6.75\times10^5$ | $127\times10^{10}$ | 5500 | 1.628 |
| Nitrobenzene | 1.523 | $7.77\times10^5$ | $917\times10^{10}$ | 5500 | 1.650 |

The wave index of refraction for air as given by Meggers and Peters[11] is:

$$(\mu-1)\times10^7 = 2726.43 + 12.288/\lambda^2\cdot10^{-8} + 0.3555/\lambda^4\cdot10^{-16}$$

with $\lambda$ measured in angstrom units. The corresponding value for the group index is then:

$$(\mu_g-1)\times10^7 = 2726.43 + 36.864/\lambda^2\cdot10^{-8} + 1.7775/\lambda^4\cdot10^{-16}.$$

[11] W. F. Meggers and Peters, Bull. Bur. Stand. **14**, 697 (1918).

TABLE I.

| Date | Weight | Average $c_0$ | Average Deviation From Daily Mean | Average Deviation From Final Mean |
|---|---|---|---|---|
| May 21, 1939 | 20 | 299,774 km/sec. | 7 km/sec. | 2 km/sec. |
| Nov. 8 | 17 | 299,775 | 9 | 1 |
| 13 | 35 | 299,759 | 10 | 17 |
| 15 | 79 | 299,772 | 9 | 4 |
| 16 | 140 | 299,780 | 8 | 4 |
| 27 | 103 | 299,781 | 13 | 5 |
| Jan. 10, 1940 | 39 | 299,774 | 5 | 2 |
| 23 | 46 | 299,774 | 3 | 2 |
| Mar. 4 | 30 | 299,757 | 3 | 19 |
| 7 | 56 | 299,745 | 9 | 31 |
| 8 | 257 | 299,754 | 3 | 22 |
| 11 | 147 | 299,749 | 9 | 27 |
| Apr. 4 | 348 | 299,808 | 9 | 32 |
| 5 | 122 | 299,774 | 10 | 2 |
| 8 | 125 | 299,769 | 7 | 7 |
| 9 | 197 | 299,771 | 7 | 5 |
| June 15 | 322 | 299,801 | 19 | 25 |
| 16 | 94 | 299,775 | 1.4 | 1 |
| 21 | 148 | 299,768 | 18 | 8 |
| July 1 | 293 | 299,789 | 12 | 13 |
| 7 | 147 | 299,741 | 3 | 35 |
| 8 | 130 | 299,758 | 9 | 18 |
| Final value | 2895 | 299,776 km/sec. | ±9 km/sec. | ±14 km/sec. |

In the previously published results[6] by the author this correction was also not applied and amounted to approximately 88 instead of 81 km/sec., making $c_0$ 299,771 km/sec.

In the present case only the correction for air must be applied as there is no glass in the path to be measured. This correction amounts to approximately 84 km/sec. and is included in the correction factor in changing from $c_a$ to $c_0$ in the results.

## Results

The long path was measured seven times for an average value of 171.8642±0.0017 m exclusive of $\Delta S$ and $\Delta Y$. $\Delta S$ had an average value of 2.4770±0.012 cm. Therefore,

$$n\lambda = 171.8147 \text{ m} + 2\Delta y.$$

Since $n=11$, and $f=19.2$ megacycles,

$$c_a = 299{,}894.8 + 34.91\Delta y \text{ km/sec.},$$

where $\Delta y$ is measured in centimeters. Inasmuch as the long path was slightly longer than an even number of wave-lengths, the lathe mirror moved in an opposite direction to that assumed in the derivation of the above equation, in order to produce a minimum. Hence $\Delta y$ was always

negative and the second term of the above equation for $c_a$ was always negative.

A summary of the final results is shown in Table I. It will be noticed that while the average deviation from the daily mean is only $\pm 9$ km/sec., the average deviation from the final mean is $\pm 14$ km/sec. This is readily accounted for on the basis of the electron transit time difficulty mentioned above. The estimated error in the absolute value of the final result is therefore $\pm 14$ km/sec. Until the transit time problem is overcome, this appears to be the limiting factor in the accuracy of this method.

In view of the above factor, no definite conclusions can be drawn regarding the periodic nature of the velocity of light, but inasmuch as this value checks very well with that of 299,771 km/sec. (group velocity correction applied) obtained by the author in 1937, and with the values of recent observers, the author is inclined to discount any probability of such a periodicity.

In conclusion the author expresses his gratitude for the financial assistance given by the Carnegie Corporation of New York, which made this research possible. It is difficult to acknowledge all of the numerous helpful suggestions made by the members of the Physics and Astronomy Departments, but appreciation must be expressed to Professors G. W. Pierce, T. Lyman, F. V. Hunt, and H. Mimno of the Physics Department, and to Professors Shapley, Bok, and Sterne of the Astronomy Department. Messrs. David Mann and Harold Benner, and members of the laboratory shops are to be commended for their excellent optical and mechanical work. Mr. Gilbert Plass showed extreme patience and accuracy in the tedious measurements of numerous records with the comparator.

# Combination of Optical Systems*

SEYMOUR ROSIN AND ORRIN H. CLARK
*Department of Physics, Columbia University, New York, New York*
(Received December 6, 1940)

THIS paper presents a method for the calculation of the cardinal points of a combination of coaxial optical systems which has the advantage of elegance and simplicity over those commonly employed. The process of combining the systems depends upon the analysis of a characteristic determinant discovered by Ferraris,[1] from which are obtained explicit formulae for the location of the cardinal points of the resultant system.

The development of the general formulae is based on a simple expression for the lateral magnification produced by two optical systems upon any pair of conjugate points.

If $F$ and $F'$ denote the object and image focal points of an optical system, $M$ and $M'$ the positions of object and image on the axis of the system and $H$ and $H'$ the principal points, and if we set

$x=FM$ $\quad f=FH=$ object, or first, focal length
$x'=F'M'$ $\quad f'=F'H'=$ image, or second, focal length

then the Newtonian relation reads

$$Y=f/x=x'/f',$$

where $Y$ is the lateral magnification of the image.

Now let there be two coaxial systems separated by a distance $d_{1\cdot2}$, where

$$d_{1\cdot2}=F'_1F_2$$

the subscripts 1 referring to the first system and the subscripts 2 referring to the second. Evidently

$$x_2=F_2M_2=F_2M'_1=F_2F'_1+F'_1M'_1=x'_1-d_{1\cdot2}.$$

Then

$$x'_2=\frac{f_2f'_2}{x_2}=\frac{f_2f'_2}{x'_1-d_{1\cdot2}}=\frac{f_2f'_2}{f_1f'_1/x_1-d_{1\cdot2}}$$

or

$$x'_2=\frac{x_1f_2f'_2}{f_1f'_1-x_1\cdot d_{1\cdot2}}. \tag{1}$$

Solving (1) for $x_1$ in terms of $x'_2$, we get also

$$x_1=\frac{x'_2f_1f'_1}{f_2f'_2+x'_2\cdot d_{1\cdot2}}. \tag{2}$$

The lateral magnification of each system separately is given by

$$Y_1=f_1/x_1, \quad Y_2=x'_2/f'_2$$

(choosing those expressions giving outside $x$'s). The lateral magnification of the image formed by the combination is

$$Y_{1\cdot2}=Y_1\cdot Y_2=\frac{f_1}{x_1}\cdot\frac{x'_2}{f'_2}. \tag{3}$$

By substituting in (3) either of (1) or (2), we get two distinct expressions for $Y_{1\cdot2}$, namely

$$Y_{1\cdot2}=\frac{f_2f'_2+x'_2\cdot d_{1\cdot2}}{f'_1f'_2}, \tag{4a}$$

$$Y_{1\cdot2}=\frac{f_1f_2}{f_1f'_1-x_1\cdot d_{1\cdot2}}. \tag{4b}$$

The familiar expressions for the cardinal points and focal lengths may now be obtained. Let us consider the particular pair of conjugate points for which $Y_{1\cdot2}=\infty$. This necessitates that the object be placed at the object side focal point of the combined system. This requirement in 4(b) leads to the equation

$$f_1f'_1=x_1\cdot d_{1\cdot2},$$

where $x_1$ here has the meaning $x_1=F_1M_1=F_1F_{1\cdot2}$, or

$$F_1F_{1\cdot2}=f_1f'_1/d_{1\cdot2}. \tag{5}$$

The requirement that $Y_{1\cdot2}=0$ gives the position of the image side focal point of the combined system, since that is where the image must be to have that particular lateral magnification.

* Publication assisted by the Ernest Kempton Adams Fund for Physical Research of Columbia University.

[1] Galileo Ferraris, "Sui cannocchiali con obiettivo composto di piu lenti a distanza le une dalle altre," Atti R. Accad. Torino **16**, 45 (1880).

Equation (4a) gives in this case

$$x'_2 = F'_2 F'_{1\cdot 2} = -f_2 f'_2 / d_{1\cdot 2}. \tag{6}$$

The principal planes are found by setting $Y_{1\cdot 2}=1$. Equation 4(b) gives $H_{1\cdot 2}$ and 4(a) gives $H'_{1\cdot 2}$ where

$$x_1 = F_1 H_{1\cdot 2} = f_1 f'_1 / d_{1\cdot 2} - f_1 f_2 / d_{1\cdot 2}, \tag{7}$$

$$x'_2 = F'_2 H'_{1\cdot 2} = -f_2 f'_2 / d_{1\cdot 2} + f'_1 f'_2 / d_{1\cdot 2}. \tag{8}$$

The focal lengths are obtained from (5) and (7)

$$f_{1\cdot 2} = F_{1\cdot 2} H_{1\cdot 2} = F_{1\cdot 2} F_1 + F_1 H_{1\cdot 2} = -f_1 f_2 / d_{1\cdot 2} \tag{9}$$

and from (6) and (8)

$$f'_{1\cdot 2} = F'_{1\cdot 2} H'_{1\,2} = F'_{1\cdot 2} F'_2 + F'_2 H'_{1\cdot 2} = f'_1 f'_2 / d_{1\cdot 2}. \tag{9a}$$

The positions of any specialized pair of conjugate points of the combined system may be obtained in terms of the constants of the separate systems in the same manner, for example, the negative principal points by setting $Y_{1\cdot 2}=-1$ in 4(a) and 4(b), the nodal points by setting $Y_{1\cdot 2}=-f_{1\cdot 2}/f'_{1\cdot 2}$, etc. Indeed by giving any value desired for $Y_{1\cdot 2}$, the positions of the object and image are at once located.

For any number of coaxial optical systems simple magnification formulae analogous to 4(a) and 4(b) may be obtained with the aid of a characteristic determinant which combines the parameters of the system in the proper manner. If the system contains $n$ components, their arrangement is specified by $n-1$ constants, which are taken to be the separations of the $n-1$ pairs of adjacent components, measured from the image focal point of the first of the pair to the object focal point of the second. The separation of the $i-1$, $i$ pair is denoted by

$$d_{i-1\cdot i} = F'_{i-1} F_i. \tag{10}$$

Then the characteristic determinant for the system of $n$ components has $n-1$ rows and is defined by

$$D_{1\cdot n} = \begin{vmatrix} d_{1\cdot 2} & f_2 & 0 & & & & \\ -f'_2 & d_{2\cdot 3} & f_3 & & & & \\ 0 & -f'_3 & d_{3\cdot 4} & \cdot & & & \\ & \cdot & \cdot & \cdot & & & \\ & & \cdot & \cdot & \cdot & & \\ & & & \cdot & \cdot & \cdot & \\ & & & & \cdot & \cdot & 0 \\ & & & & & \cdot & f_{n-1} \\ & & & & 0 & -f'_{n-1} & d_{n-1\cdot n} \end{vmatrix}. \tag{11}$$

The principal diagonal is occupied by the system separations, and the two adjacent diagonals by the focal lengths as shown, with zero's elsewhere. If we denote by $D_{i\cdot j}$ the characteristic determinant ($i=1$, $j=n$) or any $(j-i)$ rowed subdeterminant thereof with coincident principal diagonal, expansion by minors gives at once:

$$D_{i\cdot j} = d_{j-1\cdot j} D_{i\cdot j-1} + f_{j-1} f'_{j-1} D_{i\cdot j-2} \tag{12}$$

and

$$D_{i\cdot j} = d_{i\cdot i+1} D_{i+i\cdot j} + f_{i+1} f'_{i+1} D_{i+2\cdot j}. \tag{13}$$

Equations (12) and (13) are valid for all positive integral values of $n$ if we set

$$D_{k\cdot k}=1 \quad \text{and} \quad D_{l\cdot m}=0 (l>m). \tag{14}$$

Then the magnification ratio for any pair of conjugate points produced by the entire system is given by either of the following:

$$Y_{1\cdot n} = \frac{f_n f'_n D_{1\cdot n-1} + x'_n D_{1\cdot n}}{f'_1 f'_2 \cdots f'_n} \tag{15a}$$

or

$$Y_{1\cdot n} = \frac{(-1)^n f_1 f_2 \cdots f_n}{f_1 f'_1 D_{2\cdot n} - x_1 D_{1\cdot n}}. \tag{15b}$$

The proof of (15a) will be given in detail by mathematical induction. Applying (4a) it is seen to be true for $n=2$. It will now be shown that if it is true for a system consisting of $n-1$ components, it is true for the system of $n$ com-

ponents formed by adding the $n$th component. By hypothesis, then

$$Y_{1\cdot n-1}=\frac{f_{n-1}f'_{n-1}D_{1\cdot n-2}+x'_{n-1}D_{1\cdot n-1}}{f'_1f'_2\cdots f'_{n-1}}.$$

But

$$\begin{aligned}x'_{n-1}&=F'_{n-1}M'_{n-1}=F'_{n-1}F_n+F_nM_n\\&=d_{n-1\cdot n}+x_n=d_{n-1\cdot n}+f_nf'_n/x'_n\\&=(x'_nd_{n-1\cdot n}+f_nf'_n)/x'_n.\end{aligned}$$

Also

$$Y_{1\cdot n}=Y_{1\ n-1}Y_{n-1\cdot n}=Y_{1\cdot n-1}\cdot(x'_n/f'_n).$$

Hence

$$\begin{aligned}Y_{1\cdot n}&=\frac{x'_nf_{n-1}f'_{n-1}D_{1\cdot n-2}+(x'_nd_{n-1\cdot n}+f_nf'_n)D_{1\cdot n-1}}{f'_1f'_2\cdots f'_{n-1}f'_n}\\&=\frac{f_nf'_nD_{1\cdot n-1}+x'_n(d_{n-1\cdot n}D_{1\cdot n-1}+f_{n-1}f'_{n-1}D_{1\cdot n-2})}{f'_1f'_2\cdots f'_n}\end{aligned}$$

or

$$Y_{1\cdot n}=\frac{f_nf'_nD_{1\cdot n-1}+x'_n\cdot D_{1\cdot n}}{f'_1f'_2\cdots f'_n}\ \text{from (12).}$$

Hence (15a) is true for any number of components.

The proof of (15b) may be effected in a similar manner. It is easily shown that if (15b) is valid for the abbreviated system obtained by discarding the first component of any system of $n$ components, then it is valid for the complete system. But it is true for $Y_{n-1\cdot n}$ from (4b), hence it is true in general. Also (15b) may be obtained from (15a) by reversing the light path and making the following substitutions.

$$x'_n\rightarrow -x_1,\qquad d_{i\cdot i+1}\rightarrow d_{n-i\cdot n-i+1},$$
$$f_i\rightarrow -f'_{n-i+1},\qquad f'_i\rightarrow -f_{n-i+1}.$$

The positions of the focal points of the system are at once obtained from the expressions (15a) and (15b). They are given by

$$F_1F_{1\cdot n}=f_1f'_1D_{2\cdot n}/D_{1\cdot n},\tag{16a}$$

$$F'_nF'_{1\cdot n}=-f_nf'_nD_{1\cdot n-1}/D_{1\cdot n}.\tag{16b}$$

The focal lengths are given by:

$$f_{1\cdot n}=(-1)^{n-1}(f_1f_2\cdots f_n/D_{1\cdot n}),\tag{17a}$$

$$f'_{1\cdot n}=f'_1f'_2\cdots f'_n/D_{1\cdot n}.\tag{17b}$$

To solve any particular problem, it is necessary only to calculate the $D$'s, starting with $D_{1\cdot 2}=d_{1\cdot 2}$, and obtaining therefrom $D_{1\cdot 3}$, $D_{1\cdot 4}$, etc. to $D_{1\cdot n}$. In some problems it is necessary also to calculate $D_{2\cdot n}$. If $n$ is large this can be much simplified with the aid of the expression

$$D_{2\cdot n}=\frac{D_{2\cdot j-1}D_{1\cdot n}+[\prod_{i=2}^{j-1}(-f_if'_i)]D_{j\cdot n}}{D_{1\cdot j-1}},\tag{18}$$

in which by a suitable choice of $j$ the number of terms in $D_{2\cdot n}$ may be reduced drastically from the direct Laplace expansion.

Setting the expressions for the focal lengths equal to infinity, it is seen that the condition for a telescopic system is given by the equation $D_{1\cdot n}=0$. Setting this condition in (15a) or (15b) we obtain expressions for the (constant) angular magnification of the telescope, assuming the same medium on both sides.

$$Z=\frac{f'_1f'_2\cdots f'_{n-1}}{f_nD_{1\cdot n-1}}=\frac{f'_1D_{2\cdot n}}{(-1)^nf_2f_3\cdots f_n}.$$

In illustration of the simple manner in which these equations may be applied to an actual system the essential optical constants of the Gullstrand schematic eye will now be calculated.

**Data:***

| Surface | $f_i$(mm) | $f_i'$(mm) | |
|---|---|---|---|
| 1 | 20.479 | −28.179 | $d_{1\cdot 2}=$ 206.24 mm |
| 2 | −233.92 | 227.12 | $d_{2\cdot 3}=$ −36.98 mm |
| 3 | 267.20 | −277.20 | $d_{3\cdot 4}=$ −824.89 mm |
| 4 | 548.23 | −556.15 | $d_{4\cdot 5}=$ −958.66 mm |
| 5 | 404.93 | −399.16 | $d_{5\cdot 6}=$ −564.84 mm |
| 6 | 166.32 | −160.32 | |

**Computation:** (For convenience the calculation is made in decimeters.)

$D_{1\ 2}=d_{1\cdot 2}=2.0624,$

$D_{1\cdot 3}=d_{2\cdot 3}D_{1\cdot 2}+f_2f'_2=-6.0756,$

* The data are taken from J. P. C. Southall, *Mirrors, Prisms and Lenses* (Macmillan, 1936), third edition, p. 371.

$$D_{1\cdot4}=d_{3\cdot4}D_{1\cdot3}+f_3f_3'D_{1\cdot2}=34.842,$$

$$D_{1\cdot5}=d_{4\cdot5}D_{1\cdot4}+f_4f'_4D_{1\cdot3}=-148.77,$$

$$D_{1\cdot6}=d_{5\cdot6}D_{1\cdot5}+f_5f'_5D_{1\cdot4}=277.16,$$

$$D_{2\cdot6}=\frac{D_{2\cdot3}D_{1\cdot6}+f_2f'_2f_3f'_3D_{4\cdot6}}{D_{1\cdot3}}$$

$$=\frac{d_{2\cdot3}D_{1\cdot6}+f_2f'_2f'_3f'_3(d_{4\cdot5}d_{5\cdot6}+f_5f'_5)}{D_{1\cdot3}}$$

$$=-229.16,$$

$$f_{1\cdot6}=(-1)^5\frac{f_1f_2\cdots f_6}{D_{1\cdot6}}=17.052\text{ mm},$$

$$f'_{1\cdot6}=\frac{f'_1f'_2\cdots f'_6}{D_{1\cdot6}}=-22.781\text{ mm},$$

$$F'_6F'_{1\cdot6}=-\frac{f_6f'_6D_{1\cdot5}}{D_{1\cdot6}}=-143.12\text{ mm},$$

whence $A_1F'_{1\cdot6}=24.40$ mm with $A_1$ the vertex of the cornea.

$$F_1F_{1\cdot6}=f_1f'_1D_{2\cdot6}/D_{1\cdot6}=4.771\text{ mm},$$

whence $A_1F_{1\cdot6}=-15.708$ mm.

In the event one of the components is a plane refracting surface the focal lengths become infinite for that surface and the evaluation of the formulae apparently presents some difficulty. In fact, however, it is possible to omit the plane surface altogether by a simple modification of the parameters pertaining to the adjacent components. Let the $k$th component be a plane refracting surface and let $A_{k-1}$, $A_k$, and $A_{k+1}$ be the vertices of the $(k-1)$th, $k$th, and $(k+1)$th components, respectively. Then paraxial rays after entering the $k$th medium (between $A_{k-1}$ and $A_k$) proceed through $A_k$ and arrive at $A_{k+1}$ exactly as if the path $A_{k-1}A_{k+1}$ were all in the $(k+1)$th medium (between $A_k$ and $A_{k+1}$) provided the parameters which measure distance in the $k$th medium are reduced to the $(k+1)$th medium. Hence the $(k-1)$th and $(k+1)$th components may be taken as adjacent with this modification. The parameters in question are $f'_{k-1}$ and an easily determined part of $d_{k-1\cdot k+1}$. For we have:

$$d_{k-1\cdot k+1}=F'_{k-1}F_{k+1}$$
$$=F'_{k-1}A_{k-1}+A_{k-1}A_k+A_kA_{k+1}+A_{k+1}F_{k+1}$$
$$=f'_{k-1}+A_{k-1}A_k+A_kA_{k+1}-f_{k+1},$$

in which obviously $f'_{k-1}$ and $A_{k-1}A_k$ are measured in the $k$th medium and must be multiplied by $n_{k+1}/n_k$ to give the actual reduced path traversed by rays reaching $A_{k+1}$. Thus the corrected value for the separation of the $(k-1)$th and $(k+1)$th components is

$$d_{k-1\cdot k+1}=(n_{k+1}/n_k)(f'_{k-1}+A_{k-1}A_k)+A_kA_{k+1}-f_{k+1};$$

and if in addition $f'_{k-1}$ be replaced by $(n_{k+1}/n_k)f'_{k-1}$ wherever it appears explicitly the plane surface will be fully accounted for. A simple example follows. Consider two hemispheres of radius 10 cm in close contact to form a sphere, the first having index of refraction $n_1=1.5$, the second $n_2=1.7$. Then

$$f_1=20\text{ cm};\quad f'_1=-30\text{ cm};\quad f_3=170/7\text{ cm};$$
$$f'_3=-100/7\text{ cm}.$$

Hence:

$$d_{1\cdot3}=(1.7/1.5)(-30+10)$$
$$+10-170/7=-776/21,$$

and $f'_1$ must be replaced by $-1.7/1.5\times30=-34$. Thus:

$$f_{1.3}=-f_1f_3/d_{1\cdot3}=1275/97\text{ cm}=-f'_{1.3}$$

and

$$A_1F_{1.3}=A_1F_1+F_1F_{1.3}=-f_1$$
$$+f_1f'_1/d_{1\cdot3}=-155/97\text{ cm}$$

and finally

$$A_3F'_{1.3}=A_3F'_3+F'_3F'_{1.3}=-f'_3$$
$$-f_3f'_3/d_{1\cdot3}=475/97\text{ cm}.$$

This device of "skipping" the plane surface is of course applicable to any method of combining optical systems.

The treatment of reflecting systems presents no difficulty. It should be noted, however, that the treatment of reflection must conform to a convention making it a special case of refraction, and giving the Newtonian image equations in the same form as for a refracting system.

# Physical Interpretations of Resolving Power

B. P. Ramsay, O. T. Koppius and E. L. Cleveland
*Department of Physics, University of Kentucky, Lexington, Kentucky*
(Received October 18, 1940)

## I. Problems of Resolution

PHYSICISTS are concerned with the abilities of optical instruments to distinguish between two objects as well as to distinguish between two wave-lengths from a single source. The two objects whose resolution is desired may radiate either the same or different wave-lengths. Because of this, it is possible to take notice of several problems of resolution. Objective resolution is concerned with recognizing as independent two sources with a small angular separation. Spectroscopic (or chromatic) resolution is concerned with distinguishing two sources coincident in position, but differing in wave-length. Pointillist[1] resolution is a name which may be applied to problems in which the sources differ in both position and wave-length.

Although this last case has not been developed as an important topic in optics, it is worthy of reflection. For it appears that pointillist resolution might be a sort of complete differential composed of the sum of the partial differentials which constitute the other two cases. Yet the metaphor is not very apt. For in spectroscopic resolving power, the wave-lengths being resolved differ only by an increment; but in the observation of two stars, or two points of a microorganism, the wave-length difference may be large as well as abrupt. This is significant in consideration of the effect of chromatic aberration upon focusing. The effect of absorption is also important. For the maxima of adjacent wave-lengths are likely to have the same shape, but this is not true of widely different wave-lengths unless the elements of the optical system are equally transparent to both.[2] Thus pointillist resolution is a more complex problem than the other two which have been mentioned. Although it cannot be discussed here, it is felt that this is a subject of inescapable importance in certain cases. Thus, when a prismatic system is used in tandem with an instrument of high resolving power for the purpose of auxiliary dispersion, the components of the isolated line are partially resolved, and are not incident upon the second instrument from the same position.

It may be remarked that large and abrupt differences in wave-length present problems in the use of spectroscopic instruments also. These problems have been treated by the concepts of spectral range, overlapping of spectra, and visibility. It has been suggested[3] that difficulties of this kind are problems of "resolution" rather than problems of "optical resolving power." Further discussion of them will be avoided in this paper.

## II. Objective and Spectroscopic Resolving Power

The theory of spectroscopic resolving power originated with Rayleigh. His theory of objective resolving power was antedated by that of Foucault, who discussed the resolving power of telescopes, and by that of Abbe and Helmholtz, who independently discussed the resolving power of microscopes. The clarity of Rayleigh's papers, however, is responsible for the coherence with which these two types of resolving power have been understood. The Rayleigh definition for the resolving power of a spectroscopic device is

$$\rho = \lambda/\Delta\lambda, \tag{1}$$

where $\Delta\lambda$ is the smallest wave-length difference in the neighborhood of $\lambda$ which is resolvable by

[1] An art technique known as *pointillisme* may be mentioned in this regard. It was developed by the French artist Monet on the basis of suggestions offered by two physicists, Rood and Chevreul. In this method of painting, pigments are not mixed to obtain combination colors; but small streaks or dots of pigment of the fundamental colors are placed side by side on the canvas. The artistic effect is obtained by viewing the assemblage from a distance at which the eye is unable to resolve the individual points. The advantage of the method seems to be its sensitivity to contrast, intensity, and hue.

[2] The effect of absorption on the resolving power of the prism has been discussed by F. L. O. Wadsworth, Phil. Mag. **5**, 355–374, (1903). The sort of arguments used there are applicable also to lens systems.

[3] B. P. Ramsay, E. L. Cleveland and O. T. Koppius, "Criteria and the intensity-epoch slope," J. Opt. Soc. Am. **31**, 26 (1940).

the device. The corresponding expression for objective resolution is

$$r=1/\phi, \tag{2}$$

where $\phi$ is the minimum angle of resolution.

Equivalent statements of the Rayleigh definition of spectroscopic resolving power are given in terms of frequency, $\nu$, order of interference, $m$, and epoch function, $\alpha$. Thus by use of the relation

$$\nu=c/\lambda, \tag{3}$$

where $c$ is the velocity of light, the Rayleigh resolving power may be expressed[4] as

$$\rho=-\nu/\Delta\nu. \tag{4}$$

Likewise, by use of the relation

$$m=d/\lambda, \tag{5}$$

it follows[5] that

$$\rho=-m/\Delta m. \tag{6}$$

It may be observed that this result is independent of the exact formula for $d$, which is always expressible in terms of the geometry of the optical paths and changes in phase which arise from boundary conditions.[6] Formulas for $d$, which are applicable to various types of interferential devices, appear in standard references. Thus the formula usually given for the case in which light is transmitted through an optical lamina is

$$d=2T(\mu^2-\sin^2 i)^{\frac{1}{2}}=2\mu T\cos i'. \tag{7}$$

The geometry of this result is shown by Fig. 1, where $T$ is the thickness of the lamina, $\mu$ is its refractive index, $i$ is the angle of incidence, and $i'$ is the angle of refraction.

A fourth useful relation for $\rho$ is obtained from the defining equation,

$$\alpha=\gamma/2=\pi d/\lambda, \tag{8}$$

where $d$ has the same significance as in (5). The result is

$$\rho=-\alpha/\Delta\alpha. \tag{9}$$

A simple example will illustrate the use of this formula. For a grating on the Schuster criterion,

$$\Delta\alpha=\pi/k, \tag{10}$$

where $k$ is the number of rulings on the grating. The value of $\alpha$ at the maximum with which $\Delta\alpha$ is associated is

$$\alpha=m\pi. \tag{11}$$

Thus

$$\rho=m(\pi/\Delta\alpha)=km. \tag{12}$$

This is the usual result for the grating.

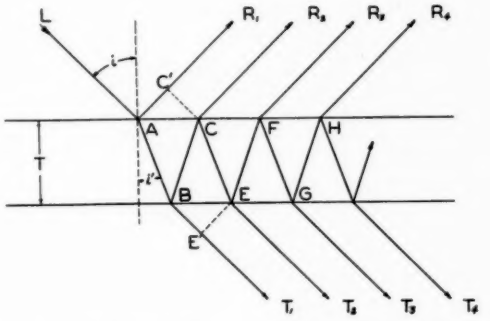


FIG. 1. Diagram to illustrate notation used in discussing optical lamina of thickness $T$, refractive index $\mu$, angle of incidence $i$, and angle of refraction $i'$.

The Rayleigh definitions (1) and (2) have been made somewhat analogous in an attempt to impart a unified significance to the concept of resolving power when applied to spectroscopic and objective instruments. All that is necessary to make them formally similar is to define a fictitious angle

$$\phi'=\Delta\lambda/\lambda. \tag{13}$$

In terms of $\phi'$, (1) and (2) are identical in form. Greater confidence in the similarity of (1) and (2) may result from carrying through some simple applications than from the introduction of the fictitious angle, $\phi'$. For, in both cases, one is concerned with the relative positions of two intensity patterns; and the distinction between the two types of resolving power seems to be based largely upon the kinds of conditions which determine the positions of the intensity patterns.

In spite of these similarities, however, it can be shown that it is impossible to construct, on the definitions (1) and (2), a single consistent theory of resolving power which will include both spectroscopic and objective resolution. For it has

[4] S. Goldman, J. Opt. Soc. Am. **23**, 70, 71 (1933).

[5] W. E. Williams, *Applications of Interferometry* (E. P. Dutton and Company, 1930), p. 79.

[6] An interesting account of effects of the latter sort is given by W. W. Sleator and A. E. Martin, J. Opt. Soc. Am. **24**, 29, 30 (1934).

been shown in a previous paper[3] that the limiting angle of resolution, $\phi$, for objective resolving power is given directly in terms of the criterion value, $b=\Delta\alpha$, by

$$\phi=2b=2\Delta\alpha. \tag{14}$$

From (9), however, it appears that

$$\phi'=\Delta\alpha/\alpha=\phi/2\alpha. \tag{15}$$

Because the meaning of $\phi'$ is different from that of $\phi$, it is impossible to discuss both spectroscopic and objective resolving power from the standpoint of a single theory until one definition or the other has been modified. Because it is not proposed at this time to follow out the consequences of altering the definitions (1) and (2), the subject of objective resolving power will not be given further consideration in this paper.

## III. The Generalized Williams Interpretation

The four statements of the definition of the Rayleigh resolving power, $\rho$, which have been noted in (1), (4), (6) and (9) do not reveal the physical quantities upon which resolving power depends. One merely knows of $\Delta\lambda$, $\Delta\nu$, $\Delta m$, and $\Delta\alpha$ that they are minimum resolvable quantities which are specified, either directly or indirectly, by a criterion for the limit of resolution. Criteria for these minimum quantities offer no assistance in providing a physical picture of resolving power. There are, however, at least four physical interpretations which indicate the quantities upon which resolving power depends.

In a previous paper,[7] it has been shown that the Rayleigh spectroscopic resolving power can be stated in a form which is a generalization of a rule which Williams[8] has found applicable to gratings. It is,

$$\rho=\Delta t/P. \tag{16}$$

Here $\rho$ is the difference in time, $\Delta t$, required to propagate energy over the extreme optical paths, where the unit of time is the period, $P$, of the wave motion. In calculating $\Delta t$, it is the group velocity, and not the phase velocity, which determines the difference in time required for the propagation of the energy.

## IV. The Indeterminacy Rule

The Rayleigh resolving power can be expressed in terms of the photon theory of light by making use of the Heisenberg indeterminacy principle which may be stated as follows:

$$\Delta\epsilon\Delta t=h. \tag{17}$$

Here $\Delta\epsilon$ is the uncertainty in the energy of a single photon, $\Delta t$ is the uncertainty in time specification, and $h$ is Planck's constant. This principle may be related[4] to $\rho$ by means of the quantum energy formula,

$$\epsilon=h\nu. \tag{18}$$

From this, $$\Delta\epsilon=h\Delta\nu, \tag{19}$$

and (17) becomes $$\Delta\nu=1/\Delta t. \tag{20}$$

Thus the Rayleigh resolving power may be expressed as the product of the frequency, $\nu$, by the uncertainty, $\Delta t$. For

$$\rho=-\nu/\Delta\nu=\nu\Delta t. \tag{21}$$

A negative sign which is properly attached to the right side of (21) has been absorbed in $\Delta t$. That is, the result is certain to have the proper sign if the difference in times is taken in the proper way. The reason for the absorption of the negative sign is to show that (21) is actually identical with (16), although the idioms in which they are stated differ. Moreover, resolving power is essentially a positive quantity, as has been stated by Williams;[9] and one can be sure that the algebraic quantities have not been manipulated in the best way if the resulting formulas yield a negative value.

The indeterminacy rule for the Rayleigh resolving power may be illustrated by applying it to the Fabry-Perot interferometer. For this instrument,

$$\Delta t=N\Delta\tau, \tag{22}$$

where $\Delta\tau$ is the time uncertainty which corresponds to a single pair of internal reflections, and $N$ is the number of such pairs of reflections which contribute to the total uncertainty, $\Delta t$.

$$\Delta\tau=t_2-t_1, \tag{23}$$

[7] B. P. Ramsay, O. T. Koppius and E. L. Cleveland. "The prism and the theory of optical resolution," J. Opt. Soc. Am. **30**, 439 (1940).

[8] W. E. Williams, reference 5, p. 27.

[9] W. E. Williams, reference 5, p. 80.

where $t_1$ is the time required for the transmission of the first beam, $t_2$ is the time required for the transmission of the second, and $t_1<t_2$. It is in this step that the sign of the ultimate value for $\rho$ is determined. From (7), it may be seen that

$$\Delta\tau=d/v=2(T/v)\cos i, \tag{24}$$

for $i=i'$, and approximately, $\mu=1$. In (24), $v$ is the velocity with which the energy is propagated; but under the assumptions which have been made, this does not differ from the phase velocity.

Examination of (10) shows that the number of rulings on the grating is

$$\pi/\Delta\alpha=k. \tag{25}$$

The corresponding relation[3] for the Fabry-Perot instrument is

$$\pi/\Delta\alpha=\pi R^{\frac{1}{2}}/1.21(1-R), \tag{26}$$

where $R$ is the intensity coefficient of reflection. Williams[9] has called this quantity the effective number of reflections. Let it be assumed that this is the number which is to be identified with $N$ in (22). Then

$$\Delta t=[\pi R^{\frac{1}{2}}/1.21(1-R)][2(T/v)\cos i]. \tag{27}$$

If $v$ equals the phase velocity for the air lamina of the Fabry-Perot instrument,

$$v=\nu\lambda. \tag{28}$$

Thus the indeterminacy rule (21) gives

$$\rho=m[\pi R^{\frac{1}{2}}/1.21(1-R)], \tag{29}$$

where $m$ is the order of interference given by

$$m=2(T/\lambda)\cos i. \tag{30}$$

Since (29) is the standard result, the assumption involved in setting

$$N=\pi/\Delta\alpha \tag{31}$$

is justified.

## V. The Dispersion Formula

It has been noted for isolated cases—such as the prism,[10] the grating,[11] and the echelon[12]—that the Rayleigh resolving power is related to angular dispersion, $D$, by the formula,

$$\rho=wD. \tag{32}$$

where $w$ is the width of the wave front incident upon the observing device. The generality of this formula has been emphasized by Monk. The argument is as follows. From (1),

$$\rho=(\lambda/\Delta i')(\Delta i'/\Delta\lambda), \tag{33}$$

where $i'$ is the angle of emergence. Since

$$D=\Delta i'/\Delta\lambda, \tag{34}$$

comparison with (32) shows that

$$w=\lambda/\Delta i'. \tag{35}$$

Although the validity of interpreting $w$ as the width of the emergent beam is well established for the prism, the grating, and the echelon, it is interesting to observe that this interpretation prevails also in the case of internal reflection devices, such as the Fabry-Perot interferometer. Direct application of (35) gives the width as

$$w=(\lambda/\Delta\alpha)(\Delta\alpha/\Delta i'). \tag{36}$$

By (7) and (8),

$$\alpha=2\pi(T/\lambda)\cos i', \tag{37}$$

where $\mu=1$, and $i=i'$. Thus,

$$\Delta\alpha/\Delta i'=-2\pi(T/\lambda)\sin i, \tag{38}$$

$$w=-(\pi/\Delta\alpha)(2T\sin i), \tag{39}$$

$$w=-N2T\sin i, \tag{40}$$

where $N$ is given by (31).

The geometrical significance of (40) appears by reference to Fig. 1. For the width of the beam transmitted by an optical lamina is

$$w=N(EE'), \tag{41}$$

where $N$ is the effective number of internal reflections which occur in the lamina. Now,

$$EE'=BE\cos(E'EB)$$
$$=2T\tan i'\cos(E'EB). \tag{42}$$

If the material of the lamina is the same as that in which $i$ is measured—e.g., air, in the case of the Fabry-Perot interferometer—it follows that $i=i'$. However, the angle $i'$ is measured in a counterclockwise direction, but $(E'EB)$ is taken clockwise from the normal to the path of the ray.

[10] M. Born, *Optik* (Julius Springer, Berlin, 1933), p. 181.
[11] L. W. Taylor, *College Manual of Optics* (Ginn and Company, New York, 1924), pp. 61 and 70–75.
[12] G. S. Monk, *Light* (McGraw-Hill, New York, 1937), pp. 198–201.

Hence,

$$(E'EB) = -i,$$

and

$$EE' = -2T \sin i. \tag{43}$$

The use of this value in (41) gives the result obtained by the abstract procedure in (40).

Since, by (26),

$$N = \pi R^{\frac{1}{2}}/1.21(1-R), \tag{44}$$

$$w = -2T \sin i[\pi R^{\frac{1}{2}}/1.21(1-R)]. \tag{45}$$

The angular dispersion is readily found from (30) to be

$$D = -m/2T \sin i. \tag{46}$$

The use of (45) and (46) in the dispersion formula (32) gives the standard result noted in (29).

The analogy between gratings and internal reflection devices can be carried one step further by noting that the quantity $EE'$ given by (43) corresponds to the grating space. For instance, the dispersion of a grating in any order is independent of the number of rulings,[13] but is inversely proportional to the grating space. This conclusion applies also to the Fabry-Perot interferometer when the analogy which has been proposed is employed.

## VI. The Epoch Slope Product

A significantly different interpretation of resolving power is suggested by comparing phenomena of resolution in the Michelson and Fabry-Perot interferometers. The intensity function for the Michelson interferometer is

$$I = 4A^2 \cos^2 \alpha.$$

Let $\lambda$ be any given wave-length, and $\lambda'$ be any other wave-length. Then at the maximum of the intensity pattern for which $\alpha_\lambda = 0$, $\alpha_{\lambda'} = 0$ for every other wave-length, $\lambda'$. But at the maxima for which $\alpha_\lambda = m\pi$, $m \neq 0$, the value of $\alpha_{\lambda'}$ is greater than $m\pi$ if $\lambda' < \lambda$, and less than this value if $\lambda' > \lambda$. Moreover, the difference $(\alpha_\lambda - \alpha_{\lambda'})$ increases with the value of $m$, the order of interference. Because of this fact, any $\Delta\lambda = \lambda' - \lambda$, however small, is resolvable simply by giving a sufficiently large value to

$$\alpha_\lambda = m\pi. \tag{47}$$

[13] L. W. Taylor, reference 11, p. 59.

On the other hand, the resolving power of a Fabry-Perot interferometer for a given order, $m$, may be different from that of a Michelson instrument employing the same order. Which has the greater resolving power depends upon the slope of the intensity maxima which they produce. It may be said in general that if the intensity value descends sharply from its maximum, $I'$, to the intensity criterion value, $I^*$, the resolving power is large, but if the intensity-epoch slope is small, the resolving power also has a small value. This point has been argued in a previous paper,[7] and values of the intensity-epoch slope have been listed.[3]

Thus it now appears that resolving power may be expressed as the product, $P$, of epoch value and intensity-epoch slope. The letter, $P$, is used instead of $\rho$, for the two quantities are not identical. The form which the mathematical expression for $P$ takes appears somewhat strange at first. It is

$$P = (\alpha/Y)(\Delta I/\Delta\alpha). \tag{48}$$

The factor, $(1/Y)$, will be discussed later. Aside from it, however, a brief examination of the expression (48) will make the meaning of $P$ clear. For $(\Delta I/\Delta\alpha)$ is simply the intensity-epoch slope which has been shown[3] to be proportional to the effective number of beams as given by (31). Moreover, as shown by (47), the epoch value, $\alpha$, is proportional to the order of interference. Thus (48) gives

$$P = CmN/Y. \tag{49}$$

The constant of proportionality, $C$, may be called the criterion coefficient, for its value is determined solely by the choice of a criterion. Its meaning becomes clear with the application of (48) to specific problems. For an intensity criterion value,

$$I^* = (4/\pi^2)I' = 0.405I', \tag{50}$$

$$\Delta I = 0.595I'. \tag{51}$$

The value of $P$ for a Fabry-Perot interferometer on this criterion (the generalized Rayleigh criterion) is

$$P = (m\pi/Y)(0.595F^{\frac{1}{2}}/1.21)I', \tag{52}$$

$$P = 0.595m(\pi F^{\frac{1}{2}}/1.21)(I'/Y), \tag{53}$$

$$P = 1.19m[\pi R^{\frac{1}{2}}/1.21(1-R)](I'/Y), \tag{54}$$

where $F$ is the coefficient of finesse given by

$$F=4R/(1-R)^2.$$

However, for a criterion value,

$$I^*=0.350I', \tag{55}$$

the value of $P$ for the same instrument is

$$P=1.30m[\pi R^{\frac{1}{2}}/1.36(1-R)](I'/Y). \tag{56}$$

Finally, for an intensity criterion value,

$$I^*=0.450I', \tag{57}$$

$$P=1.10m[\pi R^{\frac{1}{2}}/1.10(1-R)](I'/Y). \tag{58}$$

It may be observed in the first place that the criterion coefficient enters the result for $P$ in the process of evaluating the intensity-epoch slope. Thus it was noticed in the previous paper,[3] that on the generalized Rayleigh criterion the intensity-epoch slope for the Fabry-Perot interferometer has the value,

$$\Delta I/\Delta\alpha=(1.19I'/\pi)[\pi R^{\frac{1}{2}}/1.21(1-R)]. \tag{59}$$

Likewise for the grating,

$$\Delta I/\Delta\alpha=(1.19I'/\pi)k, \tag{60}$$

and for the transparent prism,

$$\Delta I/\Delta\alpha=1.19I'/\pi. \tag{61}$$

On the Schuster criterion, however, the value for the grating is

$$\Delta I/\Delta\alpha=(I'/\pi)k, \tag{62}$$

and for the transparent prism,

$$\Delta I/\Delta\alpha=I'/\pi. \tag{63}$$

Nevertheless, comparison of (54), (56) and (58), shows that the choice of a criterion affects the effective number of reflections, $N$, as well as the factor which has been placed immediately in front of $m$. Because of this, the value of $N$ as given by (31) is not equal to $k$ in the case of a grating, unless the Schuster criterion be used. In (60), for instance,

$$N=2k. \tag{64}$$

This merely means that no intrinsic significance need be attributed to the criterion coefficient. The chief value of (49) is to illustrate a similarity between $P$ and $\rho$.

The application of (48) to the prism is confusing until the meaning of $\alpha$ for this case has been determined. The source and nature of the confusion has been previously considered.[7] It is fairly obvious now that the proper value of $\alpha$ is

$$\alpha=\pi m=\pi\rho. \tag{65}$$

For the use in (48) of this value for $\alpha$ and that given by (61) for $\Delta I/\Delta\alpha$ gives for the transparent prism on the generalized Rayleigh criterion,

$$P=1.19\rho(I'/Y) \tag{66}$$

or

$$P=1.19T(\partial\mu/\partial\lambda)(I'/Y). \tag{67}$$

If an absorbing prism is considered, the value of the intensity-epoch slope is less than that given by (61). The manner in which this slope depends upon absorption has been discussed previously.[7] For a completely absorbing prism,

$$\Delta I/\Delta\alpha=0. \tag{68}$$

## VII. Conclusions

There are several respects in which the interpretation of resolving power provided by (48) is preferable to other interpretations which have been noted. In the first place, this is the only rule which shows explicitly the manner in which resolving power is related to the choice of a criterion. Here the criterion is immediately related to resolving power through the intensity-epoch slope—or, more specifically, through the intensity decrement, $\Delta I$. The coefficient of reflection, absorption, and the number of beams superposed by an interferential system affect resolving power in known ways through the epoch increment, $\Delta\alpha$. On other interpretations, these quantities affect resolving power through $\Delta t$ or $w$.

It is noteworthy that when the generalized Rayleigh criterion is used, the value of $P$—as may be seen in several cases from (54), (60), and (66)—is nineteen percent higher than the value given by the usual procedures for evaluating $\rho$. It has been urged from time to time that theoretical calculations would be in closer agreement with experimental observations if the theory gave a value approximately twenty percent higher than that given by the usual values

of $\rho$. Among those who have recommended an increase in the theoretical value are Sparrow,[14] Preston,[15] and Ditchburn.[16] The procedure proposed for obtaining this result has been the adoption of some novel criterion. The desired increase[5] in the theoretical value of resolving power results quite naturally when the epoch-slope formula (48) is used.

The discussion of (48) as the basis for a theory of resolving power is not complete without a consideration of the significance of $Y$. One obvious reason for the inclusion of this inverse factor is the certain knowledge that resolving power must be made a dimensionless quantity. It has been previously argued[3] that the unit of intensity must be $I'$, the intensity value of the maximum. This requirement would be automatically expressed by setting

$$Y=I'. \tag{69}$$

It is believed, however, that to adopt this simple identification would be to discard one of the desirable possibilities of the theory. For there are theoretical and experimental reasons[17] for making resolving power an inverse function of intensity. Because of the novelty of this possibility, it seems desirable to reserve the interpretation of $Y$ for a later paper. Enough has already been said, however, to show that (48) is a significant formula for resolving power, even if the best interpretation of $Y$ were that given by (69).

Finally, it is anticipated that the adoption of (48) as a theoretical basis for optical resolving power will facilitate the development of rules for the use of combinations of optical elements. This subject, too, merits further exposition.

[14] C. M. Sparrow, Astrophys. J. **44**, 76–86 (1916).
[15] T. Preston, *Theory of Light* (Macmillan and Company, New York, 1928), fifth edition, p. 266.
[16] R. W. Ditchburn, Proc. Roy. Irish Acad. **39**, 58–72 (1930).
[17] E.g., v. K. B. Merling-Eisenberg, Nature **89**, 416 (1937).

# Superposition Fringes in the Internally Reflected Light from a Fabry-Perot Etalon

S. MROZOWSKI*
*Department of Physics, University of California, Berkeley, California*
(Received November 18, 1940)

A system of very sharp dark fringes is observed in the spectra formed by both of the first-order reflections occurring within the quartz plates of a Fabry-Perot etalon. In the second-order reflections, two intersecting systems of fringes appear, the fringe separation in one being half of that in the other. The first-order fringes are complementary to the fringes observed many years ago by Perot and Fabry in the light passing through two nonparallel etalons of equal thickness. They arise by passage of the light through the etalon and subsequent reflection from it in the reverse direction. The two systems of fringes in the second-order reflections arise from one passage through the etalon, followed or preceded by two successive reflections from it.

IN the manufacture of Fabry-Perot etalons it is customary to make the quartz plates slightly wedge-shaped, in order to remove from the principal beam the systems of interference fringes arising from internal reflections in the plates (Fig. 1). In the most common arrangement, where an image of the fringes is formed by a lens on the slit of the spectrograph, the reflected spots containing these systems of fringes seldom reach the slit and hence do not confuse the observed pattern. Nevertheless, when an image of considerable size is projected on the slit, it is advisable to arrange the etalon in such a way as to throw the reflected light to one side or the other of the slit and not in the direction of the slit length. In the former case the reflected fringes are parallel to the slit length and do not disturb the observations by the appearance of weak, spurious components. In the latter case these appear, although it is true that they can usually be easily distinguished from the main pattern by the difference in the separation of orders.

In the arrangement, perhaps somewhat less frequently used, where the etalon is inserted in the spectrograph between the prism and one of the lenses, the second arrangement is more practicable. One then observes, above and below the main spectrum, weaker spectra of the reflected light. Their position can be adjusted by turning either or both of the etalon plates about an axis in the direction of the light. In Fig. 2 is shown an enlargement of an overexposed photograph of a line with both first-order reflections ($R_1$ and $S_1$ in Fig. 1) directed to the same side. It is very easy to distinguish the two types of reflections designated $R_n$ and $S_n$. The fringes formed by $S_n$ are exact copies of the main interference pattern caused by $L'$, while the fringes from $R_n$ are extensions of the main interference pattern, having the same appearance that it would have if the source slit were wide enough or long enough for it to appear in the corresponding position. The beams reflected successively from the surfaces $A$ and $D$ cannot be observed. as they overlap with much more intense beams coming from reflections lower in order by two ($L'$ and $R_{n-2}$ or $S_{n-2}$).

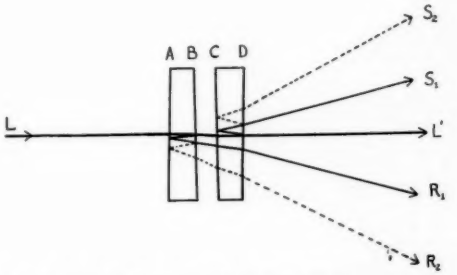


FIG. 1. Internal reflection of light passing through a Fabry-Perot etalon.

Recently, in the course of some work on hyperfine structure using such an arrangement, I noticed fine white lines on the negatives crossing the patterns in the reflected images. Two such lines are visible in Fig. 2 and are marked with arrows. A closer examination showed that all the reflected images are crossed by very sharp dark fringes. Since these fringes do not seem to have been described before, their behavior was

* Now at Ryerson Physical Laboratory, University of Chicago.

studied more carefully and the results, with their explanation, are presented here.

These systems of fringes can be more easily observed using a source of continuous spectrum. In the first-order reflections $R_1$ and $S_1$ they consist of single sets of fringes, of constant separation for a given wave-length, but drawing together as they extend toward the violet. The extreme sharpness of the fringes may be seen in Fig. 3. The sharpness decreases in the direction of

FIG. 2. The direct and the two first-order reflection spectra of a complex line.

shorter wave-lengths. The spacing is inversely proportional to the thickness of the etalon spacer and directly proportional to wave-length. Rotation of the etalon around an axis parallel to the edge of the wedge (normal to the surface of the paper in Fig. 1) produces a shift of the fringe system in a direction perpendicular to the dispersion of the spectrograph. At the same time the fringes in the reflected spectra $R_1$ and $S_1$ become more and more inclined. Rotation of the etalon around the other axis (parallel to $B$ and $C$ in the plane of the paper) has only a very slight influence on the fringe system. In both cases the fringes lose their sharpness with larger angles of rotation. Parallelism of the silvered surfaces $B$ and $C$ is essential for the appearance of these fringes, but they are more persistent than the usual high order fringes given by the etalon for discrete lines in the direct spectrum $L'$. They are still visible (although very diffuse) when no traces of fringes in a discrete spectrum in $L'$ can be seen. Widening the slit of the spectrograph does not affect the sharpness of the fringes in $S_1$, but lowers that in $R_1$.

In the second-order reflections, $S_2$ and $R_2$, two overlapping systems of dark fringes are visible (Fig. 4). The fringe separation in one system is exactly half of that in the other. These fringes have a more complicated dependence of sharpness on wave-length than have those in the first order. In addition to the gradual decrease of sharpness towards the violet, two broad regions are observed, one in the yellow-green, the other in the violet, where the fringes are so broad that they practically disappear. The intensity of the reflected light is also somewhat smaller in these regions. The relative position of the two intersecting systems of fringes is the same in both $R_2$ and $S_2$.

The explanation of these fringes is quite elementary. They are low order fringes of a kind observed by Perot and Fabry as early as 1899, and called by them "superposition" fringes. They are essentially of the type known as Brewster's fringes.[1] They appear as bright fringes when light passes in succession through two Fabry-Perot etalons slightly inclined to each other, and having equal separations, or separations in a simple ratio. For two etalons $BC$ and $C'B'$ of equal thickness $t$ and with an angle of inclination $\alpha$ (Fig. 5), a beam of light passing through is split by reflection on the silvered surfaces into several components. The two components arising from a twofold reflection in the first and in the second etalon are shown in Fig. 5. Their optical path difference is

$$aa'b'+c'd'-ab-cde-fg=4t\sin(\beta-\alpha/2)\sin\alpha/2.$$

For different directions $\beta$, in the plane of the paper, we get interference fringes at infinity with a $\sin^2$ distribution of intensity and with a zero fringe at $\beta=\alpha/2$. The presence of the $2n$-times reflected beams in both etalons, and their interference, changes this intensity distribution into

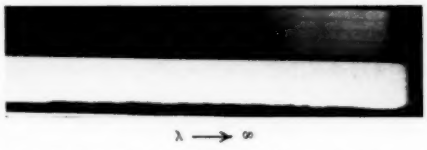


FIG. 3. Interference fringes in a continuous spectrum caused by the first-order reflection.

[1] W. E. Williams, *Applications of Interferometry* (Methuen, London), p. 104; see especially p. 88 and the references given on p. 104.

narrow bright fringes, the width of which depends on the reflecting power of the silvered surfaces. The distance of the fringes is inversely proportional to $t$ and proportional to $\lambda$.

Referring to Fig. 1 we see that for the beam $S_1$ the light first goes along $LL'$ through an etalon $BC$ and then, after changing direction, falls again on the first surface of a second etalon $CB$ at a slightly different angle. This angle is double the wedge angle of the quartz plate. The

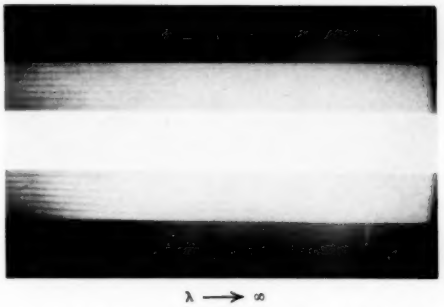


FIG. 4. Interference fringes caused by both first- and second-order reflections.

light transmitted through this second etalon (to the left, and not shown in Fig. 1) will contain the fringe system described above. It is the pattern produced by two etalons in tandem, which was rather thoroughly investigated by Perot and Fabry. The beam $S_1$ reflected from the second etalon is complementary to this system, and therefore will consist of sharp dark fringes on a bright background. It must be noted that in both cases there is a continuous background, that is, the dark fringes are not completely dark at their minima, because the light directly transmitted by the first etalon and reflected from the front surface of the second is much stronger than any light that enters the second. For the reflected beam $R_1$ we get the same dark fringe system, since only the order of events, transmission through one etalon and reflection from a second, is inverted.

The beams $S_2$ and $R_2$ show effects similar to those expected for three etalons of the same thickness, and inclined at angles 0, $\alpha$ and $2\alpha$. In $S_2$ the transmission through the first and reflection from the second gives an interference system

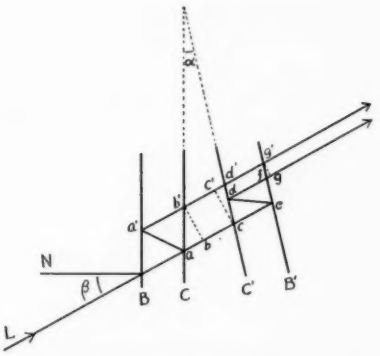


FIG. 5. Illustrating the origin of superposition fringes.

of the same type described for $S_1$, but besides this, transmission through the first and reflection from the third gives a second fringe system having half the fringe separation, since the inclination is $2\alpha$. For both systems the remaining etalon acts only as a mirror, giving rise to no interference.

A third system of fringes is to be expected, caused by successive reflection from two etalons, i.e., the second and third, the first acting only as a screen weakening the intensity. This is too weak to be observed, because the background in this case is many times stronger than that of the bright fringes to be expected. The high reflecting power of the silvered surface makes the noninterfering part of the light directly reflected from the front surfaces of both etalons very strong, and the weak fringes disappear on this bright background.

The two regions of diffuseness, and the decrease in intensity of the reflections $S_2$ and $R_2$, are caused by partial polarization of the light on internal reflection. Upon insertion of a Polaroid film in front of the etalon similar broad bands, completely dark near the center, appear in the same spectral regions for $S_1$ and $R_1$. The lowering of the intensity is undoubtedly connected with the rotation of the plane of polarization in crystalline quartz, the polarization arising from internal reflection.

In both of the photographs in Figs. 3 and 4 the background looks completely continuous. Actually it consists of the extremely fine and closely spaced parabolic fringes of high order always

given by the etalon in a continuous spectrum. They are not visible because of the relatively small dispersion and fairly large slit width. Therefore in the above considerations this structure has been disregarded.

The extreme sharpness of the superposition fringes described here appears at first sight to be rather promising for certain applications, such as in the determination of indices of refraction of liquids. The liquid could be introduced between the silvered surfaces of the etalon and the separation of the fringes with and without the liquid very exactly determined. It would only be necessary to count the number of fringes, and the fractional part of a fringe, from the zero fringe out to a certain point; by varying the inclination of the etalon. However, it appears that the method could not give more accurate results than the well-known standard procedures, because of the low order of the fringes, which compensates for their greater sharpness.

The author is greatly indebted to Professors F. A. Jenkins and H. E. White for helpful discussions of this subject and for their kindness in making available the facilities for this investigation.

# The Theory of Anomalous Diffraction Gratings and of Quasi-Stationary Waves on Metallic Surfaces (Sommerfeld's Waves)

U. FANO
*Carnegie Institution of Washington, Cold Spring Harbor, New York*

(Received January 8, 1941)

The theory of Wood's anomalous diffraction gratings, which was developed some years ago, has been reexamined in order to visualize its physical meaning. Each wave diffracted by a grating is identified through the component of its "wave vector" tangential to the grating. Surface waves similar to those found in total internal reflection are included (§2). The amplitudes of these waves can be calculated by successive approximations (§3). One feature of the anomalies is connected with the infinite dispersion of spectra at grazing emergence (§4). Emphasis is put on the existence of polarized quasi-stationary waves which represent an energy current rolling along the surface of a metal (§5). These waves can be strongly excited on the surface of metallic gratings under critical conditions depending also on the profile of the grooves; secondary interference phenomena arise then in the observed spectra (§6). The connection of the quasi-stationary surface waves with the wireless ground waves is discussed (§7). A general formulation is introduced to discuss the significance of the approximation used (Appendix).

## 1. THE EXPERIMENTAL FACTS

THIS paper is concerned with the intensity of the waves diffracted by a metallic diffraction grating, when the primary wave is plane and monochromatic and travels in a direction perpendicular to the grooves. The main elements which may influence the intensity are: (a) the wave-length of the light; (b) the angle of incidence; (c) the angle of emergence of the diffracted waves; (d) the geometry of the grating, i.e., the profile of its grooves, which may be suitably represented by a Fourier expansion:

$$\zeta(x)=\sum_{p=-\infty}^{\infty}\zeta_p \exp(2\pi i p x/\delta);$$

(e) the optical properties of the metal of the grating, as represented by the complex refractive index: $n=(\epsilon+2i\sigma/\nu)^{\frac{1}{2}}$ ($\epsilon$ and $\sigma$ are the dielectric constant and the conductivity respectively and both are functions of the frequency $\nu$) see Fig. 1; (f) the polarization.

The intensity of diffraction is expected *a priori* to be a slow varying function of these elements. If white light is used, instead of monochromatic light, the photometry of the spectrum will give a plot of the intensity as a function of the wave-length. Anomalies appear in the spectra of some individual gratings[1] as large and sharp irregularities of this function.

One may distinguish two anomalies:

(A) A *sharp* anomaly—that is, an "edge" of intensity—appears as a discontinuous change of intensity along the spectrum at sharply defined frequencies. These frequencies are governed by a relation discovered by Rayleigh, involving the elements (a), (b) and (c). The angle of incidence being given, the edge occurs at those wave-lengths which would be diffracted at grazing emergence in spectra of higher order[2] (Fig. 2).

(B) A *diffuse* anomaly extends for a wide interval from the "edge" towards the red and consists generally of a minimum and a maximum of intensity (one dark band and one bright band).

The characteristic properties of the anomalies are:

(1) Both anomalies are strongly affected by the geometry of the grating, the presence of sharp edges in the profile of the grooves apparently being a necessary condition for the exist-

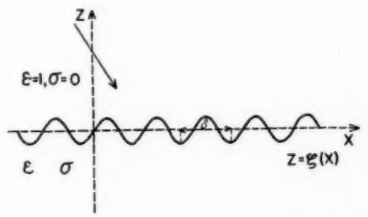


FIG. 1. Showing the parameters which characterize a metallic reflection grating.

[1] R. W. Wood, Phil. Mag. **4**, 393 (1902); **23**, 310 (1912); Phys. Rev. **48**, 928 (1935); J. Strong, Phys. Rev. **49**, 291 (1936).

[2] Lord Rayleigh, Phil. Mag. **14**, 60 (1907).

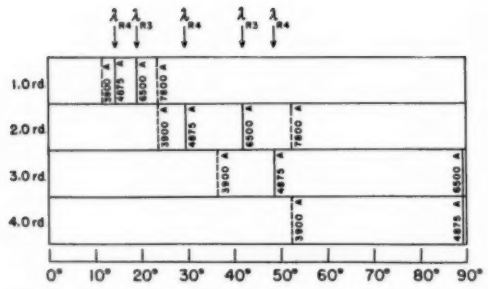


FIG. 2. Analysis of a spectrum in different orders. The wave-lengths $\lambda_{R3}$(6500A) and $\lambda_{R4}$(4875A) represent the limits of the spectra of third and fourth order respectively; they appear in every spectrum as Rayleigh's wave-lengths.

ence of the anomalies. Rubbing of the grating (which strips off small ridges between grooves) destroys the phenomenon completely, unless the grooves are very narrow, in which case the bottoms of the grooves act, presumably, themselves as ridges which cannot be stripped off.

(2) Anomaly B depends upon the optical constants: A change of $n$ shifts the position of the bands as compared to the edge.

(3) Both anomalies affect only light polarized with its magnetic vector parallel to the grating.

A qualitative explanation of the anomalies shows up in the development of a procedure for calculating the intensities of the diffracted waves.[3,4]

## 2. Construction of the Diffracted Waves

According to the usual method of treating electromagnetic phenomena at the boundary between two homogeneous media (vacuum and metal in our case) the electromagnetic field is represented by a set of plane waves of equal frequency, including the incident wave and all reflected, refracted and diffracted waves. The amplitudes of these waves must be determined in such a way that the set as a whole fulfills the boundary conditions on the surface of the grating (requiring continuity of the tangential components of the electric and magnetic fields).[5] (Mathematically the problem is thus reduced to the determination of the coefficients of the Fourier expansion of its unknown solution.)

The *whole* set of diffracted waves may be suitably determined representing diffraction as a momentum transfer by the grating to the impinging wave. (To apply momentum considerations to the propagation of waves is equivalent to treating the corresponding mathematical problem through Fourier expansion.) To each plane wave there corresponds a "wave vector" $\mathbf{k}=\mathbf{1}/\boldsymbol{\lambda}$ whose length is the wave number and whose direction is the direction of propagation. The "wave vector" may be considered as the "momentum" of the wave. Let $\mathbf{k}_o$ be the momentum of the incident wave and $k_{ot}$, $k_{on}$ be its components, tangential and normal to the grating. Since the frequency of light is unaffected by the grating, the modulus $|\mathbf{k}|$ of the momentum of any wave must be equal to $|\mathbf{k}_o|=k_o$ in vacuum, and to $nk_o$ within the metal. Momentum transfer by the grating can thus change only the direction of momentum: Any change of the normal component is possible, but changes of the tangential component must be integral multiples of $1/\delta$ (inverse of the spacing of the grating). (In the case of three-dimensional gratings, e.g. crystals, even the change of the normal component is subject to a condition.) To each integral number $p$ there corresponds one diffracted wave in vacuum and one within the metal, with a tangential momentum component: $k_{pt}=k_{ot}+p/\delta$. The normal components are then determined from the tangential component and the known value of the modulus (their sign is determined by boundary conditions at infinite distance). This gives in vacuum the well-known construction of $k_{pn}=(k_o^2-k_{pt}^2)^{\frac{1}{2}}$ shown in Fig. 3, which, however, applies only if $p$ is so small that $k_{pt}\leq k_o$. If on the contrary $k_{pt}>k_o$, $k_{pn}$ is imaginary; this corresponds to *superficial waves* traveling with momentum $k_{pt}$ along the surface of the grating and exponentially damped in the normal direction. Similar waves take place in the less refracting medium in the case of total internal reflection. They represent an energy current flowing from the surface a short distance into the vacuum and then being forced back to the surface after a tangential displacement.

[3] U. Fano, Ann. d. Physik **32**, 393 (1938).

[4] This phenomenon is closely analogous to the so-called "Dellen" in the diffraction of molecular rays (discovered by Stern and Frisch), whose explanation in connection with superficial adsorption phenomena was first given by Lennard-Jones and Devonshire (Nature **137**, 969 (1936), Proc. Roy. Soc. **A158**, 253 (1937)) and then further developed (reference 3).

[5] Lord Rayleigh, Proc. Roy. Soc. **A79**, 399 (1907).

This picture may be clarified by an investigation of the lines of current of Poynting's vector.[6]

In representing the optical properties of metals ($n^2=\epsilon+2i\sigma/\nu$), the large conductivity shows up as a large negative value of the dielectric constant rather than as the "conductivity" $\sigma$ itself. The oscillating electric field acting on free metallic electrons gives rise to a current 90° out of phase, representing a negative dielectric polarization. The resistance of the metal results in the generation of heat through a small component of the current *in* phase, proportional to the "conductivity" $\sigma$. Therefore we shall consider the negative coefficient $\epsilon$ as the important characteristic and $\sigma$ as a correction representing energy losses. This approximation is justified by the quantitative results. A negative value of $\epsilon$ means a material less dense optically than a vacuum. Then every wave striking such a medium will experience total reflection, very much as in the case of total internal reflection in transparent media. $\sigma$ gives rise to a partial absorption of that radiation, which penetrates the metal during the reflection process. Mathematically: the component $k_{pn}=(n^2k_o^2-k_{pt}^2)^{\frac{1}{2}}$ of the momentum of waves within the metal is always complex; it is purely imaginary if $\sigma$ is neglected. In our phenomenon then, a superficial wave is produced within the metal for every value of $p$.

### 3. The Method of Successive Approximations

The amplitudes of the plane waves with tangential momentum component $k_{pt}$ in vacuum and in metal will be respectively indicated by $A_{p+}$, $A_{p-}$. $A_{o+}$ is, for instance, the amplitude of the regularly reflected wave (central image). The boundary conditions involve all the quantities $A_{p+}$, $A_{p-}$ together, and determine *all* of them as solutions of a *single* system of equations. Hence it is difficult to investigate the behavior of the amplitudes of the different waves because of their close interdependence. Rayleigh[5] devised an analysis of this interdependence, which enables us to calculate the amplitudes by successive approximations. A generalized mathematical formulation which is given in the Appendix indicates how to consider the case when the approximation is not accurate.

Rayleigh considered diffraction as a perturbation of the elementary case of a plane metallic mirror, which means mathematically expanding the boundary conditions in powers of the depth of the grooves. Wood's anomalies are often found in gratings showing strong central images, in which case this approximation is accurate.

In the *first approximation* the boundary conditions can be split into a set of systems of two equations, each of them determining the amplitudes $A_{p+}^{(1)}$, $A_{p-}^{(1)}$ of the $p$th pair of waves. This means that each pair of waves is assumed to be excited independently of the other ones. The $p$th component $\zeta_p \exp(2\pi ipx/\delta)$ of the Fourier expansion of the profile of the grooves contributes the momentum transfer $p/\delta$ and is responsible for the excitation of the $p$th pair of waves. Thus $A_{p+}^{(1)}$ and $A_{p-}^{(1)}$ are proportional to $\zeta_p$[7] (it is recalled that only the first-order spectrum is intense if the grooves are purely sinusoidal).

In the *second approximation* one must consider a perturbation coupling the amplitudes of the various diffracted waves. The additional amplitudes $A_{p+}^{(2)}$ or $A_{p-}^{(2)}$ are linear functions of the first approximation amplitudes of all other waves. Contributions arising from this "second-order diffraction" are thus superposed to the waves determined according to the first approximation. This superposition may conceivably give rise to *anomalous interference effects*.[8]

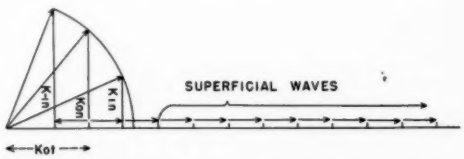


FIG. 3. Construction of the normal momentum component of the diffracted waves. The construction cannot be applied to the waves of third or higher order, thus showing that these waves have imaginary normal momentum components, i.e. that they are superficial waves.

[6] Reference 2, Appendix 1. See also a paper by T. Westerdijk, Ann. d. Physik **36**, 696 (1939).

[7] The zero-order approximation ($\zeta(x)=0$) determines $A_{p+}^{(0)}$ and $A_{o-}^{(0)}$ according to Fresnel's formulae.

[8] The balance of intensity is determined by interference affecting *only* the central image which, within this approximation, acts as an infinitely powerful bank on which the various diffracted waves draw independently of one another. Here, as in the case of the "Dellen" (reference 4), to consider that anomalous dark bands are due to a "lack"

## 4. A General Property Concerning Anomaly A

When the angle of emergence of a diffracted wave approaches 90°, it becomes, in the limit, an infinitely fast varying function of the frequency, i.e., one has *infinite dispersion of spectra at grazing emergence.* Hence the intensity may vary quite rapidly with frequency on account of its dependence on the emergence angle. Actual calculation shows that the derivative of $A_{p+}^{(1)}$ with respect to the frequency tends to infinity at grazing emergence on account of its dependence on the angle of emergence. This does not mean that our method of approximation breaks down; we find only that $A_{p+}^{(1)}$ as a function of frequency meets a discontinuity (a "step" in the graphical plot) at grazing emergence. This is the limit at which the $p$th wave goes over from a diffracted outgoing wave to a superficial wave on the metal. We do not even know, whether the discontinuity is quantitatively important (whether the "step" is high) or not; we only know that a *sharp* intensity change must be present as a consequence of the infinite dispersion at grazing emergence.

This fact has a wider influence in the second approximation, whenever incidence angle and frequency fulfill Rayleigh's condition (i.e., when the spectrum of a certain order $q$ is diffracted at grazing emergence). Since the quantities $A_{p+}^{(2)}$, for any value of $p$, are linear functions of the first approximation amplitudes of all the diffracted waves, the discontinuity of $A_{q+}^{(1)}$ will be carried over to the amplitudes of all other waves. *This just represents the anomaly A;* the only difficulty is that we have yet no reason to believe that a discontinuity in only one of the terms contributing to the second approximation is quantitatively important enough to affect the whole result appreciably.

We may now understand the meaning of the geometrical condition (1) indicated in §1. The $q$ value corresponding to grazing emergence is not likely to be a very small number (it may be of the order of 5). Therefore *the presence of sharp edges* in the profile of the grating, mathematically expressed by large values of the higher harmonics $\zeta_q$, will enhance $A_{q+}^{(1)}$ itself and its contribution to $A_{p+}^{(2)}$ and to the total $A_{p+}=A_{p+}^{(1)}+A_{p+}^{(2)}$.

## 5. The Superficial Waves

According to the physical picture of Rayleigh's first approximation, the light which has received a large tangential momentum $p/\delta$ from the grating, so that $k_{pt}>k_0=\nu/c$, is diffracted into a *pair of superficial waves.* This light cannot leave the neighborhood of the surface, since it is bent again and again towards it, both in vacuum and in metal. A double superficial wave is then excited under the action of the grating and no part of its energy is dispersed outside the surface region (unless a repeated action of the grating takes place). Energy is dissipated only by a slow transformation into heat by the electric resistance of the metal. One may then wonder whether this phenomenon of energy transport along lines of current undulating up and down, above and below the surface, might not represent a form of quasi-stationary state taking place almost independently of the excitation. Under the excitation of the impinging waves the oscillation would then be exceedingly intense.

One may consider as a geometrical optical model of undulating energy transport a wave traveling between two parallel mirrors with repeated reflections at their surfaces. For instance, a light wave may travel within a glass plate between a vacuum and a metal as between two mirrors (if its angle of incidence on the surface glass-vacuum exceeds the critical angle so that total reflection takes place). See Fig. 4. In the usual picture of total or metallic reflection, the penetration (or "tail") of the waves beyond the reflecting surface appears as a slight correction to the geometrical approximation. In our case the thickness of the intermediate glass plate vanishes, so that only the "tails" beyond the reflecting surfaces of both metal and vacuum are left, without any trace of the geometrical model.

Considering further the case of a glass plate, a wave progressing along the plate must be a standing wave in transverse direction. Therefore the thickness of the plate must contain exactly an integral number of half-wave-lengths *plus an additional fraction* of wave-length to allow for

of radiation arising from strong absorption by other processes is equivalent to assuming that the approximation method diverges.

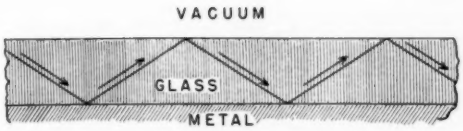


FIG. 4. Schematic path of a light wave progressing within a glass plate between a metal and a vacuum.

the condition that the phase has a particular value at each reflecting surface. This value is determined by frequency, incidence and *polarization*. Thus physical optics establishes an equation connecting the thickness of the plate with the transverse wave-length, that is, determining the permissible ("proper") values for the transversal and tangential momentum components, or else for the incidence angle, for any given thickness. The number of proper values decreases with the thickness. See Fig. 5.

Our question is: "Is there left any proper value when the thickness vanishes?" To allow for vanishing thickness, not only the number of transversal wave-lengths but also the "additional fraction" must vanish, that is, the sum of the "phases" at the surfaces must be a multiple of 180°. (This condition is, of course, independent of the properties of the glass plate considered.) The answer given by actual calculation[9] is: *One and only one proper value exists and this only if the wave is polarized with its magnetic vector parallel to the surface.* The possibility of a solution is essentially due to the negative sign of $\epsilon$, that is, to the possibility of concentrating such strong charges on a metallic surface as to invert the direction of the normal component of the electric field. The dependence on the polarization is then obvious, since no analogous magnetic property exists. The proper value $\chi$ of the tangential momentum component is always *slightly larger than the modulus* $k_o=1/\lambda$ *of the momentum in vacuum.*

We now consider the effects of absorption by heat production. This absorption results in a longitudinal damping of the waves which cannot be considered any longer to be truly stationary (the term "quasi-stationary" may be used). The proper value of the tangential momentum component is no longer real and will be indicated by $\chi+i\gamma$ where $\gamma$ represents the damping. The damping is always small for metals with large negative values of $\epsilon$; although heat production is proportional to the "conductivity" $\sigma$, increasing $\sigma$ at constant $\epsilon$ has the effect of expelling the wave from the metal and of increasing the fraction of the time spent by the radiation outside the metal.

## 6. Explanation of the Anomalies

The pairs of waves with tangential momentum components $k_{pt}=k_{ot}+p/\delta$, which are excited by the impinging wave on the surface of a grating, behave as forced oscillations. The conclusion of §5 is that, although pairs of superficial waves do not dissipate any energy outwards from the grating, they cannot oscillate intensively as quasi-stationary waves unless the corresponding $k_{pt}$ approaches the proper value $\chi$. If, on the other hand, one $k_{pt}$ approaches $\chi$, a phenomenon takes place which is analogous to the *resonance* of a mechanical oscillating system excited with its proper frequency. The smaller $|\chi-k_{pt}|$, the larger become the amplitudes $A_{p+}^{(1)}$ and $A_{p-}^{(1)}$; their value remains finite at resonance only because of the absorption in the metal, just as friction opposes breakdown in the case of resonance of mechanical systems. The width of the interval around $\chi$, in which the effect of the resonance is felt, is proportional to the damping $\gamma$. It is a well-known result of the theory of resonance of induced oscillations, that the amplitude of oscillation (that is, $A_{p+}^{(1)}$ and $A_{p-}^{(1)}$) is inversely proportional to a factor of the form $k_{pt}-\chi-i\gamma$. Increasing the conductivity of the metal makes the resonance phenomenon sharper and sharper because the damping $\gamma$ vanishes; at the same time $\chi$ approaches $k_o$. Rayleigh studied only the limiting case of a perfectly reflecting metal, in which the superficial wave is completely expelled from the metal and becomes a regular plane wave in vacuum grazing the surface of the metal.

The amplitude of the superficial waves can rise to anomalously large values *only if* the same *conditions* which govern Wood's anomalies *are*

[9] The equation determining the proper value of the momentum is:

$$n^2\xi_{n+}+\xi_{n-}=n^2(k_o^2-\xi_t^2)^{\frac{1}{2}}+(n^2k_o^2-\xi_t^2)^{\frac{1}{2}}=0,$$

if the magnetic vector is parallel to the surface, and:

$$\xi_{n+}+\xi_{n-}=(k_o^2-\xi_t^2)^{\frac{1}{2}}+(n^2k_o^2-\xi_t^2)^{\frac{1}{2}}=0,$$

if the electric vector is parallel to the surface.

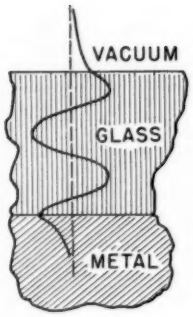


FIG. 5. Amplitude of vibration of a standing wave in the various layers of a set of three media: vacuum, glass, metal.

*fulfilled*. First, the high order Fourier coefficients $\zeta_p$ must be large (in agreement with *property 1* of §1; see also §4). Secondly, the light must be *polarized* with its magnetic vector parallel to the grating (*property 3*, see §5). Finally one of the quantities $k_{pt}=k_{ot}+p/\delta$ must be approximately equal to $\chi$ which is in turn only slightly larger than $k_o$; this means that *Rayleigh's condition* requiring that one wave be diffracted at grazing emergence ($k_{pt}=k_o$) must also be approximately fulfilled.

Both quantities $k_o=1/\lambda$ and $k_{pt}=k_{ot}+p/\delta$ decrease with increasing wave-length, but their ratio $k_{pt}/k_o$ increases. If at a certain wave-length $k_{pt}$ is only slightly smaller than $k_o$, the $p$th pair of diffracted waves can be anomalously intense because of being sufficiently similar to a quasi-stationary wave ($k_{pt}\approx k_o\approx\chi$). Increasing the wave-length so as to make $k_{pt}$ exactly equal to $k_o$ causes the amplitude of the $p$th diffracted wave to undergo a discontinuity which, on account of the intensity of the wave, can so affect all other waves through second-order diffraction as to give rise to *anomaly A* (as shown in §4).

At a certain larger wave-length, *shifted towards the red* as compared to that of anomaly A, $k_{pt}$ becomes equal to $\chi$. Then, owing to the form of the denominator $k_{pt}-\chi-i\gamma$, the amplitude of the $p$th (superficial) wave reaches its maximum value and undergoes a *rapid phase change* of nearly 180°, as the sign of $k_{pt}-\chi$ is changed. Hence the perturbation of the observed spectra which is due to the superficial anomalous wave (Rayleigh's second approximation, see §3) reaches its maximum and changes suddenly its phase. Thus the superposition of first- and second-order diffraction may give rise to the characteristic succession of dark and bright bands within a short wave-length interval (*anomaly B*). A change in the optical constants of the grating affects the values of $\chi$ and $\gamma$ and, therefore, affects the distance of anomalies A and B in the spectrum as well as the total width of the phenomenon. This may be obtained by changing the spectral region through a shift of the incidence angle or by use of another metallic coat on the grating (*property 2*). If at least one of the quantities $k_{pt}$ is nearly equal to $\chi$ for every wave-length (this occurs if $\lambda$ is small and $\delta$ large), the anomalies form an almost continuous succession along the spectrum.[10]

Thus it has been shown how the anomalies *may* originate. The phases and the amplitudes of the interfering waves which are diffracted according to the first and second approximation are, however, somewhat complicated algebraic functions of the parameters $\epsilon$, $\sigma$, and of all $\zeta_p$. Since these last coefficients are never known for a particular grating, we are not able to determine the size and shape of the anomalous bands in any particular case. The only necessary condition safely established both theoretically and experimentally is that an irregular shape of the grooves is required in order to give large values to the high order Fourier coefficients $\zeta_h$.

## 7. Connection with Sommerfeld's Superficial Waves and with Brewster's Polarization Phenomenon

The first explanation by Rayleigh[11] of Wood's anomalies was given in terms of Huygens' construction: One considers, that each groove $A$ of the grating is a center of diffusion of the incident light and hence is the origin of a scattered spherical wave. Rayleigh's condition (existence of a diffracted wave at grazing emergence) requires that the part of the scattered wave traveling along the grating with phase velocity $c$ reaches the neighboring groove $B$ in phase with the incident wave and with the waves scattered by the grooves $A'$, $A''$ . . . (see Fig. 6). Second-

[10] The apparent spectral width of the bands might not be due entirely to absorption of superficial waves within the metal. Second-order diffraction, i.e., the interaction with other diffracted waves, is also effective as an absorption (see Appendix).

[11] Lord Rayleigh, Phil. Mag. **14**, 60 (1907).

order diffraction of the scattered waves by the groove $B$ is superposed on the first-order diffraction of the incident wave, giving rise to an interference effect. This phenomenon may be expected to be very intense since all grooves $A$, $A'$, $A''$ . . . , that is, practically the whole grating, contribute to it. It was pointed out later,[12] that the optical properties of the metal may influence the phase velocity of that part of the scattered wave which travels along the grating. This introduces a perturbation into the elementary law determining the existence of a diffracted wave at grazing emergence.

The problem of propagation of light traveling along a grating is analogous to the problem of the radiation by an antenna near the surface of a conducting body. This problem has been discussed mainly by Sommerfeld. The spherical wave diffracted by a groove is analogous to that irradiated by a hypothetical resonating oscillator lying in the vacuum just above the groove. This wave is equivalent to a superposition of plane waves with total momentum $k_0=1/\lambda$, each plane wave being characterized by its tangential momentum component $k_t$ and by its direction within the plane of the grating. All waves having $k_t \leq k_0$ will experience regular metallic reflection, and their superposition far away from the surface will give rise to a wave that is approximately spherical. Superficial waves will arise having $k_t > k_0$; we might expect them to destroy each other by interference, since they are progressing along the surface with a continuous spectrum of phase velocities $ck_0/k_t$. Actually they are not destroyed, however, since the waves with magnetic field polarization parallel to the surface and with $k_t \approx \chi$ give rise to the resonance phenomenon of the quasi-stationary waves and are enhanced far above the background of all other waves. Their amplitudes are inversely proportional to $k_t - \chi - i\gamma$ and hence their superposition gives rise to a single damped wave with momentum component $\chi$, whose amplitude decreases exponentially along the grating with a range of $\chi/\gamma$ wave-lengths.

The agreement between Rayleigh's explanation and the experimental results is very much improved by taking into account the fact that waves scattered along the surface of the grating act as a single damped wave of momentum $\chi$.[13] The change of momentum from $k_0$ to $\chi$ corresponding to a reduction of the phase velocity, shifts the anomalies towards the red. Damping broadens the resonance and avoids the collective action of the grooves of the whole grating, since only grooves within a distance of $\chi/\gamma$ wave-lengths cooperate in producing the interference of the scattered waves.

The superficial damped waves deduced here through the picture of superficial quasi-stationary waves had already been obtained mathematically by Sommerfeld in the discussion of radio waves progressing on the surface of the earth; his result applies to every frequency and every conducting surface. Our picture represents Sommerfeld's waves as a *group of undamped waves*, whose interference appears as a damping.

However this representation is not as straightforward in the case of radio waves on sea water as it is in our case, because of the difference in electrical properties. A conductor like sea water does not reflect radio waves as a metal does light; its dielectric constant is not negative and therefore there is no total reflection by the conducting surface and no pair of quasi-stationary superficial waves in the two media, whose energy travels undulating along the surface. It is not yet clear what picture is suitable for the case of radio waves; it has been pointed out that Sommerfeld's representation of the field of a radio antenna might not be suitable.[14] The physical interpretation of Sommerfeld's method is particularly satisfactory in the case of optical frequencies and metallic conductors.

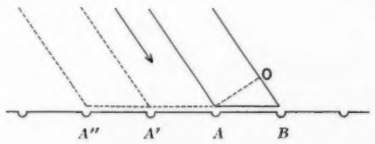


FIG. 6. Geometrical representation of Rayleigh's condition: $AB-OB=p\lambda$.

Analogy with Sommerfeld's waves gives, finally, a connection with Brewster's polarization

[12] See discussion by R. W. Wood, Phys. Rev. **48**, 928 (1935).

[13] U. Fano, Phys. Rev. **50**, 573 (1936).

[14] H. Weyl, Ann. d. Physik **60**, 481 (1919).

phenomenon: Light polarized in the same way as that of Wood's anomalies impinging with characteristic angle of incidence on the surface of a dielectric is not partially reflected but is fully transmitted. Sommerfeld's superficial waves go over into a pair of incident plus refracted Brewster's waves if the conductivity of the conducting body tends toward zero. The physical meaning is this: Brewster's waves, Sommerfeld's waves and the quasi-stationary waves discussed in §5 represent for media of different electric properties the same singular case defined by the same mathematical equation: They are pairs of plane waves, one on each side of the boundary between two media, which are able ("almost able" in the case of *quasi*-stationary waves) to fulfill the boundary conditions by themselves. The lack of symmetry between electric and magnetic properties of matter makes it impossible to give a solution to this problem, if the waves are polarized with their magnetic vector within the plane of incidence.

## Appendix

There are two boundary conditions on the surface of the grating which determine the amplitudes $A_{p+}$, $A_{p-}$ of the diffracted waves, when the polarization is given. These conditions are expressed by linear equations whose coefficients depend on the characteristics of the experimental set-up listed in §1 and are functions of the coordinate $x$ (see Fig. 1). Hence their form is:

$$\sum_{p,s} \alpha_{ps}^{(1)}(x) A_{ps} = \beta^{(1)}(x) I, \quad \sum_{p,s} \alpha_{ps}^{(2)}(x) A_{ps} = \beta^{(2)}(x) I, \ ^{15}$$

where $s$ has the two values $+$ and $-$, and $I$ is the amplitude of the impinging wave. The functions $\alpha$ and $\beta$ are periodic and can be expanded into a Fourier series, as, for instance:

$$\alpha_{p+}^{(1)}(x) = \sum_{p'} a_{p'1,\,p+} \exp\,(2\pi i p' x/\delta)$$

($\delta$ is the distance between the grooves of the grating). The boundary conditions are then transformed into an infinite system of linear equations involving the coefficients of the Fourier series:

$$\sum_{p,s} a_{p'1,\,ps} A_{ps} = b_{p'1} I; \quad \sum_{p,s} a_{p'2,\,ps} A_{ps} = b_{p'2} I. \ ^{16}$$

This system can be condensed in the form:

$$\sum_{n} c_{n'n} x_n = y_{n'},$$

where $n$ and $n'$ represent the pairs of indices $ps$, $p's'$ ($s'=1, 2$; $c_{n'n} = a_{p's',\,ps}$; $x_n = A_{ps}$; $y_{n'} = b_{p's'} I$). The quantities $c_{n'n}$ represent the characteristics of the system of diffracted waves, whereas the $y_{n'}$ represent various components of the action of the impinging light.

In any practical case the solution of this system of equations exists and has the form:

$$x_n = \sum_{n'} C_{n'n} y_{n'},$$

where the resolvent matrix $C_{n'n}$ is somewhat analogous to the Green's function in the theory of linear differential equations.[17] $C_{n'n}$, according to its definition, is the value of $x_n$ when all the quantities $y$ vanish except $y_{n'}$ which is equal to one. The quantities $y$ represent the excitation which is furnished by the light impinging on the grating and induces the diffracted waves. Each $y_{n'}(n'=p', s')$ may be considered as a "component of the excitation" having the tangential momentum $k_{p't} = k_{ot} + p'/\delta$; ($k_{ot}$ is contributed by the impinging wave, $p'/\delta$ by the grating). When Rayleigh's first approximation holds, i.e., when the equations depend linearly on the depth of the grooves, each pair of "components" $y_{p'1}$, $y_{p'2}$, represents the whole action of a hypothetical purely sinusoidal grating with spacing $\delta/p'$ (see §3 and note (18)). Although no such physical interpretation of the "components of the excitation" can be given independently of Rayleigh's approximation, it is an important result that the amplitude of any diffracted wave can *always* be represented by formula (1) as the superposition of different contributions. A rapid change of phase of one contribution may thus always be the origin of the rapid succession of dark and bright bands in Wood's anomalies (as explained in §6).

There are two "components of the excitation" with the same tangential momentum $k_{qt}$ (i.e., $y_{q1}$ and $y_{q2}$). Their contributions to the amplitudes of the single diffracted waves are determined by those elements of the matrix $C_{n'n}$ which lie on the pair of rows identified by the index $p'=q$ and by both values $s'=1, 2$. The four elements of

---

[15] See reference 14, p. 404. When the magnetic vector is parallel to the grating, it is:

$$\alpha_{p+}^{(1)}(x) = \exp\,[2\pi i(px/\delta + k_{pn+}\zeta(x))];$$
$$\alpha_{p+}^{(2)}(x) = n^2(k_{pn+} - k_{pt} d\zeta/dx)\alpha_{p+}^{(1)}(x);$$
$$\alpha_{p-}^{(1)}(x) = -\exp\,[2\pi i(px/\delta - k_{pn-}\zeta(x))];$$
$$\alpha_{p-}^{(2)}(x) = -(k_{pn-} + k_{pt} d\zeta/dx)\alpha_{p-}^{(1)}(x);$$
$$\beta^{(1)}(x) = -\exp\,(-2\pi i k_{on+}\zeta(x));$$
$$\beta^{(2)}(x) = -n^2(k_{on+} + k_{ot} d\zeta/dx)\beta^{(1)}(x).$$
$$k_{pn+} = (k_o^2 - k_{pt}^2)^{\frac{1}{2}}; \qquad 0 \leqslant \mathrm{Arg}\ (k_{pn+}) < \pi;$$
$$k_{pn-} = (n^2 k_o^2 - k_{pt}^2)^{\frac{1}{2}}; \qquad 0 \leqslant \mathrm{Arg}\ (k_{pn-}) < \pi.$$

[16]
$$\exp\,(2\pi i k_{pn+}\zeta(x)) = \sum_q \overset{(p)}{g}_q \exp\,(2\pi i q x/\delta)$$
$$\exp\,(-2\pi i k_{pn-}\zeta(x)) = \sum_q \overset{(p)}{h}_q \exp\,(2\pi i q x/\delta)$$
$$a_{p'1,\,p+} = \overset{(p)}{g}_{p'-p}; \quad a_{p'1,\,p-} = \overset{(p)}{h}_{p'-p}$$
$$a_{p'2,\,p+} = n^2\left[k_{pn+} - \frac{k_{pt}}{k_{pn+}}\frac{p'-p}{\delta}\right]\overset{(p)}{g}_{p'-p}$$
$$a_{p'2,\,p-} = \left[k_{pn-} - \frac{k_{pt}}{k_{pn-}}\frac{p'-p}{\delta}\right]\overset{(p)}{h}_{p'-p}$$
$$b_{p'1} = -\overset{(0)}{g}_{-p'}{}^*; \quad b_{p'2} = n^2\left[k_{on+} - \frac{k_{ot}}{k_{on+}}\frac{p'}{\delta}\right]\overset{(0)}{g}_{-p'}{}^*.$$

[17] $C_{n'n}$ is determined by an algebraic formula in the case of a finite system of linear equations.

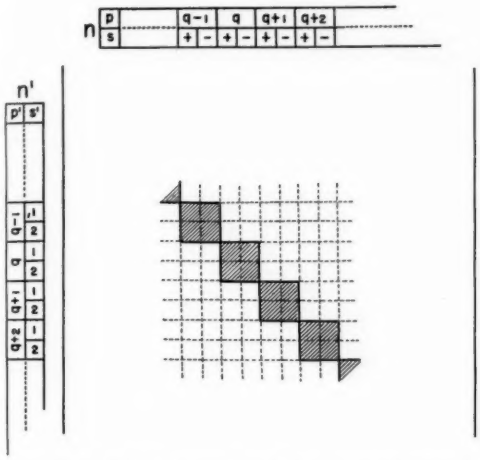


FIG. 7. Rayleigh's approximation is accurate when the important elements of both matrices $c_{n'n}$ and $C_{n'n}$ are concentrated within the set of "diagonal squares."

these rows which belong to the columns $p=p'=q$, $s=\pm$, i.e., which lie within one $2\times2$ square along the main diagonal line of the matrix $C_{n'n}$ (see Fig. 7), determine the contribution to the pair of diffracted waves having the same tangential momentum $k_{qt}$.

Rayleigh's approximation method assumes that the action of the grating inducing tangential momentum transfers is small. Then all the coefficients of the Fourier expansions interconnecting plane waves with different tangential momentum are small; among them are all those elements of the matrix of coefficients $c_{n'n}$ [18] for which

$$\exp(2\pi i k_{pn+}\zeta(x)) = 1+2\pi i k_{pn+}\zeta(x)-\cdots$$
$$g_q^{(p)} = \delta_q+2\pi i k_{pn+}\zeta_q-\cdots;\quad h_q^{(p)} = \delta_q-2\pi i k_{pn-}\zeta_q-\cdots;$$
$$\delta_q=1 \text{ when } q=0;\quad \delta_q=0 \text{ when } q\neq0.$$

$p\neq p'$, i.e., which lie outside the set of $2\times2$ diagonal squares (Fig. 7). Hence in the first approximation, neglecting those coefficients which are small, the infinite system of equations can be split into a set of systems of two equations, each of them involving one pair of unknowns $A_{p+}$, $A_{p-}$. It is then possible to calculate the resolvent matrix $C_{n'n}$. Its elements vanish unless they belong to the diagonal squares, meaning that each "component of the excitation" induces only the pair of waves with the same tangential momentum. The four elements within each of these squares are inversely proportional to the corresponding $2\times2$ determinant of coefficients $c_{ps',ps}(s'=1,2;\ s=\pm)$. This determinant is essentially equivalent to the expression $k_{pt}-\chi-i\gamma$ to which the anomalous amplitudes are inversely proportional (§6) and hence it has a minimum at $k_{pt}=\chi$. If $k_{pt}$ were to assume the complex value $\chi+i\gamma$ the determinant would vanish and then the *homogeneous system* $\Sigma_s c_{ps',ps}x_{ps}=0$ $(s'=1,2)$ would have a finite solution representing a self-sufficient wave without any excitation.

[18] Rayleigh's method involves expansion of exponentials in powers of the depth of the grooves $\zeta(x)$, or better, of its ratio to the transversal wave-length.

This is a damped superficial wave of Sommerfeld's type;[19] the damping is due to heat production in the metal and is represented by the imaginary part of $k_{pt}$. Thus, according to the results of §6, whenever $k_{pt}$ approaches $\chi$, the elements of $C_{n'n}$ within a diagonal square become anomalously large, meaning that a pair of superficial waves is excited with anomalous intensity.

*If Rayleigh's approximation is not accurate*, the mathematical problem is complicated because the infinite system cannot be split and hence one cannot calculate the quantities $C_{n'n}$ within a diagonal square by means of the coefficients $c_{n'n}$ within the corresponding square. The physical aspect of it is, however, still understandable: A superficial wave of Sommerfeld's type can still exist, but it undergoes an additional damping because it must supply a whole set of diffracted waves originating from it. Accordingly, the infinite homogeneous system $\Sigma_n c_{n'n}x_n=0$ must still have a solution, even when it cannot be split into parts, but for this the tangential momentum must assume a complex value with a sufficiently large imaginary part.[20, 21] Therefore one may still expect that a superficial wave is strongly excited, i.e., that the elements of the matrix $C_{n'n}$ belonging to a diagonal square become anomalously large, when the tangential momentum of one "component of the excitation" approaches the characteristic momentum of Sommerfeld's wave; this anomaly becomes, however, less intense as Rayleigh's approximation becomes less accurate. An intense superficial wave must, on the other hand, give rise by diffraction to other intense waves; hence an anomaly must also affect the elements of the resolvent matrix $C_{n'n}$ lying on the same rows including the one anomalous diagonal square but outside it. This anomaly *does not depend critically* on the accuracy of Rayleigh's approximation because it is subject to opposite influences. On one hand, the importance of all the elements lying outside the diagonal squares is increased as the approximation becomes less accurate. When, on the other hand, damping of superficial waves by diffraction becomes more important than damping by heat production, the whole anomalous phenomenon is damped so that even its effect on the amplitude of the observed spectra must be finally reduced.[22]

[19] See, e.g., the article by A. Sommerfeld in Ph. Frank-R. von Mises, *Die Differentialgleichungen der Mathematischen Physik* (Vieweg, Braunschweig, 1935), second edition, Vol. II, p. 876.

[20] One can see that the additional damping to be added to $\gamma$ is approximately proportional to the square of the depth of the grooves.

[21] The influence of the grating on the energy traveling within a superficial wave is not too close, however, because the wave stretches up to an appreciable distance from the grating into vacuum.

[22] When it is possible to bring the matrix $C_{n'n}$ into a diagonal form, represented by a set of values $\gamma_m$, that is, to solve the homogeneous system:

$$\sum_n c_{n'n}x_n^{(m)} = \gamma_m x_{n'}^{(m)}, \qquad \left(\sum_n |x_n^{(m)}|^2 = 1\right),$$

the matrix $C_{n'n}$ is given by the formula:

$$C_{n'n} = \sum_m x_{n'}^{(m)} x_n^{(m)}/\gamma_m.$$

Wood's anomalies are represented by anomalously small values of one of the quantities $\gamma_m$. Within Rayleigh's first approximation the $\gamma_m$ are factors of the $2\times2$ determinants

On account of general properties of the Fourier expansion the elements of both matrices $c_{n'n}$ and $C_{n'n}$ converge rapidly towards zero as the difference $|p'-p|$ of their Fourier indices, that is, their distance from the diagonal line, increases. Also the coefficients $y_{n'}$ decrease with increasing $p'$. This is probably why Wood's anomalies are not frequent (§4).

In conclusion, the possibility of analyzing different contributions to the amplitude of diffracted waves is independent of Rayleigh's approximation method. This method shows how and why the anomaly affecting the resolvent matrix $C_{n'n}$ arises from the behavior of the coefficients $c_{n'n}$ lying within one diagonal square. The anomaly is felt inasmuch as the coefficients belonging to the diagonal squares have a leading influence in determining the solution of the infinite system of equations, but for this the coefficients lying outside the same squares must not necessarily be negligible. The physical explanation of Wood's anomalies rests on the similarity between a pair of diffracted waves and a wave of Sommerfeld's type on a metallic surface. This requires that Rayleigh's approximation be accurate at least to such an extent that the existence of plane waves on the surface of the grating (with $k_{pt}$ only slightly larger than $k_0$) is not completely effaced by the perturbation arising from the grating itself.

*Note added in proof.*—Throughout this paper, as well as in the previous treatments of Rayleigh's theory of diffraction gratings, it has not been duly pointed out that Rayleigh's approximation becomes inaccurate for superficial waves with very large tangential momentum. In fact, the grooves cannot be considered merely as a perturbation to these waves which are very strongly damped in transversal direction:[18] Analysis of the radiation field into a set of plane diffracted waves (§2) is appropriate to the study of the phenomena far away from the grating but not to the description of the field within the grooves; this description requires the superposition of a large number of superficial waves with large tangential momentum. Mathematically, the matrix elements $c_{n'n}$ become very large when $p$ is large.

All this, however, should not upset the essential results obtained in this paper. Although the treatment which has been given is not strictly correct, it probably represents the phenomena fairly enough. This treatment considers mainly relations among the waves diffracted outwards from the grating and the anomalous superficial wave which also stretches appreciably outwards on account of its small transversal damping ($\chi$ is only slightly larger than $k_0$). The objection introduced here, namely that waves with large tangential momentum are essentially involved by the phenomena within the grooves, does not directly interfere with the relations among the waves stretching outwards from the grating. Mathematically, Wood's anomalies have been traced back to relations among the matrix elements $c_{n'n}$ with rather small values of the indices $p$ and $p'$. The existence of very large elements of the same matrix with large values of these indices might conceivably reduce the quantitative import of the relations mentioned above but not their qualitative effects.

of diagonal squares of $c_{n'n}$. It is easy to discuss the order of magnitude of the quantities $x_n^{(m)}$ at different stages of Rayleigh's approximation.

# Interreflections in Finite Cylinders

PARRY MOON
*Electrical Engineering Department, Massachusetts Institute of Technology, Cambridge, Massachusetts*
(Received December 10, 1940)

## 1. INTRODUCTION

THE interreflections of light within a circular cylinder of finite length have been treated in detail by Buckley[1] and by Yamauti.[2] Cylinders with rectangular cross sections, corresponding to lightwells in buildings and to rectangular apertures in furnace walls, have been considered by Hisano[3] and by Hottel and Keller.[4] In the present paper the work of the foregoing investigators is extended to cover the general right cylinder having any cross section, with or without ends, and with arbitrary initial luminosities for top, bottom, and cylinder. The subject is of more than academic interest, since its practical applications include the predetermination of daylight illumination in lightwells, the calculation of the performance of experimental blackbodies, and the determination of illumination and brightness distribution produced in rooms by artificial lighting systems. Some of these applications will be considered in future papers.

The following assumptions will be made: (a) All surfaces are perfectly diffusing and each has a uniform reflection factor. (b) The medium within the cylinder is transparent and nondissipative. (c) The luminosity of the cylinder walls is a function of the distance from the end and is independent of the position around the cylinder. (d) Initial and final luminosities are uniform over an end disk. (e) The kernel of the integral equation can be approximated by an exponential function.

The simplification introduced by the last three assumptions makes possible a solution of the integral equation. Without assumption (c), the problem would be a two-dimensional one which could be solved, if at all, only by arduous numerical methods. The assumption is rigorously correct for a circular cylinder illuminated by a uniform sky, but is an approximation for cylinders of other cross sections. For rectangular lightwells, both theoretical[5] and experimental[6] investigations show that luminosity variations at constant depth are unimportant; and thus it is reasonable to believe that assumptions (c) and (d) do not introduce large errors.

Assumption (e) may seem shocking, in view of the departures from exponential form of the actual kernels. Luckily, however, the kernel always appears under the integral sign, and the integration process has wonderful powers of smoothing out irregularities. For this reason the final results are believed to be sufficiently accurate for most engineering purposes,[7] and they have the very real advantage of an analytical form sufficiently simple to be used in practical work. The basic thesis is that an approximate formula is better than no formula at all; or, to use the Dutch proverb, "Beter een vogel in de hand dan tien in de lucht."

## 2. THE INTEGRAL EQUATION

Let

$K_{11}(s-t)$ = average illumination produced at the depth $s$ by a luminous band at $t$, per unit luminosity and per unit width of band;

$K_{12}(t)$, $K_{13}(t)$ = average illumination produced on an end of the cylinder by a luminous band at $t$, per unit luminosity and per unit width of band;

$K_{21}(s)$, $K_{31}(s)$ = average illumination produced at $s$ by one luminous end of the cylinder, per unit luminosity of the end;

$K_{32}(l)$ = average illumination on 2 produced by 3, per unit luminosity of 3;

[1] H. Buckley, "On the radiation from the inside of a circular cylinder," Phil. Mag. **4**, 753 (1927); **6**, 447 (1928); **17**, 576 (1934).

[2] Z. Yamauti, "Recherche d'un radiateur intégral au moyen d'un corps cylindrique," Com. Int. Poids et Mésures, Procès-verbaux **16**, 243 (1933).

[3] K. Hisano, "Light flux distribution in a rectangular parallelepiped and its simplifying scale," Researches Electrotech. Lab., Tokyo, No. 394 (1936).

[4] H. C. Hottell and F. Keller, "Effect of reradiation on heat transmission in furnaces and through openings," A. S. M. E. annual meeting (December, 1932).

[5] A. D. Moore, "Interreflection by the increment method as applied to a light court," Trans. I. E. S. **24**, 629 (1929).

[6] H. F. Meacock and G. E. V. Lambert, "Efficiency of lightwells," Dept. Sci. Ind. Research, Tech. Pap. No. 11 (1930).

[7] See Parry Moon, "Interreflections in lightwells," to appear in this journal.

$K_{23}(l)$ = average illumination on 3 produced by 2, per unit luminosity of 2;
$p$ = perimeter of an end ($m$);
$S$ = area of an end ($m^2$);
$\alpha = p/S$;
$L_1(s)$ = average luminosity of cylinder wall at depth $s$ (lumen $m^{-2}$);
$L_2$, $L_3$ = average luminosity of end disks (lumen $m^{-2}$);
$L_{01}(s)$ = average initial luminosity (no interreflections) of cylinder wall at depth $s$;
$L_{02}$, $L_{03}$ = average initial luminosity of end disks;
$\rho_1$, $\rho_2$, $\rho_3$ = reflection factors.

Certain relations can be established among the various $K$'s. For example, $K_{21}(s)$ is the illumination produced on the cylinder wall by the luminous disk 2; and this illumination is obviously equal to the illumination produced by a uniformly luminous cylinder ($L=1$) extending upward from $t=0$ to $t=-\infty$. Thus,

$$K_{21}(s)=\int_{-\infty}^{0} K_{11}(s-t)dt. \tag{1}$$

Similarly,

$$K_{31}(s)=\int_{l}^{\infty} K_{11}(s-t)dt. \tag{2}$$

The illumination produced on disk 3 by disk 2 is the same as that produced by a uniformly luminous cylinder ($L=1$) from 0 to $-\infty$, or

$$K_{23}(l)=\int_{-\infty}^{0} K_{13}(t)dt. \tag{3}$$

By the reciprocity principle, the flux from 2 to 3 is equal to the flux from 3 to 2, the luminosity of the source being the same in both cases. Thus,

$$K_{23}(l)=K_{32}(l). \tag{4}$$

Also, the flux from the band at $t$ to disk 2 is (for unit luminosity)

$$dF_{12}=(K_{12}dt)S,$$

which is equal to the flux from 2 to the band:

$$dF_{21}=K_{21}(pdt).$$

Therefore,

$$K_{12}=K_{21}\alpha, \tag{5}$$

$$K_{13}=K_{31}\alpha. \tag{6}$$

It is convenient, also, to know the definite values:

$$K_{21}(0)=\tfrac{1}{2}\quad K_{31}(l)=\tfrac{1}{2}\quad K_{23}(0)=1, \tag{7}$$

which are obtained by use of the unit-sphere principle.[8]

On the basis of the foregoing notation, the luminosity equations can be written immediately as

$$\left.\begin{aligned} L_1(s)&=L_{01}(s)+\rho_1\left\{\int_0^l K_{11}|s-t|\,L_1(t)dt \right.\right.\\ &\qquad\left.\left.+K_{21}(s)\cdot L_2+K_{31}(s)\cdot L_3\right\}\right.\\ L_2&=L_{02}+\rho_2\left\{\int_0^l K_{12}(t)L_1(t)dt+K_{32}(l)\cdot L_3\right\},\\ L_3&=L_{03}+\rho_3\left\{\int_0^l K_{13}(t)L_1(t)dt+K_{23}(l)\cdot L_2\right\}.\end{aligned}\right\} \tag{8}$$

Among these three simultaneous equations, $L_2$ and $L_3$ can be eliminated, giving the single integral equation:

$$L_1(s)=L_0(s)+\rho_1\int_0^l K(s,t)L_1(t)dt, \tag{9}$$

where

$$\begin{aligned} L_0(s)&=L_{01}(s)+\frac{\rho_1}{1-\rho_2\rho_3K_{23}{}^2}\\ &\quad\times\{[K_{21}(s)+\rho_3K_{31}(s)K_{23}(l)]L_{02}\\ &\quad+[K_{31}(s)+\rho_2K_{21}(s)K_{23}(l)]L_{03}\}, \end{aligned} \tag{10}$$

$$\begin{aligned} K(s,t)&=K_{11}(s-t)+\frac{\alpha}{1-\rho_2\rho_3K_{23}{}^2}\\ &\quad\times\{[K_{21}(s)+\rho_3K_{31}(s)K_{23}(l)]\rho_2K_{21}(t)\\ &\quad+[K_{31}(s)+\rho_2K_{21}(s)K_{23}(l)]\rho_3K_{31}(t)\}. \end{aligned} \tag{11}$$

After $L_1(s)$ is obtained by solution of Eq. (9), the other luminosities are easily found from Eq. (8), or

$$\begin{aligned} L_2&=\frac{1}{1-\rho_2\rho_3K_{23}{}^2}\left\{L_{02}+\rho_2K_{23}(l)\cdot L_{03}\right.\\ &\quad+\alpha\rho_2\int_0^l[K_{21}(t)+\rho_3K_{31}(t)\\ &\quad\left.\times K_{23}(l)]L_1(t)dt\right\}, \end{aligned} \tag{12}$$

[8] Parry Moon, "Basic principles in illumination calculations," J. Opt. Soc. Am. **29**, 108 (1939).

$$L_3=\frac{1}{1-\rho_2\rho_3K_{23}{}^2}\Big\{L_{03}+\rho_3K_{23}(l)\cdot L_{02}+\alpha\rho_3\int_0^l[K_{31}(l)+\rho_2K_{21}(t)\times K_{23}(l)]L_1(t)dt\Big\}. \quad (13)$$

Equations (9), (12) and (13) are of great generality, since they apply to right cylinders having any shape of cross section and any length, with or without ends, and with arbitrary reflection factors and initial luminosities.

### 3. The Exponential Kernel

The actual kernel $K(s, t)$ for the finite cylinder is always too complicated to allow an exact solution of Eq. (9). Even for a semi-infinite circular cylinder without ends, Eq. (9) has not been solved exactly. Buckley[1] has shown, however, that the kernel for the *circular* cylinder can be closely approximated by an exponential, which gives an easy solution. It appears that kernels for cylinders of other cross sections can also be approximated by exponentials. For rectangular sections, for instance, exponential kernels can be used; and though the approximation is not as close as for the circular cylinder, it is good enough for engineering purposes.

Thus the kernel $K_{11}|s-t|$ will be written *for all cylinders* as

$$K_{11}|s-t|=Ae^{-a|s-t|}. \quad (14)$$

The absolute-value signs must be used to make the kernel symmetric.[9] The other $K$'s can now be written by use of Eqs. (1) to (6):

$$K_{21}(s)=A\int_{-\infty}^{0}e^{-a(s-t)}dt=\frac{A}{a}e^{-as}, \quad (1a)$$

$$K_{31}(s)=A\int_{l}^{\infty}e^{-a(t-s)}dt=\frac{A}{a}e^{-a(l-s)}, \quad (2a)$$

$$K_{23}(l)=K_{32}(l)=\alpha\int_l^\infty K_{21}(t)dt=\frac{\alpha A}{a}\int_l^\infty e^{-at}dt=\frac{\alpha A}{a^2}e^{-al}. \quad (5a)$$

The values of Eq. (7) can be introduced, giving

$$A=a/2, \quad \alpha=2a. \quad (7a)$$

Thus,

$$K_{11}|s-t|=(a/2)e^{-a|s-t|}, \quad (14a)$$

$$K_{21}(s)=\tfrac{1}{2}e^{-as}, \quad (1b)$$

$$K_{31}(s)=\tfrac{1}{2}e^{-a(l-s)}, \quad (2b)$$

$$K_{23}(l)=e^{-al}. \quad (5b)$$

Substitution in Eqs. (10) and (11) gives

$$L_0(s)=L_{01}(s)+(\rho_1/2M)[N_{23}(s)\cdot L_{02}+N_{32}(s)\cdot L_{03}], \quad (10a)$$

$$K(s,t)=(a/2)\{e^{-a|s-t|}+(1/M)[N_{23}(s)\rho_2e^{-at}+N_{32}(s)\rho_3e^{-a(l-t)}]\}, \quad (11a)$$

where

$$M=1-\rho_2\rho_3e^{-2al}, \quad (15)$$

$$N_{23}(s)=e^{a(l-s)}+\rho_3e^{-a(l-s)}, \quad (16)$$

$$N_{32}(s)=e^{as}+\rho_2e^{-as}. \quad (17)$$

From Eqs. (12) and (13),

$$L_2(l)=\frac{1}{M}\Big\{L_{02}+\rho_2e^{-al}\times\Big[L_{03}+a\int_0^l N_{23}(t)\cdot L_1(t)dt\Big]\Big\}, \quad (12a)$$

$$L_3(l)=\frac{1}{M}\Big\{L_{03}+\rho_3e^{-al}\times\Big[L_{02}+a\int_0^l N_{32}(t)\cdot L_1(t)dt\Big]\Big\}. \quad (13a)$$

### 4. Solution of the General Integral Equation

The solution of Eq. (9) will now be obtained for the general case of three reflection factors ($\rho_1$, $\rho_2$, $\rho_3$) and three different initial luminosities ($L_{01}$, $L_{02}$, $L_{03}$). The solution is of the form

$$L_1(s)=B\cosh ks+C\sinh ks+D. \quad (18)$$

[9] Parry Moon, "On interreflections," J. Opt. Soc. Am. **30**, 195 (1940).

The constants $B$, $C$, and $D$ are evaluated by substituting Eq. (18) in Eq. (9) and performing the indicated integrations. Then it is found that

$$B=\frac{2(a^2-k^2)}{a}\frac{\nu\sigma-\mu\tau}{\lambda\sigma-\rho\mu}, \tag{19}$$

$$C=\frac{2(a^2-k^2)}{a}\frac{\lambda\tau-\nu\rho}{\lambda\sigma-\rho\mu}, \tag{20}$$

$$D=L_{01}/(1-\rho_1), \tag{21}$$

$$k=a(1-\rho_1)^{\frac{1}{2}}, \tag{22}$$

where

$$\lambda=(1+\rho_2)\{[(a+k)-\rho_3(a-k)]e^{kl}+[(a-k)-\rho_3(a+k)]e^{-kl}\}+2a(1-\rho_2)(e^{al}+\rho_3e^{-al}),$$

$$\rho=(1-\rho_2)\{[(a+k)-\rho_3(a-k)]e^{kl}+[(a-k)-\rho_3(a+k)]e^{-kl}\}-2a(1-\rho_2)(e^{al}-\rho_3e^{-al}),$$

$$\mu=(1+\rho_2)\{[(a+k)-\rho_3(a-k)]e^{kl}-[(a-k)-\rho_3(a+k)]e^{-kl}\}-2k(1+\rho_2)(e^{al}+\rho_3{}^{-al}),$$

$$\sigma=(1-\rho_2)\{[(a+k)-\rho_3(a-k)]e^{kl}-[(a-k)-\rho_3(a+k)]e^{-kl}\}+2k(1+\rho_2)(e^{al}-\rho_3e^{-al}),$$

$$\nu=L_{02}(e^{al}+\rho_3e^{-al})+L_{03}(1+\rho_2)-D\{(1-\rho_2)(e^{al}+\rho_3e^{-al})+(1+\rho_2)(1-\rho_3)\},$$

$$\tau=-L_{02}(e^{al}-\rho_3e^{-al})+L_{03}(1-\rho_2)+D\{(1-\rho_2)(e^{al}-\rho_3e^{-al})-(1-\rho_2)(1-\rho_3)\}.$$

Further algebraic manipulation yields the simpler expressions:

$$B=\frac{\rho_1\{L_{02}n+(1-\rho_1)^{\frac{1}{2}}(1+\rho_2)L_{03}-D[(1-\rho_2)n+(1-\rho_1)^{\frac{1}{2}}(1+\rho_2)(1-\rho_3)]\}}{(1-\rho_2)n+(1-\rho_1)^{\frac{1}{2}}(1+\rho_2)m}, \tag{23}$$

$$C=\frac{\rho_1\{-L_{02}m+(1-\rho_2)L_{03}+D[(1-\rho_2)m-(1-\rho_2)(1-\rho_3)]\}}{(1-\rho_2)n+(1-\rho_1)^{\frac{1}{2}}(1+\rho_2)m}, \tag{24}$$

where

$$m=(1-\rho_3)\cosh kl+(1-\rho_1)^{\frac{1}{2}}(1+\rho_3)\sinh kl, \tag{25}$$

$$n=(1-\rho_3)\sinh kl+(1-\rho_1)^{\frac{1}{2}}(1+\rho_3)\cosh kl. \tag{26}$$

Substitution of Eqs. (23), (24), (21) and (22) in Eq. (18) gives the luminosity distribution on the cylinder. This form of solution applies when $\rho_1<1$. If $\rho_1=1$, the transcendental solution breaks down into an algebraic solution, and the foregoing equations are inapplicable. The algebraic solution for $\rho_1=1$ is obtainable rather easily but will not be considered in this paper because it has little practical significance. The limitation to $\rho_1<1$ is stated here because attempts are often made to check interreflection equations by considering what happens if the reflection factor reaches unity. Evidently no such check can be applied to any equation developed in this paper.

The luminosity of the end disks is obtained from Eqs. (12a) and (13a). The introduction of Eqs. (16) and (18) gives

$$L_2(l)=\frac{1}{M}\left\{L_{02}e^{al}+\rho_2\left[L_{03}+a\int_0^l(e^{a(l-t)}+\rho_3e^{-a(l-t)})\cdot(D+B\cosh kt+C\sinh kt)dt\right]\right\},$$

or the luminosity of the top disk is

$$L_2(l)=(1-\rho_2\rho_3e^{-2al})^{-1}\left\{L_{02}+\rho_2e^{-al}\left[L_{03}+\frac{L_{01}}{1-\rho_1}\{v_3-(1-\rho_3)\}\right.\right.$$

$$+\frac{B}{\rho_1}\{v_3-(1-\rho_3)\cosh kl-(1-\rho_1)^{\frac{1}{2}}(1+\rho_3)\sinh kl\}$$

$$\left.\left.+\frac{C}{\rho_1}\{(1-\rho_1)^{\frac{1}{2}}u_3-(1-\rho_3)\sinh kl-(1-\rho_1)^{\frac{1}{2}}(1+\rho_3)\cosh kl\}\right]\right\}. \tag{12b}$$

Similarly, the luminosity of the bottom disk is

$$L_3(l)=(1-\rho_2\rho_3e^{-2al})^{-1}\left\{L_{03}+\rho_3e^{-al}\left[L_{02}+\frac{L_{01}}{1-\rho_1}\{v_2-(1-\rho_2)\}\right.\right.$$

$$+\frac{B}{\rho_1}\{v_2\cosh kl-(1-\rho_1)^{\frac{1}{2}}u_2\sinh kl-(1-\rho_2)\}$$

$$\left.\left.+\frac{C}{\rho_1}\{u_2\sinh kl-(1-\rho_1)^{\frac{1}{2}}u_2\cosh kl+(1-\rho_1)^{\frac{1}{2}}(1+\rho_2)\}\right]\right\}, \quad (13b)$$

where

$$u_2=e^{al}+\rho_2e^{-al}, \quad v_2=e^{al}-\rho_2e^{-al}, \quad u_3=e^{al}+\rho_3e^{-al}, \quad v_3=e^{al}-\rho_3e^{-al}.$$

## 5. Uniformly Luminous Cylinder without Ends

For the special case of a cylinder without ends, Eqs. (19) and (20) can be written in a simpler form. Let the cylinder walls have a uniform initial luminosity $L_{01}$, and let

$$L_{02}=L_{03}=0, \quad \rho_2=\rho_3=0.$$

Then

$$B=-\frac{L_{01}\rho_1}{1-\rho_1}\,\frac{(1-\rho_1)^{\frac{1}{2}}(\cosh kl+1)+\sinh kl}{2(1-\rho_1)^{\frac{1}{2}}\cosh kl+(2-\rho_1)\sinh kl}, \quad (23a)$$

$$C=\frac{L_{01}\rho_1}{1-\rho_1}\,\frac{(\cosh kl-1)+(1-\rho_1)^{\frac{1}{2}}\sinh kl}{2(1-\rho_1)^{\frac{1}{2}}\cosh kl+(2-\rho_1)\sinh kl}, \quad (24a)$$

$$D=L_{01}/(1-\rho_1), \quad (21)$$

$$k=a(1-\rho_1)^{\frac{1}{2}}. \quad (22)$$

If the cylinder is of finite length and has nonreflecting ends, there is an advantage in so formulating the result that the inherent symmetry about a center section is emphasized. Let $l'$ be the half-length of the cylinder and $s'$ be the axial distance measured from the center section, or

$$l=2l', \quad s=s'+l'.$$

Substitution of these values in Eqs. (23a) and (24a) gives

$$B=-\frac{L_{01}\rho_1}{1-\rho_1}\,\frac{\cosh kl'}{\cosh kl'+(1-\rho_1)^{\frac{1}{2}}\sinh kl'}, \quad (23b)$$

$$C=\frac{L_{01}\rho_1}{1-\rho_1}\,\frac{\sinh kl'}{\cosh kl'+(1-\rho_1)^{\frac{1}{2}}\sinh kl'}. \quad (24b)$$

Thus the final luminosity is

$$L_1(s')=D+[B\cosh kl'+C\sinh kl']\cosh ks'+[B\sinh kl'+C\cosh kl']\sinh ks',$$

which reduces to the simple equation:

$$L_1(s')=\frac{L_{01}}{1-\rho_1}\left\{1-\frac{\rho_1\cosh ks'}{\cosh kl'+(1-\rho_1)^{\frac{1}{2}}\sinh kl'}\right\}. \quad (18a)$$

If the length of the cylinder exceeds approximately 3, the two ends have little effect on each other

and it is usually permissible to consider that $l \to \infty$. Then, from Eqs. (23a) and (24a),

$$B = -\frac{L_{01}}{1-\rho_1}[1-(1-\rho_1)^{\frac{1}{2}}], \quad C = \frac{L_{01}}{1-\rho_1}[1-(1-\rho_1)^{\frac{1}{2}}]$$

and Eq. (18) becomes, for the semi-infinite cylinder,

$$L_1(s) = \frac{L_{01}}{1-\rho_1}\{1-[1-(1-\rho_1)^{\frac{1}{2}}]e^{-ks}\}, \tag{18b}$$

where $s$ is measured from the open end.

## 6. Cylinder without Ends, Illuminated by Uniform Sky

A cylinder of arbitrary cross section has an open top and a nonreflecting bottom. The cylinder wall is illuminated by a sky of uniform luminosity $L_u$. The problem may be considered in two ways:

(a) The top has the initial luminosity $L_u$ and zero reflection factor, while initial luminosities of sides and bottom are zero.

(b) The top of the cylinder is nonexistent. The initial luminosity of the wall is equal to its reflection factor times its initial illumination, or

$$L_{01}(s) = \rho_1 K_{21}(s) L_u. \tag{27}$$

The only place in the integral equation where the initial luminosities enter is in $L_0(s)$ of Eq. (10). By the former method,

$$L_{02} = L_u, \quad L_{01} = L_{03} = 0, \quad \rho_2 = \rho_3 = 0,$$

and Eq. (10) becomes

$$L_0(s) = 0 + \rho_1 K_{21}(s) L_u. \tag{10a}$$

By the second method, Eq. (27) is substituted into Eq. (10) and gives (10a) directly. Thus,

$$B = \rho_1 L_u \frac{(1-\rho_1)^{\frac{1}{2}} \cosh kl + \sinh kl}{2(1-\rho_1)^{\frac{1}{2}} \cosh kl + (2-\rho_1) \sinh kl}, \tag{23c}$$

$$C = -\rho_1 L_u \frac{\cosh kl + (1-\rho_1)^{\frac{1}{2}} \sinh kl}{2(1-\rho_1)^{\frac{1}{2}} \cosh kl + (2-\rho_1) \sinh kl}, \tag{24c}$$

$$D = 0, \quad K = a(1-\rho_1)^{\frac{1}{2}}.$$

The final luminosity distribution is therefore

$$L_1(s) = \frac{\rho_1 L_u}{2(1-\rho_1)^{\frac{1}{2}} \cosh kl + (2-\rho_1) \sinh kl}\{[(1-\rho_1)^{\frac{1}{2}} \cosh kl + \sinh kl] \cosh ks - [\cosh kl + (1-\rho_1)^{\frac{1}{2}} \sinh kl] \sinh ks\}. \tag{18c}$$

For a semi-infinite cylinder, $\cosh kl = \sinh kl = \frac{1}{2}e^{kl}$, and Eq. (18c) becomes

$$L_1(s) = L_u[1-(1-\rho_1)^{\frac{1}{2}}]e^{-ks}. \tag{18d}$$

Thus, in any cylinder where $l > 3$, illuminated by a uniform sky, *the luminosity of the walls is an exponential function of the depth.* Equation (18d) can be applied advantageously to lightwells.

### 7. Cylinder with Reflecting Bottom, Uniform Sky

The conditions are

$$L_{02}=L_u, \quad L_{01}=L_{03}=0, \quad \rho_2=0,$$

which give the following results:

Substitution in Eqs. (23) and (24) gives

$$B=\frac{\rho_1 L_u[(1-\rho_1)^{\frac{1}{2}}(1+\rho_3)\cosh kl+(1-\rho_3)\sinh kl]}{2(1-\rho_1)^{\frac{1}{2}}\cosh kl+[(1-\rho_3)+(1-\rho_1)(1+\rho_3)]\sinh kl}, \tag{23d}$$

$$C=\frac{-\rho_1 L_u[(1-\rho_1)^{\frac{1}{2}}(1+\rho_3)\sinh kl+(1-\rho_3)\cosh kl]}{2(1-\rho_1)^{\frac{1}{2}}\cosh kl+[(1-\rho_3)+(1-\rho_1)(1+\rho_3)]\sinh kl}, \tag{24d}$$

$$D=0, \quad K=a(1-\rho_1)^{\frac{1}{2}}.$$

If one introduces the abbreviations:

$$U=(1-\rho_1)^{\frac{1}{2}}(1+\rho_3)\cosh kl+(1-\rho_3)\sinh kl,$$
$$V=(1-\rho_1)^{\frac{1}{2}}(1+\rho_3)\sinh kl+(1-\rho_3)\cosh kl,$$
$$W=2(1-\rho_1)^{\frac{1}{2}}\cosh kl+[(1-\rho_3)+(1-\rho_1)(1+\rho_3)]\sinh kl,$$

the luminosity of the wall is

$$L_1(s)=(L_u\rho_1/W)[U\cosh ks-V\sinh ks]. \tag{18e}$$

The luminosity of the bottom disk is obtained from Eq. (13a), where

$$M=e^{al}, \quad N_{32}(t)=e^{at}.$$

Thus,

$$L_3=\rho_3 e^{-al}\left\{L_u+a\int_0^l e^{at}[B\cosh kt+C\sinh kt]dt\right\},$$

which reduces to

$$L_3=\rho_3 L_u e^{-al}\left\{1+\frac{1}{W}[U\{e^{al}[\cosh kl-(1-\rho_1)^{\frac{1}{2}}\sinh kl]-1\}\right.$$
$$\left.-V\{e^{al}[\sinh kl-(1-\rho_1)^{\frac{1}{2}}\cosh kl]+(1-\rho_1)^{\frac{1}{2}}\}]\right\}. \tag{13c}$$

From Eq. (12a),

$$L_2=L_u. \tag{12c}$$

According to Eq. (18e) the luminosity of the wall becomes zero if the sky luminosity is zero or if the cylinder wall has zero reflection factor, as would be expected. Furthermore, if the depth $l$ is several times the width,

$$\cosh kl \cong \sinh kl \cong \tfrac{1}{2}e^{kl}$$

and

$$U=V=\frac{e^{kl}}{2}[(1-\rho_1)^{\frac{1}{2}}(1+\rho_3)+(1-\rho_3)],$$

$$W=\frac{e^{kl}}{2}[1+(1-\rho_1)^{\frac{1}{2}}][(1-\rho_1)^{\frac{1}{2}}(1+\rho_3)+(1-\rho_3)].$$

Thus,

$$\frac{U}{W}=\frac{1}{1+(1-\rho_1)^{\frac{1}{2}}}=\frac{1}{\rho_1}[1-(1-\rho_1)^{\frac{1}{2}}]$$

and

$$L_1(s)=L_u[1-(1-\rho_1)^{\frac{1}{2}}]e^{-ks}, \tag{18d}$$

which is independent of the reflection factor of the bottom.

If $l$ is large, the luminosity of the bottom becomes

$$L_3=\rho_3 L_u[1+(1-\rho_1)^{\frac{1}{2}}]\frac{U}{W}[\cosh kl-\sinh kl]=\rho_3 L_u e^{-kl}. \tag{13d}$$

## 8. Room with Nonreflecting Floor, Indirect Lighting

Consider a room having a horizontal cross section of any shape. The room is lighted by an indirect system, which provides an initial uniform luminosity $L_{02}$ over the entire ceiling and zero initial luminosity on the walls and floor. The reflection factor of the floor is so low that it is neglected. Thus,

$$\rho_3=0, \quad L_{01}=L_{03}=0, \quad D=0.$$

Substitution in Eqs. (23) and (24) gives

$$B=(L_{02}\rho_1/T)[(1-\rho_1)^{\frac{1}{2}}\cosh kl+\sinh kl], \tag{23e}$$
$$C=-(L_{02}\rho_1/T)[\cosh kl+(1-\rho_1)^{\frac{1}{2}}\sinh kl] \tag{24e}$$

and the solution is

$$L_1(s)=(L_{02}\rho_1/T)[R\cosh ks-S\sinh ks], \tag{18f}$$

where

$$R=(1-\rho_1)^{\frac{1}{2}}\cosh kl+\sinh kl,$$
$$S=\cosh kl+(1-\rho_1)^{\frac{1}{2}}\sinh kl,$$
$$T=2(1-\rho_1)^{\frac{1}{2}}\cosh kl+[(1-\rho_2)+(1-\rho_1)(1+\rho_2)]\sinh kl,$$
$$k=a(1-\rho_1)^{\frac{1}{2}}.$$

The luminosity of the ceiling is obtained from Eq. (12a), where $M=e^{al}$, $N_{23}(t)=e^{a(l-t)}$, and $N_{32}(t)=e^{at}$. Substitution gives

$$L_2=L_{02}\{1+\rho_1\rho_2\sinh kl/T\} \tag{12e}$$

and for the floor, of course, Eq. (13a) reduces to

$$L_3=0. \tag{13e}$$

For the *special case of a very large room of small height*, $\cosh kl\leqq 1$, $\sinh kl\leqq 0$, and

$$R\leqq(1-\rho_1)^{\frac{1}{2}}, \quad T\leqq 2(1-\rho_1)^{\frac{1}{2}}.$$

Thus the wall luminosity becomes

$$L_1(s)\leqq L_{02}\rho_1 R/T=L_{02}\rho_1/2. \tag{18g}$$

The corresponding ceiling luminosity is

$$L_2=L_{02}\left\{1+\frac{\rho_1\rho_2\sinh kl}{2(1-\rho_1)^{\frac{1}{2}}}\right\}\leqq L_{02}. \tag{12f}$$

For a *very high room*, $\cosh kl\leqq e^{kl/2}$ and

$$R=S=(e^{kl}/2)[1+(1-\rho_1)^{\frac{1}{2}}],$$
$$T=(e^{kl}/2)[2(1-\rho_1)^{\frac{1}{2}}+(1-\rho_2)+(1-\rho_1)(1+\rho_2)].$$

Thus the wall luminosity is

$$L_1(s)=L_{02}\rho_1\frac{R}{T}e^{-ks} \tag{18h}$$

and the ceiling luminosity is

$$L_2=L_{02}\left\{1+\frac{\rho_1\rho_2}{2(1-\rho_1)^{\frac{1}{2}}+(1-\rho_2)+(1-\rho_1)(1+\rho_2)}\right\}. \tag{12g}$$

## 9. Room with Nonreflecting Floor, Wall Lighting

The room of Section 8 is now lighted so that the initial illumination on the walls is uniform (lighting of a picture gallery, for instance). The initial illumination of the ceiling is zero, and the floor has a negligible reflection factor. Under these conditions,

$$\rho_3=0, \quad L_{02}=L_{03}=0$$

and

$$B=-\frac{\rho_1 L_{01}}{1-\rho_1}\frac{[(1-\rho_2)R+(1-\rho_1)^{\frac{1}{2}}(1+\rho_2)]}{T}, \tag{23e}$$

$$C=\frac{\rho_1 L_{01}}{1-\rho_1}\frac{(1-\rho_2)(S-1)}{T}, \tag{24e}$$

$$D=L_{01}/(1-\rho_1). \tag{21}$$

The luminosity of the wall is

$$L_1(s)=\frac{L_{01}}{1-\rho_1}\left\{1+\frac{\rho_1}{T}\left[-[(1-\rho_2)R+(1-\rho_1)^{\frac{1}{2}}(1+\rho_2)]\cosh ks+(1-\rho_2)(S-1)\sinh ks\right]\right\}. \tag{18i}$$

The luminosity of the ceiling is obtained from Eq. (12a):

$$L_2(l)=\frac{L_{01}}{1-\rho_1}\left\{\left[1+\frac{\rho_1}{T}(1-\rho_2)(R-S)\right]-e^{-al}\left[1+\frac{\rho_1}{T}((1-\rho_1)^{\frac{1}{2}}(1+\rho_2)S+(1-\rho_2)R)\right]\right\}. \tag{12h}$$

## 10. Room with Nonreflecting Walls

Let $\rho_1=0$; $L_{01}=0$; $D=0$; $k=a$. $B$ and $C$ are zero because the coefficient $\rho_1$ is zero in each case. Thus,

$$L_1(s)=0.$$

The fact that $B$ and $C$ are zero does not eliminate the terms containing these quantities in Eqs. (12b) and (13b) because of the $\rho_1$ in the denominator. However, it can be shown that terms containing $B$ and $C$ are actually zero. The luminosities of the end disks reduce to the simple equations:

$$L_2(l)=\frac{L_{02}+\rho_2 e^{-al}L_{03}}{1-\rho_2\rho_3 e^{-2al}}, \tag{12i}$$

$$L_3(l)=\frac{L_{03}+\rho_3 e^{-al}L_{02}}{1-\rho_2\rho_3 e^{-2al}}. \tag{13i}$$

This result, incidentally, can be obtained by elementary methods, without the use of integral equations. Evidently,

$$\left.\begin{aligned}L_2(l)&=L_{02}+\rho_2 K_{32}(l)\cdot L_3\\ L_3(l)&=L_{03}+\rho_3 K_{23}(l)\cdot L_2\end{aligned}\right\}, \tag{28}$$

since

$$K_{32}(l)=K_{23}(l)=(\alpha A/a^2)e^{-al}. \tag{5a}$$

Eq. (28) becomes

$$\left.\begin{aligned}L_2(l)&=L_{02}+\rho_2 L_3 e^{-al}\\ L_3(l)&=L_{03}+\rho_3 L_2 e^{-al}\end{aligned}\right\}. \tag{28a}$$

If these two equations are solved simultaneously, they give Eqs. (12h) and (13h). The results can be obtained also by writing down the individual reflections and summing terms from 1 to $\infty$, as is so often done in the theory of the integrating sphere.

## 11. Illumination on a Horizontal Plane

The preceding sections have given expressions for the *luminosity*, $L$. It is often desirable to obtain also the *illumination*, $E$. Evidently,

$$L_1(s) = L_{01}(s) + \rho_1 E_1(s) \quad \text{or} \quad E_1(s) = [L_1(s) - L_{01}(s)]/\rho_1. \tag{29}$$

Similarly, for top and bottom,

$$E_2(l) = (L_2(l) - L_{02})/\rho_2, \tag{30}$$

$$E_3(l) = (L_3(l) - L_{03})/\rho_3. \tag{31}$$

In the lighting of rooms, the engineer is often interested in the average illumination on the upper side of a fictitious horizontal plane called the "working plane." An expression for this average illumination $E_{Av}(h)$ at any distance $h$ below the ceiling is easily obtained from the results of the preceding paragraphs. From the definitions of the $K$'s,

$$E_{Av}(h) = K_{23}(h) \cdot L_2 + \int_0^h K_{13}(t) \cdot L_1(t)\,dt, \tag{32}$$

where

$$K_{13}(t) = \alpha K_{31}(t) = (\alpha A/a)e^{-a(h-t)}, \tag{2b}$$

$$K_{23}(h) = (\alpha A/a^2)e^{-ah}. \tag{5b}$$

Thus,

$$E_{Av}(h) = L_2 e^{-ah} + ae^{-ah} \int_0^h e^{at}[D + B\cosh kt + C\sinh kt]\,dt.$$

Integration gives the average illumination:

$$E_{Av}(h) = L_2 e^{-ah} + \frac{L_{01}}{1-\rho_1}(1-e^{-ah}) + \frac{B}{\rho_1}\{[\cosh kh - (1-\rho_1)^{\frac{1}{2}}\sinh kh] - e^{-ah}\}$$
$$+ \frac{C}{\rho_1}\{[\sinh kh - (1-\rho_1)^{\frac{1}{2}}\cosh kh] + (1-\rho_1)^{\frac{1}{2}}e^{-ah}\}. \tag{32a}$$

## 12. Effect of Cross Section

As stated previously, the equations of this paper apply not only to circular cylinders but to cylinders of any cross section. An examination of the equations shows that the only way in which the cross section enters is in the factor $k = a(1-\rho_1)^{\frac{1}{2}}$. Moreover, $k$ and $a$ never occur singly but always in combination with $l$ or $s$ in $e^{al}$, cosh $ks$, sinh $kl$, etc.

Evidently, $al$ is dimensionless and $a$ has the dimensions $[L^{-1}]$. The unit of length used in the specification of $s$ and $l$ can be selected at will and is entirely independent of the unit of length used in the luminosity. The luminosities in any of the equations may be expressed, for example, in lumens per square meter; while $l$ and $s$ in these same equations may be in feet or in other units. With circular cylinders, it is customary to employ a unit of length equal to the radius of the cylinder; for in that way, $a$ has a fixed value for all cylinders, irrespective of size. Similarly, it is often convenient to take the width of a rectangular lightwell as the unit of length.

Values of $a$ depend on the unit of length that has been chosen and on the shape of the cross section. According to Section 3,

$$a = p/2S, \tag{33}$$

where $p$ = perimeter of cross section and $S$ = area of cross section. For a *circular cylinder*, $p = 2\pi r$, $S = \pi r^2$, and if the radius is taken as unity,

$$a = 1.$$

The kernel is therefore approximated by

$$K(s-t) = \tfrac{1}{2}e^{-|s-t|}$$

as was done by Buckley.

For an *elliptical cylinder* with the semi-minor axis taken as unity and the semi-major axis as $b$,

$$S=\pi b$$
$$p\cong\pi[2(1+b^2)]^{\frac{1}{2}}$$

and thus,

$$a\cong[(1+b^2)/2b^2]^{\frac{1}{2}}.$$

For a cylinder having a cross section in the form of a *regular hexagon*, with each side taken as unity,

$$S=3\sqrt{3}/2, \quad p=6, \quad a=2/\sqrt{3}=1.155.$$

If the cross section is a *right triangle*, with sides 1 and $w$,

$$S=w/2$$
$$p=1+w+(1+w^2)^{\frac{1}{2}},$$
$$a=(1/w)[1+w+(1+w^2)^{\frac{1}{2}}].$$

If the cross section is *rectangular*, with sides 1 and $w$,

$$S=w, \quad p=2(1+w), \quad a=(1+w)/w. \quad (34)$$

It is interesting to note that if the luminosity distribution be plotted for the circular cylinder, *this same graph can be used for a cylinder of any cross section*, by proper change in the unit of length. It is merely necessary that $al$ be the same in both cases. To use the circular-cylinder graph for a hexagonal cylinder, for instance, all lengths in the latter are reduced in the ratio 1 : 1.155.

This unifying principle is particularly useful for the family of rectangular parallelepipeds. Everything can be worked out on the basis of a square cross section, and results for all other rectangles are then easily obtained by changing the unit of length. If a rectangular room has the dimensions $W_2$, $W_3$ and the height $W_1$, then

$$al=(W_2+W_3)W_1/W_2W_3, \quad (35)$$

or, if the square cross section ($a=2$) is taken as standard,

$$l=(W_2+W_3)W_1/2W_2W_3. \quad (36)$$

Similarly, at any actual distance of $h'$ below the ceiling,

$$s=(W_2+W_3)h'/2W_2W_3. \quad (37)$$

All combinations of $W_1$, $W_2$, and $W_3$ which give the same value of $l$ will have the same luminosity distribution, and all combinations of $W_2$, $W_3$ and $h'$ resulting in a given $s$ will result in a given value of luminosity. Thus, any of the formulas of the preceding sections can be used in calculating a luminosity distribution for a square room ($a=2$). The curve is plotted against the variable $s$ and can be used for all rooms where Eq. (36) is satisfied.

Equation (37) was obtained in 1936 by Hisano,[3] who called it the *simplifying scale* for the rectangular parallelepiped. Apparently, Hisano had no theoretical basis for his formula but found it to give results in agreement with a large number of experimental data. It is interesting that exactly the same equation is now obtained by the use of integral equations.

## 13. Conclusions

Multiple reflections of light within enclosures are of considerable practical importance, and the subject is now being attacked successfully by means of integral equations. This paper obtains a general solution for the luminosity distributions in right cylinders. The cylinders may be of any cross section, with or without end disks, and with different reflection factors and initial luminosities for the various parts. The solutions are not rigorously correct, but they are obtained in simple analytic form that will be useful in engineering practice. Various special cases are considered and a simplifying scale is discussed.

# Operational Analysis of the Diffraction Grating

ROY C. SPENCER
*Brace Laboratory of Physics, University of Nebraska, Lincoln, Nebraska*
(Received December 31, 1940)

Operational analysis is used to express the formula for the Fraunhofer diffraction pattern for a grating of $N$ slits in terms of that for a single slit.

STUDENTS of physical optics usually have difficulty in comprehending the derivation of the formula for the Fraunhofer diffraction pattern for the grating, even though they may understand that for the single slit. The purpose of this note is to bridge the gap between the two as directly as possible by use of operational analysis.

The effect of a grating is that of a double integration which may be considered as two successive operations. The first operation indicated by $P_1(a)$ is that of integration over the interval covered by the slit shown in Fig. 1. It is a function of the slit width $a$. The second operation indicated by $P_2$ is the sum of $N$ displacements each separated by a distance $d$. (See Fig. 2.) Since both operators are linear, their product[1,2] is the operator for the grating.

Fig. 1 Fig. 2

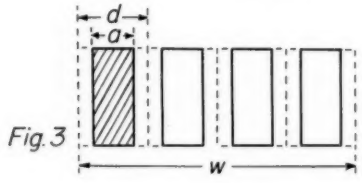

Fig. 3

$$P=P_1(a)P_2. \tag{1}$$

Now, let the slit width $a$ increase until it equals $d$ as indicated by the dotted lines in Fig. 3. The grating then reduces to a single slit of width $w=Nd$ which causes (1) to reduce to

$$P_1(w)=P_1(d)P_2. \tag{2}$$

Eliminating $P_2$ from (1) and (2)

$$P=P_1(a)P_1(w)/P_1(d) \tag{3}$$

in which each of the operators on the extreme right has the form of the single slit operator, but with $w$ and $d$ substituted, respectively, for $a$.

The above result may now be applied to the problem of Fraunhofer diffraction for which

$$P_1(a)=\frac{a\sin\alpha}{\alpha}, \quad \alpha=\frac{\pi a\sin\theta}{\lambda}. \tag{4}$$

Substitution of (4) into (3) results in the usual grating formula

$$P=\frac{a\sin\alpha}{\alpha}\frac{\sin N\beta}{\sin\beta}, \quad \beta=\frac{\pi d\sin\theta}{\lambda}. \tag{5}$$

[1] H. T. Davis, *The Theory of Linear Operators* (Principia Press, Bloomington, Indiana, 1936), p. 6–7.
[2] R. C. Spencer, Phys. Rev. **55**, 239A (1939).

# A Portable Visual Adaptometer

GEORGE WALD*
*Biological Laboratories, Harvard University, Cambridge, Massachusetts*
(Received January 15, 1941)

THE measurement of visual threshold and adaptation is a powerful tool in the study of retinal function, of vitamin A deficiency,[1–3] and of certain types of central nervous imbalance.[4] For precise and significant work four properties of the test field must be controlled:[5] (1) its brightness; (2) its size and distance from the eye; (3) its retinal position with reference to a fixation point; and (4) the duration of its exposure. A shutter in the light path controls the last factor, and is imperative in any case to minimize the "personal equation." In a number of procedures in present use the operator steadily raises the intensity of a continuous field until told to stop by the subject. In such arrangements the true end point is necessarily overshot by various amounts, depending upon the speed with which the intensity is raised and the reaction times of the workers. This error is eliminated when the subject is presented with a series of flashes graded in brightness, and spaced so that he may report on each flash before being exposed to the next.

The present adaptometer was built originally for a vitamin A deficiency survey in Northern Newfoundland and Labrador, which entailed considerable transportation, sometimes by dog-sled and on skis.[6] It has therefore been tried under particularly rigorous conditions. Lacking some of the flexibility of more elaborate instruments, it attempts to combine their precision with maximal simplicity, inexpensiveness, ruggedness, and portability.

## DESIGN

The entire instrument, except for the eyepiece, is enclosed in a cabinet 8.5×8.5×11.5 inches in size, and weighs about 18.5 pounds. It consists of a test unit connected by a long cord to storage cells and a control panel. The panel bears an on-off switch, a voltmeter and rheostat for setting the line voltage, and a calibrated rheostat with dial for regulating the intensities of the test and fixation lights. The test unit is of the size and approximate shape of a pocket lamp.

FIG. 1. Adaptometer mounted for stationary use. The test unit is clamped on a burette stand. In this instance the subject (left) operates the shutter-plunger, while the operator adjusts the brightness-dial. When not in use the eyepiece is detached, and the test unit and cord are replaced in the cabinet through the door shown in its side.

It provides a fixation point and a field of controlled brightness, size, and position, illuminated for short flashes through a shutter activated by a plunger. A funnel-shaped eyepiece may be fitted on the front of this unit to set the position of the subject's head and protect the eyes from stray light.

The complete assembly is shown in Fig. 1, set up as a table instrument. The test unit has been clamped on an ordinary burette stand. Alter-

* This research was supported in part by a grant from the Josiah Macy, Jr., Foundation.

[1] G. Wald, H. Jeghers and J. Arminio, "An experiment in human dietary night-blindness," Am. J. Physiol. **123**, 732 (1938).

[2] S. Hecht and J. Mandelbaum, "The relation between vitamin A and dark adaptation," J. Am. Med. Assn. **112**, 1910 (1939).

[3] G. Wald and D. Steven, "An experiment in human vitamin A deficiency," Proc. Nat. Acad. Sci. **25**, 344 (1939).

[4] R. A. McFarland and W. H. Forbes, "The effects of variations in the concentration of oxygen and of glucose on dark adaptation," J. Gen. Physiol. **24**, 69 (1940–41).

[5] Cf. reference 2. S. Hecht and S. Shlaer, "An adaptometer for measuring human dark adaptation," J. Opt. Soc. Am. **28**, 269 (1938).

[6] D. Steven and G. Wald, "Vitamin A deficiency: a field study in Newfoundland and Labrador," J. Nutrition, in press.

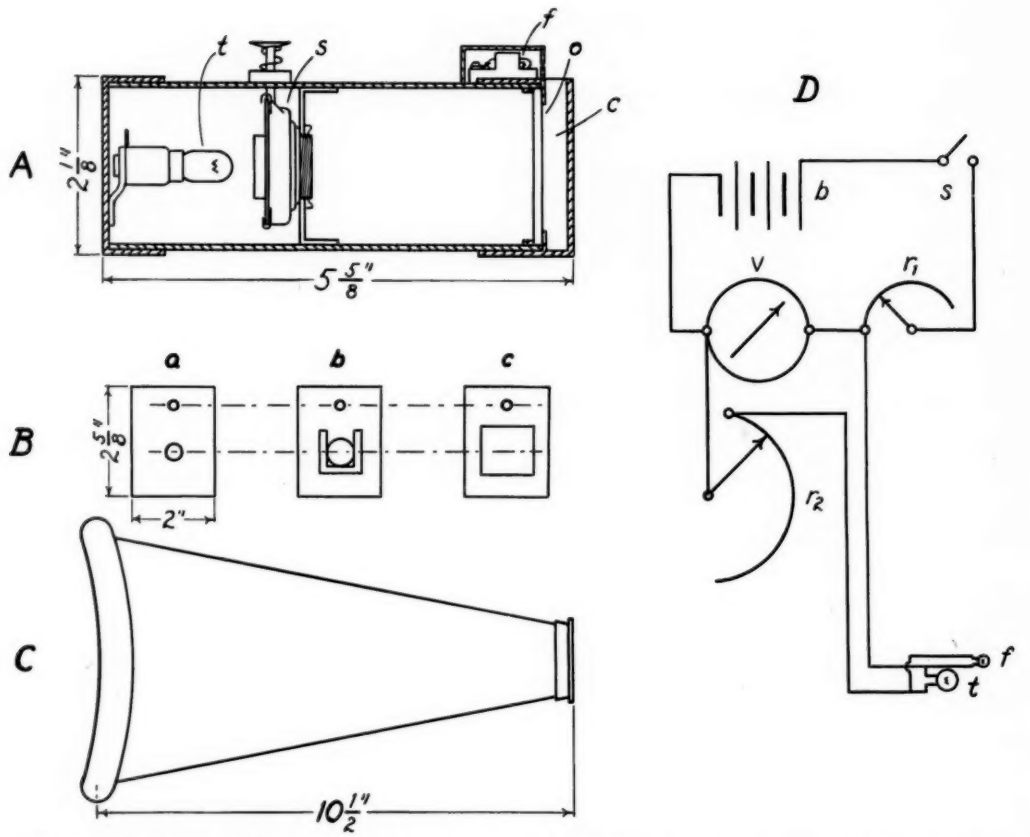


FIG. 2A. Sagittal section of the test unit: *c*, channel for eyepiece and diaphragms; *f*, fixation lamp; *o*, opal glass screen; *s*, shutter; *t*, test lamp. B. The diaphragms, drawn to half the scale of A: (*a*) for field size and position; (*b*) to hold 1-inch square filters; (*c*) the back of the eyepiece. C. Top view of the eyepiece, drawn to half the scale of A. D. The circuit: *b*, storage cells; *s*, on-off switch; $r_1$, rheostat, and *v*, voltmeter, for setting the line voltage; $r_2$, calibrated rheostat for regulating the brightness of *f*, the fixation lamp, and *t*, the test lamp.

natively the operator may hold the test unit in one hand, clicking the shutter with his thumb, while regulating the brightness dial with his other hand.

**Test unit**

A sagittal section of this is shown in Fig. 2A. The removable rear cap bears a radio pilot light receptacle and lamp. The latter is rated at 6–8 volts and 0.15 ampere; since it is always burned at lower voltages it lasts indefinitely. Close to the lamp a photographic shutter is mounted, operated by a spring plunger. This can be set to transmit bulb, time, and 1/25 or 1/50 second exposures. At the front end of the unit an opal glass disk held against a fixed diaphragm 1.5 inches in diameter forms the basic field. Just in front of this is a channel to receive further diaphragms, filters and the eyepiece.

A small housing mounted above the field, which contains a miniature lamp, and at its front a fine opening covered with red Cellophane, provides a red fixation point.

The diaphragms are shown in Fig. 2B. Diaphragm (*a*) fixes the size and position of the field. These may be varied within the limits of the fixed opening at the front of the unit. Fields centered at 6.5° below the fixation point may be varied in diameter up to about 8°. Alternatively a 1° field may be centered from 3° to 10° below the fixation point.

Diaphragm (*b*) bears a frame for 1-inch square

filters. Diaphragm (*c*) is the back of the eyepiece itself. Its square opening fits over the filter frame of (*b*), holding filters securely in position. The complete eyepiece, a top view of which is is shown in Fig. 2C, is made of thin tin-plate, and is cushioned at its front end with sponge rubber. It holds the eyes at a distance of about 11 inches from the field.

**Brightness control**

The circuit of the instrument is shown in Fig. 2D. Current is supplied by three 2-volt low discharge storage cells (Willard DA. 2.1). These are rated at 26 ampere hours and in the present apparatus they function for long periods without recharge or other attention. A voltmeter and 10-ohm rheostat are used to set a standard voltage across the test circuit. The test and fixation lamps are connected in parallel, both in series with a calibrated 40-ohm rheostat with scale. The brightnesses of the test and fixation lights thus rise and fall together, and the fixation light is kept automatically at a level appropriate to each stage of visual adaptation.

## Calibration

The use of a rheostat to regulate brightness is cheap and convenient, but is complicated by the fact that the spectral distribution of the light varies with its intensity. Both factors independently determine the visibility, and for this reason a calibration in terms of absolute energy output should be valueless. This difficulty may be met in two ways:

(1) The test light may be restricted to a narrow spectral band with a "monochromatic" filter. Wave-length changes are thus eliminated, and the rheostat varies the intensity alone. A filter cuts the brightness down to only a few percent of its full value, so that with the present arrangements the highest thresholds could no longer be measured; but this does not seriously interfere with most uses to which the instrument may be put. In general, filters should be employed which transmit in the green, where both cone and rod visibilities are high: the Wratten 74, or the Corning 401 should be suitable. The intensity of the monochromatic light may be calibrated visually or with any available physical method.

(2) So far we have employed a simpler though less elegant procedure with satisfactory results. The full radiation of the test lamp is calibrated visually with a Macbeth illuminometer. This measures the brightness for the human eye, regardless of wave-length composition, compared

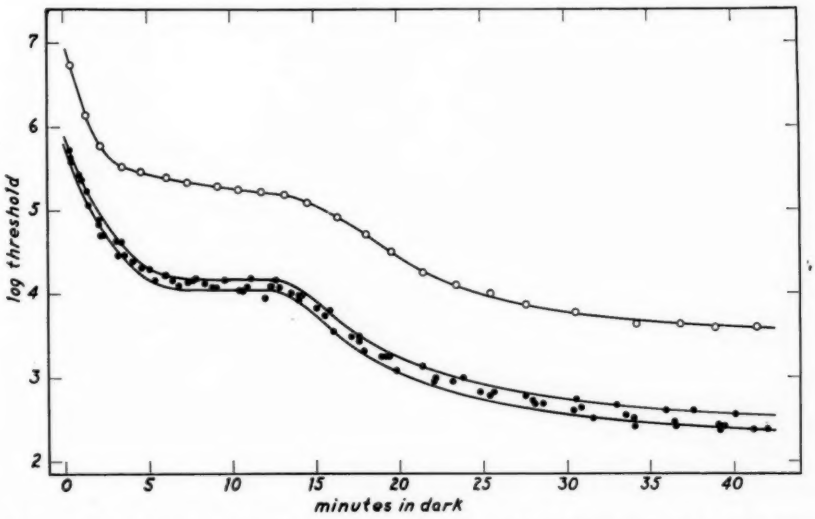


FIG. 3. Dark adaptation following 4 minutes exposure to 2940 millilamberts. Each point represents a single reading of the threshold. *Open circles:* data of one monocular experiment, displaced 1 log unit upward. *Solid circles:* data of four binocular experiments on different days. Thresholds in millimicrolamberts ($10^{-6}$ millilambert). Field 2° in diameter, centered 6° below the fixation point, 1/50 second test flashes.

with a standard white. Such visual measurements can be made with adequate precision over the entire working range of the lamp. The data of Fig. 3 were obtained with this type of calibration.

The total effective range of the present instrument (without filters) is about 4 logarithmic units. This is sufficient to measure the entire extent of dark adaptation under most conditions. Over a range of about 3 log units the variation of log brightness with scale reading is accurately linear. Toward the bottom of the intensity range the brightness falls more rapidly, due perhaps to the reddening of the test light.

## Procedures

### Thresholds

In the course of a measurement the subject looks steadily at the fixation point. The field is set initially at a subthreshold intensity. Either the subject or the operator clicks the shutter about once per second. Between clicks the operator raises the intensity by equal logarithmic steps—equal dial spacings—until the subject reports just seeing the flash of light. It is not necessary that he see the outline of the field. To avoid fatigue such threshold determinations should ordinarily be spaced at least one minute apart.

### Dark adaptation

A series of measurements is shown in Fig. 3. The points are individual readings, obtained with an excellent trained subject. Following 4 minutes light adaptation to 2940 millilamberts, the threshold was measured repeatedly during about 40 minutes in darkness. A 2.0° test field was employed, centered 6.0° below the fixation point, and exposed for flashes of 1/50 second. The initial fall of threshold is due to cone adaptation, and reaches a minimum maintained until about the thirteenth minute. The second fall of threshold to a final level is due to the rods. The monocular run illustrates the precision obtainable in a single experiment. The plot of four binocular experiments shows the day-to-day variability; the data are contained within parallel-sided bands, 0.13 log unit wide for the cones, and 0.17 log unit wide for the rods.

### A survey procedure

For many purposes it is practicable to measure only the threshold of the completely dark adapted eye. This maintains its level indefinitely; it may be checked repeatedly, its scatter determined, and the reliability of the measurement greatly increased by averaging. The final threshold constitutes the most obvious basis for grading absolute visual sensitivities, and is the most sensitive single index of vitamin A deficiency now available.[1] It lends itself readily to the design of a rapid and efficient group procedure.

In our survey work several subjects are admitted to the dark room simultaneously. Measurements on the first subject are begun after about 20 minutes in darkness. Following exposure to ordinary indoor illuminations, dark adaptation is virtually complete within this interval. Readings are continued until 3–6 check determinations have been obtained. As each subject leaves the dark room another enters. In this way, following the initial 20-minute delay, measurements may be continued without interruption. Readings on each subject are usually completed within 5 minutes.

Measurements made in this manner ordinarily scatter within a range of about 0.1 log unit at each sitting, and within 0.3 log unit from day to day. The procedure has not yielded reliable results with children under 6 years of age, nor with about $\frac{1}{4}$ of the subjects aged 6 to 8 years.

# A Chart for Transferring Spherical Coordinates

FRANK BENFORD* AND JOHN E. BOCK†
*General Electric Company, Schenectady, New York*
(Received October 18, 1940)

WHEN dealing with highly unsymmetrical lighting units it is customary to plot the photometric data on a special web that represents a hemisphere centered on the unit. Lines of equal intensity (isocandles) on this web give a detailed analysis of the distribution of light about the unit. It is important for certain engineering purposes that equal spherical areas in all parts of the hemisphere be represented by equal areas on the web. The development of Fig. 1 preserves areas, but there is distortion of form. The isocandle diagram is used as the basis for computing illumination, and for this purpose the north-south axis of the isocandle web should be perpendicular to the plane to be illuminated. This requirement is kept in mind when placing the unit in the photometer for test, but it often happens that some practical advantage is to be gained by installing the unit tilted at a different angle. The computation of illumination when the angles of test and installation do not agree is extremely complicated and is seldom done. For this case it would be useful to have a method of transferring the photometric data to new positions on the web and thus simplify the further work of computing illumination.

In Fig. 2 is shown a plane projection of a hemisphere with equal-angle spaced lines of latitude and longitude, and there is here evident the familiar distortion of areas that goes with this type of projection. If data are to be transferred on this web, using a perpendicular to the center of the web as an axis of rotation, each point moves along an arc of a circle, such as from $(e_1, s_1)$ to $(e_2, s_2)$ and another point will move along an equal arc $(e_3, s_3)$ to $(e_4, s_4)$. These two arcs are equal in angular dimensions but differ in linear length. It would simplify matters if these two arcs could be represented by two straight lines of equal length, and the chart here presented was designed with this plan in mind.

The details of rectifying equal concentric arcs so that they become equal parallel straight lines are given in Fig. 3, and will not be gone into here.

The chart is shown in Fig. 4. The scale of degrees on the right (marked Equator, South Pole, Equator, North Pole, Equator) is the scale used to make all measurements. The point $(e_1, s_1)$ of Fig. 2 has the coordinates 70° from east $(e_1)$ and 30° from south $(s_1)$, and on the chart this point is located at the intersection of the curve from 70° longitude on the central longitude scale, and the curve starting at 30° from the south pole on the right of the chart. The point $(e_1, s_1)$ was rotated counterclockwise through 60° in Fig. 2 and accordingly 60° are measured upward on the chart in a direction parallel to the right-hand scale and having a length taken from the same scale. The new location $(e_2, s_2)$ is found to be (29°, 73°); that is, 29° from the east point of Fig. 2 and 73° from the south pole. A second point (60°, 70°) when rotated 60° counterclockwise moves through the same vertical distance to (57°, 103.5°). This

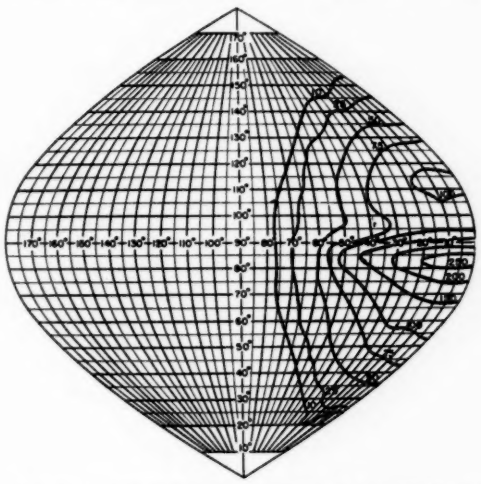

FIG. 1. This true-area development of a hemisphere is used to plot the distribution of intensity of radiation about a lighting unit. The curves shown are isocandles or lines of equal intensity.

* Research Laboratory, General Electric Company.
† Illuminating Laboratory, General Electric Company.

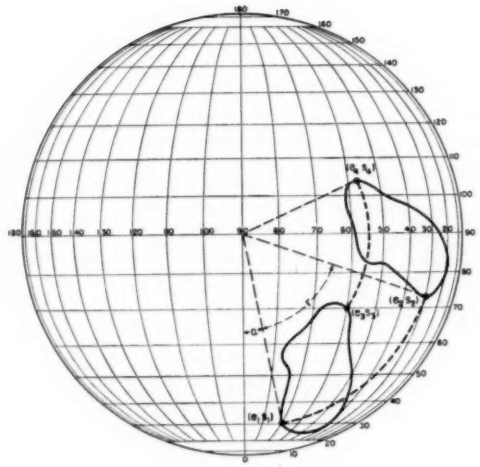

FIG. 2. This is the familiar projection of a hemisphere used in map making and it has distortions of areas that limit its use for engineering purposes. The data curve is shown in two positions 60 degrees apart. The chart here described is intended to facilitate such a transfer without computations, or the use of a distorted-area web.

vertical distance indicates the same angular rotation every place on the chart, and this uniformity of scale makes the use of the chart a relatively simple matter.

If the rotation is in the opposite direction—that is, clockwise on Fig. 2—the direction of transfer is downward as indicated by the arrow near the left edge of the chart.

It will be noted that 90° east occurs on all three longitude scales, at the top, middle and bottom of the chart; in fact, the entire line at the left of the chart is the (90°, 90°) point of Fig. 2. Measurements along this line are meaningless because rotation of the central point of Fig. 2 about itself is meaningless; that is, it produces no change in position.

The top and bottom longitude scales are identical, and they represent the half of the equator to the left of the center of Fig. 2. If the chart is bent into a cylinder so that these two scales are brought into coincidence, then angular measurements can be made across the joining line; these measurements correspond to an arc crossing the 90°–180° section of the equator in Fig. 2.

The scales of longitude are meaningless except on the equator, and the stub marks are given only as a guide in estimating positions between lines. Any radial line from the center of Fig. 2 becomes a straight horizontal line on the chart. The spacings of degree marks along this line are to a non-uniform scale except at the equator, but of course points on it can be evaluated by interpolation between the curves of the web.

The accuracy of any graphical method is always important to know, and a study has been

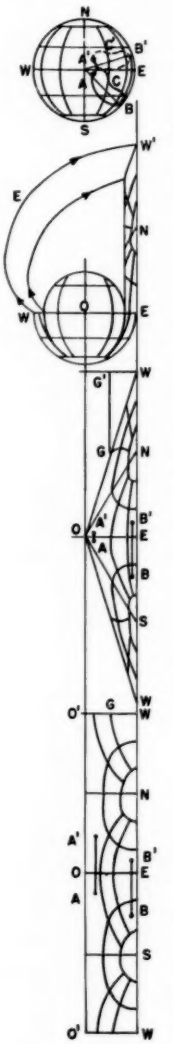


(a) This web is formed by the uniformly spaced lines of longitude and latitude of a hemisphere projected onto the plane of the paper. A curve $A\ B\ C$ is to be moved to a new position $A'B'C'$ by rotation about the center of the web. Each point on the curve moves over a circular arc whose linear length varies as its distance from the center of the web.

(b) If the upper part of the hemisphere is cut into narrow concentric strips, and these strips are pulled around until they are parallel to the vertical axis, any concentric circles on the original projection will become straight parallel lines of unchanged length. The lines of longitude and latitude will be distorted as shown on the right side of the drawing.

(c) When the complete hemisphere has been rectified, a triangular outline results, and the arcs $AA'$ and $BB'$ of Fig. (a) become straight parallel lines $AA'$ and $BB'$. In order to have length $AA'$ equal length $BB'$ it is necessary to extend all vertical elements of (c) to a common length. The vertical element passing through $G$, for example, is uniformly stretched to $G'$ and the triangle is thus changed into a rectangle.

(d) Here all concentric circles of the original projection have been extended to a common length $WEW$, and the original arcs $AA'$ and $BB'$ of unequal linear length have become straight parallel lines of equal length. The measurement of a group of equal circular arcs is obviously more easily made on (d) than on the original web (a).

FIG. 3. The details of changing a spherical projection of the type of Fig. 2 into a projection having the property of representing equal angles by equal straight lines is here outlined.

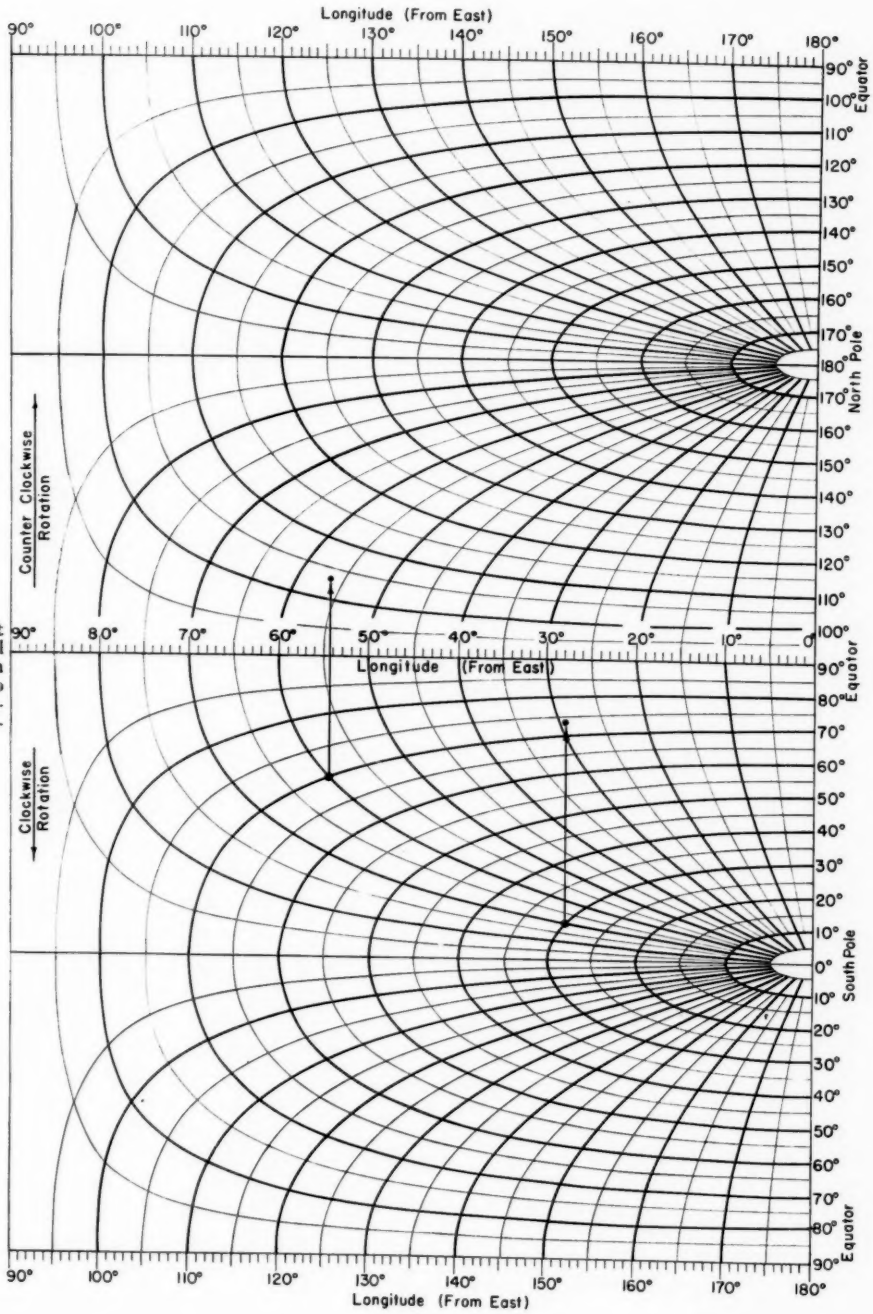
Longitude (From East)
90° 100° 110° 120° 130° 140° 150° 160° 170° 180°
Equator
North Pole
South Pole
Counter Clockwise Rotation
Clockwise Rotation
90° 80° 70° 60° 50° 40° 30° 20° 10° 0°
Longitude (From East)

FIG. 4. This chart is a working model of Fig. 3(d), with changes in scale to improve its accuracy and convenience of use.

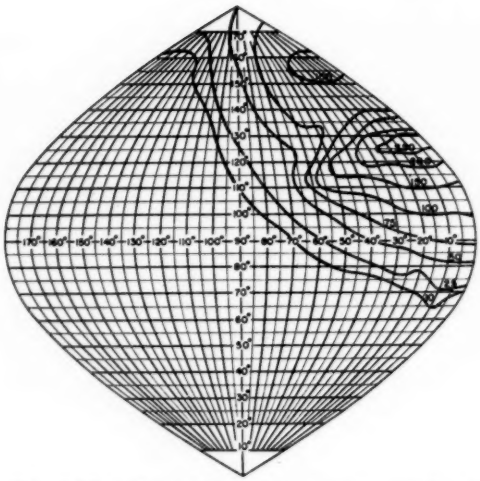

FIG. 5. These isocandles are the same curves as those of Fig. 1, but they have been rotated counterclockwise through 60 degrees. Since the shapes are changed, the curves must be rotated point by point.

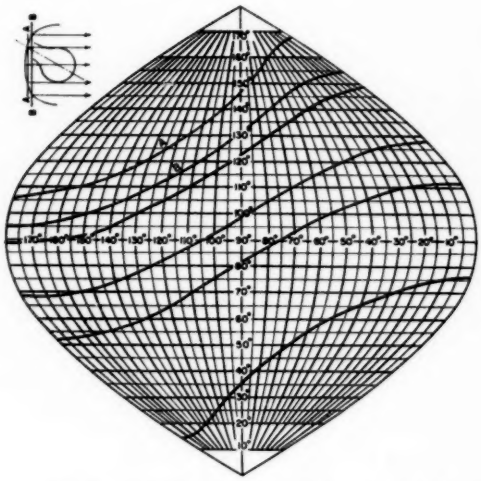

FIG. 6. The plotted curves represent the traces of cones from the light center to boundaries of various zones of a composite form of floodlighting reflector. Radiation in the region above curve *B* falls upon the central paraboloid of the reflector. Light in the region between *A* and *B* is reflected into the floodlight beam without interference, while light in the region above *A* passes through the lamp bulb after reflection.

made on a 12″×18″ white print, using the 64 intersections of the 10° curves in one-quarter of the chart, and making a 60° counterclockwise rotation of the points. The results were compared with accurately computed transfers, and the tabulated results gave the following probable errors for a single reading:

Probable error in longitude = 0.387°;
Probable error in latitude = 0.203°.

The change of coordinates may be computed in cases where the accuracy of the chart is not high enough. In Fig. 2 a point designated as $(e_1, s_1)$ is to be rotated counterclockwise through $r$ degrees, and it is desired to find the new spherical coordinates $(e_2, s_2)$ of the point. It is convenient to introduce an auxiliary angle $a$ measured in the plane of the paper from the north-south axis to a radial line joining the projection of $(e_1, s_1)$ with the center of the sphere. The following equations are arranged for logarithmic computations of $(e_2, s_2)$ from a given value of $(e_1, s_1)$ and $r$.

$$\tan s_1 \cos e_1 = \tan a,$$

$$\frac{\cos s_1 \cos (a+r)}{\cos a} = \cos s_2,$$

$$\frac{\tan (a+r)}{\tan s_2} = \cos e_2.$$

In using the chart it is best for two people to work together, one to read original coordinates and plot the new coordinates, while the other uses the chart. It is found that holding the chart on a drafting board and using a T-square and triangle makes the operation very rapid. If two ink spots are made on a celluloid triangle the proper vertical distance apart, the scales and lines on the chart are left exposed to view and the location and the reading of points are made easier. The isocandle curves of Fig. 5 are the curves of Fig. 1 thus rotated through 45° in a counterclockwise direction. It will be noted that while certain peculiarities of each curve remain recognizable, the general form is distorted. This distortion arises from the distortion of angles on the web that was previously mentioned.

The chart has been used for the design and analysis of multiple surface reflectors. Some of these reflectors were made up of combinations of paraboloids, spheres, and cylinders, and to analyze the complete unit it was necessary to know how much light fell upon each surface. When the lamp was coaxial with the reflector, this analysis was easily enough made from the photometric curve of the lamp; but when the

lamp axis was placed at an angle with that of the reflector, the lamp zones and the reflector zones no longer coincided.

In Fig. 6 the curves represent the angular boundaries of the sections of a reflector when it is tipped 30° to the lamp axis. The isocandles of the lamp are not plotted, as they would be merely straight lines parallel to the lines of latitude of the web. In place of plotting these isocandles, the lumens in each zone were computed and hence the lumens falling on each small quadrilateral of the web is known. The spherical area between the left boundary of the web and curve *A* represents the solid area filled by light falling upon the rear paraboloid of the reflector and then transmitted through the lamp bulb. The area between *A* and *B* is filled with light that is reflected around the edges of the bulb and enters the beam without interference. By counting the number of small quadrilaterals between curves, and giving to each its proper lumen rating, the true zonal lumens are found. The computation can then be finished by correcting the light from each reflector zone for reflection and transmission losses. This process, when carried out for all the zones of the mirror, leads to a figure for the performance of the complete reflector. The work of computing and comparing various designs is thus brought within practical limits of time and effort.

# The Refractive Index of Liquid Water in the Near Infra-Red Spectrum

MELCHOR CENTENO V
*New York, New York*

(Received January 8, 1941)

THE dispersion of liquid water was investigated by Rubens[1] to wave-length 1.256 microns and by Seegert[2] to 2.327 microns, by means of the refractometer. Rubens and Ladenburg[3] extended the range to 18 microns by applying the Cauchy formula[4] of the reflection of unpolarized radiation at normal incidence

$$R=[(n-1)^2+g^2]/[(n+1)^2+g^2],$$

where $R$ is the reflectivity, $g$ the extinction coefficient and $n$ the relative index of refraction, at the interface. The extinction coefficient is the numerical exponent in the Bouguer-Lambert relation giving the transmission through a thickness of material equal to the wave-length divided by $4\pi$. Knowing the reflectivity and the extinction coefficient, the Cauchy formula renders the corresponding value of the index of refraction relative to air, since the first two quantities are usually measured in air.

The formula has been verified experimentally in numerous instances,[5] in the regions of normal as well as in the regions of anomalous dispersion.

In computing the values of $n$ for liquid water by means of the formula, Rubens and Ladenburg used values of $R$ and $g$ which were not accurate. Therefore, it was thought desirable to repeat the computations using the more accurate values of the reflectivity and extinction coefficient of water which are now available.

The *reflectivity* of liquid water has been measured by various investigators.[6] From the average of their results, the smoothed-mean values given in the second column of Table I were graphically secured.

From the general reviews,[7] the compilations[8] and the results of other investigations[9] of the absorption of radiation by liquid water, average values were obtained to a wave-length of 8.5 $\mu$.

The results of the transmission measurements

[1] H. Rubens, Ann. d. Physik **45**, 253 (1892).
[2] B. Seegert, Dissertation, Berlin Universität (1908).
[3] H. Rubens and E. Ladenburg, Verh. d. D. Phys. Ges. **1**, No. 1, 16 (1909).
[4] A. L. Cauchy, Comptes rendus **8**, 560 (1839); J. Jamin, Ann. de chim. et phys. **22**, 311 (1848); A. Beer, Pogg. Ann. **92**, 402 (1854); F. Eisenlohr, Pogg. Ann. **104**, 337 and 346 (1858); P. Drude, *Physik des Aethers* (1894), p. 557.
[5] See, for example:
B. Walter, *Die Oberflächen oder Schiller Farben* (Vieweg, Braunschweig, 1895), p. 31.
A. Pflüger, Ann. d. Physik **65**, 173 (1898).
R. W. Wood, Phys. Rev. [1] **14**, 315 (1902).
A. Minor, Ann. d. Physik **10**, 581 (1903).
C. K. Edmunds, Phys. Rev. [1] **18**, 193, 385 (1904).
A. H. Pfund, Astrophys. J. **24**, 19 (1906).
J. T. Tate, Phys. Rev. [1] **34**, 321 (1912).
R. B. Wilsey, Phys. Rev. **8**, 391 (1916).
M. Czerny, Zeits. f. Physik **65**, 600 (1930).
Cl. Schaefer, Zeits. f. Physik **75**, 687 (1932).

[6] A. H. Pfund, reference 5.
H. Rubens and E. Ladenburg, Verh. d. D. Phys. Ges. **10**, 227 (1908); also Sitz. Preuss. Akad. Wiss. **274**, 1140 (1908); also reference 3.
F. Gehrts, Ann. d. Physik **47**, 1059 (1915).
K. Brieger, Ann. d. Physik **57**, 287 (1918).
E. P. T. Tyndall, Int. Crit. Tab. (compilation) **5**, 256 (1929).
M. Weingeroff, Zeits. f. Physik **70**, 104 (1931).
[7] F. E. Fowle, Smith. Misc. Coll. **68**, No. 8 (Publ. 2484) (1917).
J. Lecompte, Trans. Faraday Soc. **25**, 864 (1929).
Cl. Schaefer and F. Matossi, *Das Ultrarote Spektrum* (J. Springer, Berlin, 1930).
L. H. Dawson and E. O. Hulburt, J. Opt. Soc. Am. **24**, 175 (1934).
[8] J. Becquerel and J. Rossignol, Int. Crit. Tab. **5**, 268 (1929).
N. E. Dorsey, *Properties of Ordinary Water Substance In all Its Phases* (Reinhold, 1940), Table 160.
[9] E. Aschkinass, Ann. d. Physik [3] **55**, 401 (1895).
H. Kreusler, Ann. d. Physik [4] **6**, 412 (1901). As corrected by N. E. Dorsey (reference 8).
W. W. Coblentz, Bull. Bur. Stand. **2**, No. 3, 457 (1906).
W. W. Coblentz, Bull. Bur. Stand. **7**, No. 4, 619 (1911).
D. A. Goldhammer, *Dispersion und Absorption des Lichtes* (Teubner, Leipzig, 1913).
E. J. Schaeffer, M. G. Paulus and H. C. Jones, Physik. Zeits. **15**, 447 (1914).
J. R. Collins, Phys. Rev. **20**, 486 (1922).
T. Dreisch, Zeits. f. Physik **30**, 200 (1924).
E. K. Plyler, J. Opt. Soc. Am. **9**, 545 (1924).
S. W. Leifson, Astrophys. J. **63**, 73 (1926).
J. Kaplan, J. Opt. Soc. Am. **14**, 251 (1927).
E. O. Hulburt, J. Opt. Soc. Am. **17**, 15 (1928).
K. Tsukamoto, Rev. d'optique **7**, 89 (1928). As corrected by N. E. Dorsey (reference 8).
C. D. Hodgman, J. Opt. Soc. Am. **23**, 426 (1933).
E. Haas, Biochem. Zeits. **282**, 224 (1935).
D. Williams, R. D. Weatherford and E. K. Plyler, J. Opt. Soc. Am. **26**, 149 (1936).
J. R. Collins, Phys. Rev. **55**, 470 (1939).
G. Hüfner and E. Albrecht, Wied. Ann. **42**, 1 (1891).
W. H. Julius, Verh. Konink. Neder. Akad. Wet. **1**, No. 1 (1892).
F. Paschen, Wied. Ann. **51**, 21; **52**, 216; **53**, 334 (1894).
W. W. Coblentz, Phys. Rev. [1] **20**, 252 (1905); [1] **23**, 125 (1906).
J. J. Fox and A. E. Martin, Proc. Roy. Soc. London **174**, 234 (1940).

TABLE I. *Optical constants of water in the near infra-red.*

| WAVE-LENGTH IN MICRONS | PERCENTAGE REFLECTIVITY | EXTINCTION COEFFICIENT | REFRACTIVE INDEX | WAVE-LENGTH IN MICRONS | PERCENTAGE REFLECTIVITY | EXTINCTION COEFFICIENT | REFRACTIVE INDEX | WAVE-LENGTH IN MICRONS | PERCENTAGE REFLECTIVITY | EXTINCTION COEFFICIENT | REFRACTIVE INDEX |
|---|---|---|---|---|---|---|---|---|---|---|---|
| 1.00 | 1.96 | $3.5\times10^{-6}$ | 1.326 | 4.03 | 2.19 | 0.00642 | 1.347 | 7.80 | 1.68 | 0.0472 | 1.294 |
| 1.05 | 1.95 | 3.1 | 1.325 | 4.10 | 2.18 | 0.00709 | 1.346 | 8.00 | 1.66 | 0.0472 | 1.292 |
| 1.10 | 1.94 | 1.7 | 1.324 | 4.20 | 2.16 | 0.00871 | 1.344 | 8.20 | 1.64 | 0.0472 | 1.289 |
| 1.20 | 1.93 | $1.21\times10^{-5}$ | 1.323 | 4.30 | 2.15 | 0.0108 | 1.343 | 8.40 | 1.62 | 0.0473 | 1.287 |
| 1.30 | 1.91 | 1.29 | 1.321 | 4.40 | 2.14 | 0.0133 | 1.342 | 8.60 | 1.57 | 0.0476 | 1.282 |
| 1.40 | 1.90 | $1.30\times10^{-4}$ | 1.320 | 4.50 | 2.13 | 0.0164 | 1.341 | 8.80 | 1.51 | 0.0483 | 1.276 |
| 1.50 | 1.88 | 3.12 | 1.318 | 4.60 | 2.11 | 0.0194 | 1.339 | 9.00 | 1.44 | 0.0498 | 1.268 |
| 1.60 | 1.87 | 1.12 | 1.316 | 4.70 | 2.10 | 0.0202 | 1.338 | 9.2 | 1.35 | 0.0518 | 1.257 |
| 1.70 | 1.85 | 1.08 | 1.315 | 4.80 | 2.08 | 0.0199 | 1.336 | 9.4 | 1.27 | 0.0542 | 1.247 |
| 1.80 | 1.82 | 1.43 | 1.312 | 4.90 | 2.05 | 0.0188 | 1.334 | 9.6 | 1.18 | 0.0562 | 1.236 |
| 1.90 | 1.79 | 8.14 | 1.309 | 5.00 | 2.02 | 0.0169 | 1.331 | 9.8 | 1.09 | 0.0595 | 1.224 |
| 2.00 | 1.74 | 14.3 | 1.304 | 5.10 | 1.98 | 0.0152 | 1.327 | 10.0 | 0.99 | 0.0601 | 1.212 |
| 2.20 | 1.63 | 5.11 | 1.293 | 5.20 | 1.93 | 0.0143 | 1.322 | 10.2 | 0.92 | 0.0621 | 1.202 |
| 2.40 | 1.47 | 10.1 | 1.276 | 5.30 | 1.86 | 0.0143 | 1.315 | 10.4 | 0.85 | 0.0687 | 1.190 |
| 2.50 | 1.37 | 20.1 | 1.265 | 5.40 | 1.80 | 0.0146 | 1.309 | 10.6 | 0.78 | 0.0802 | 1.175 |
| 2.60 | 1.25 | 51.8 | 1.252 | 5.50 | 1.73 | 0.0174 | 1.302 | 10.8 | 0.73 | 0.0946 | 1.159 |
| 2.70 | 0.96 | 0.0183 | 1.216 | 5.60 | 1.66 | 0.0232 | 1.295 | 10.9 | 0.70 | 0.0993 | 1.150 |
| 2.74 | 0.75 | 0.0273 | 1.187 | 5.70 | 1.57 | 0.0340 | 1.284 | 11.0 | 0.72 | 0.1138 | 1.143 |
| 2.77 | 0.90 | 0.0364 | 1.206 | 5.80 | 1.40 | 0.0515 | 1.263 | 11.1 | 0.77 | 0.1290 | 1.137 |
| 2.80 | 1.41 | 0.0490 | 1.266 | 5.85 | 1.25 | 0.0653 | 1.242 | 11.2 | 0.84 | 0.1471 | 1.129 |
| 2.85 | 2.00 | 0.0578 | 1.324 | 5.90 | 1.50 | 0.0799 | 1.266 | 11.3 | 0.92 | 0.1637 | 1.121 |
| 2.90 | 2.48 | 0.0637 | 1.367 | 6.00 | 2.02 | 0.1220 | 1.304 | 11.4 | 0.97 | 0.1751 | 1.114 |
| 2.95 | 2.87 | 0.0670 | 1.401 | 6.04 | 2.16 | 0.1372 | 1.312 | 11.5 | 1.02 | 0.1831 | 1.111 |
| 3.00 | 3.40 | 0.0680 | 1.446 | 6.10 | 2.28 | 0.1216 | 1.331 | 11.6 | 1.09 | 0.1880 | 1.118 |
| 3.02 | 3.90 | 0.0683 | 1.453 | 6.20 | 2.46 | 0.0940 | 1.358 | 11.7 | 1.19 | 0.1937 | 1.130 |
| 3.07 | 4.39 | 0.0682 | 1.525 | 6.30 | 2.34 | 0.0768 | 1.352 | 11.8 | 1.30 | 0.1991 | 1.144 |
| 3.10 | 4.30 | 0.0681 | 1.517 | 6.40 | 2.22 | 0.0626 | 1.344 | 12.0 | 1.47 | 0.2058 | 1.165 |
| 3.16 | 4.12 | 0.0658 | 1.504 | 6.50 | 2.12 | 0.0524 | 1.336 | 12.5 | 2.15 | 0.2438 | 1.219 |
| 3.20 | 4.00 | 0.0611 | 1.495 | 6.60 | 2.05 | 0.0462 | 1.331 | 13.0 | 3.02 | 0.2918 | 1.270 |
| 3.30 | 3.65 | 0.0370 | 1.471 | 6.70 | 2.00 | 0.0450 | 1.326 | 13.5 | 3.55 | 0.3202 | 1.297 |
| 3.40 | 3.37 | 0.0225 | 1.449 | 6.80 | 1.98 | 0.0448 | 1.324 | 14.0 | 4.10 | 0.3582 | 1.309 |
| 3.50 | 3.05 | 0.0128 | 1.423 | 6.90 | 1.97 | 0.0451 | 1.323 | 14.5 | 4.72 | 0.4028 | 1.313 |
| 3.60 | 2.80 | 0.00783 | 1.402 | 7.00 | 1.95 | 0.0457 | 1.321 | 15.0 | 5.12 | 0.4298 | 1.315 |
| 3.70 | 2.59 | 0.00619 | 1.381 | 7.20 | 1.87 | 0.0463 | 1.313 | 16.0 | 5.29 | 0.4088 | 1.374 |
| 3.80 | 2.36 | 0.00596 | 1.363 | 7.40 | 1.77 | 0.0466 | 1.303 | 17.0 | 6.15 | 0.4070 | 1.468 |
| 3.90 | 2.25 | 0.00590 | 1.353 | 7.60 | 1.72 | 0.0484 | 1.298 | 18.0 | 6.21 | 0.4585 | 1.401 |

made by Rubens and Ladenburg[3] on a thin film of water containing ten percent of glycerin were corrected for the reflection[10] and the absorption[11] due to glycerin, and for the reflection due to water (by means of the smoothed-mean values already obtained). These corrections were made under the hypothesis, practically correct in view of the small percentage of glycerin, that the reflective and absorptive effects were directly proportional to the respective amounts of water and glycerin forming the film. In this manner, the absorption of liquid water was determined to 18 $\mu$.

TABLE II. *Dispersion of water, from the ultraviolet to the near infra-red. At 20°C.*

| WAVE-LENGTH IN MICRONS | REFRACTIVE INDEX | WAVE-LENGTH IN MICRONS | REFRACTIVE INDEX |
|---|---|---|---|
| 0.1151 | Met. refl. | 0.65628 | 1.331151 |
| 0.1829 | 1.46379 | 0.70652 | 1.330019 |
| 0.20255 | 1.41993 | 0.76820 | 1.32890 |
| 0.25020 | 1.37734 | 0.808 | 1.3286 |
| 0.30822 | 1.35671 | 0.871 | 1.3273 |
| 0.35871 | 1.34795 | 0.943 | 1.3262 |
| 0.40466 | 1.342724 | 1.028 | 1.3250 |
| 0.44715 | 1.339423 | 1.130 | 1.3234 |
| 0.50157 | 1.336363 | 1.256 | 1.3215 |
| 0.54607 | 1.334466 | 1.617 | 1.3149 |
| 0.58926 | 1.332988 | 1.968 | 1.3078 |

The calculated values of the *extinction coefficient g* are given in the third column of Table I. From these and the smoothed-mean values of $R$, the corresponding values of the *index of refraction*

[10] A. H. Pfund, reference 5.

[11] C. Friedel, Ann. d. Physik [3] **55**, 453 (1895).
W. Weniger, Phys. Rev. **31**, 388 (1910).
W. W. Coblentz, Bur. Stand. Sci. Papers, No. 418 (1921).

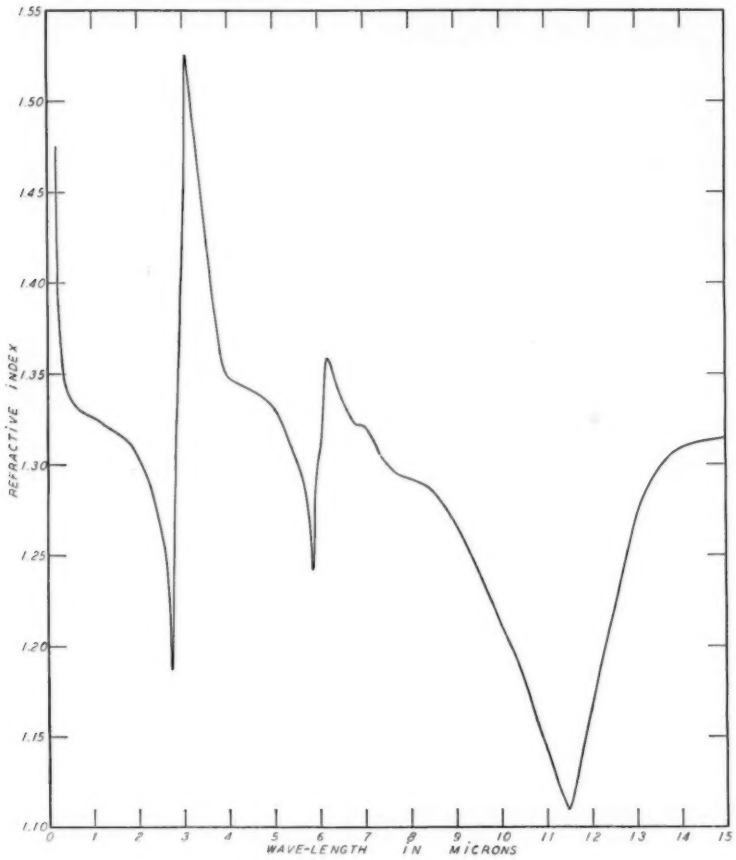


FIG. 1. Dispersion of water in the near infra-red.

$n$ given in the last column of Table I were calculated.

The values of $R$, $g$ and $n$ are for a temperature of 20°C, excepting those of $g$ for wave-lengths greater than 9 microns, for which the temperature is 18°C.

The values of the index given in Table II were obtained from the following sources: for the ultraviolet from the compilation by Chéneveau;[12] for the visible region from Tilton and Taylor[13] and from the compilation by Dorsey;[14] and the infra-red values, from Seegert[2] whose measurements were made at 19.8°C, and partially (up to 1.256 microns) from Rubens[1] whose measurements were made at 12°C. Rubens' values were corrected to 20°C by extrapolating the temperature coefficient of the visible region.[15] The averages of Seegert's and Rubens' values are those given in Table II.

Since the precision of measurement is not great, the error of extrapolating the temperature coefficient to 1.256 microns is probably negligible. Similarly, a correction for a temperature difference of two degrees in the extinction coefficient beyond 9 microns, would not affect the values of the index given in Table I.

Seegert[2] determined an index of 1.2997 for a wave-length of 2.327 microns. This is probably incorrect, due perhaps to the difficulties of using the Abbe refractometer at a wave-length where

[12] C. Chéneveau, Int. Crit. Tab. **7**, 12 (1929).
[13] L. W. Tilton and J. K. Taylor, J. Research Nat. Bur. of Stand. **20**, 419 (1938). (R.P. 1085.)
[14] N. E. Dorsey, reference 8, Table 137.
[15] N. E. Dorsey, reference 8, Tables 135 and 141.

water has a strong absorption ($g=7.04\times10^{-4}$). The Rubens and Ladenburg[3] values lead to an index of 1.283, and Table I to an index of 1.282, at the same wave-length.

In Fig. 1 are plotted the values of the index as a function of the wave-length. The principal maxima and minima are located as follows:

*Maxima:* 1.525 at 3.07 $\mu$
1.358 at 6.20 $\mu$
*Minima:* 1.187 at 2.74 $\mu$
1.242 at 5.85 $\mu$
1.110 at 11.47 $\mu$.

There appears to be another maximum of 1.47 at about 17.1 $\mu$.

The values of the maxima are larger and of the minima smaller than the corresponding values found by Rubens and Ladenburg. The spectral locations of the maxima and minima are also different.

The minima are particularly interesting because they indicate little diffusion of radiation through a cloud of water droplets, as compared, for example, with that existing in the visible region.

# Oscillator Strengths for the Liquid Phase*

ARCHIE I. MAHAN†
*The Johns Hopkins University, Baltimore, Maryland*
(Received December 19, 1940)

The following paper gives a discussion of the methods involved in evaluating the oscillator strengths from both the dispersion and absorption equations for liquids. The resulting equations are then applied to a set of infra-red bands on which the absorption and dispersion were measured.

## THEORY

FROM the standpoint of the classical theory of absorption and dispersion, any absorbing medium can be looked upon as being made up of a series of charged particles which, under the influence of some outside disturbance, may vibrate about given positions of equilibrium. These particles may, with sufficient approximation, be regarded as harmonically bound to these rest positions. Any such oscillator suspended in the liquid phase through which an electromagnetic wave is traveling will be subjected to three forces in addition to the assumed type of binding force: The first will be the frictional force, the second the field of force created by the other closely adjacent oscillators, and the last that due to the electromagnetic wave itself as it progresses through the medium. If one assumes a frictional force to be proportional to the velocity of the motion, it can be shown[1] that the reaction of the medium to the electromagnetic wave is given by[2]

$$m'd^2P/dt^2+bdP/dt+kP = N\epsilon^2(E_0e^{i\omega t}+4\pi P/3), \quad (1)$$

$m'$ being the reduced mass of the oscillator, $P$ the polarization per unit volume, $b$ the damping coefficient, $k$ the binding constant, $N$ the number of polarizable particles per unit volume, $E_0$ the electrical amplitude of the incoming electromagnetic wave of frequency $\nu$, and $\epsilon$ the effective charge of the oscillator.

If one solves this equation in detail,[1] the solution results in a refractive index given by

$$n^2=1+\frac{4\pi N\epsilon^2/m'}{\omega_0^2-4\pi N\epsilon^2/3m'-\omega^2+ib\omega/m'}, \quad (2)$$

where $\omega_0=(k/m')^{\frac{1}{2}}$ is $2\pi$ times the frequency of the free undamped oscillator, and $\omega$ is $2\pi$ times the frequency of the incoming wave. The significance of a complex refractive index is well known in classical physics,[3] for it is quite easy to show that it represents an absorption given by Lambert's law which is of the form

$$I_z=I_0e^{-4\pi\nu n'\kappa z/c}, \quad (3)$$

$I_0$ being the initial intensity, $I_z$ the intensity a distance $z$ into the medium, $n'$ the real part of the refractive index and $n'\kappa$ the imaginary part. In order to determine the rate of energy decay with distance, Eq. (2) must be separated into its real and imaginary parts. Performing this operation results in the familiar equations[4]

$$n'^2(1-\kappa^2)=1+\sum_0\frac{N\epsilon^2f_0/\pi m'\cdot(\bar\nu_0^2-\nu^2)}{(\bar\nu_0^2-\nu^2)^2+(b_0\nu/2\pi m')^2}, \quad (4)$$

$$2n'^2\kappa=\sum_0\frac{N\epsilon^2f_0/\pi m'\cdot(b_0\nu/2\pi m')}{(\bar\nu_0^2-\nu^2)^2+(b_0\nu/2\pi m')^2}, \quad (5)$$

where a change to frequency units has been made and $\bar\nu_0^2=\nu_0^2-Nf_0\epsilon^2/3\pi m'$. The previous $N_0$ has now been replaced by a product $Nf_0$ where $f_0$ has the meaning of the number of oscillators per molecule with charge $\epsilon$ and resonant frequency $\bar\nu_0$ and $N$ is now the number of molecules

* Submitted in partial fulfillment of the degree of Doctor of Philosophy from The Johns Hopkins University, Baltimore, Maryland, June, 1940.
† Now at Georgetown University.
[1] J. C. Slater and N. H. Frank, *Introduction to Theoretical Physics* (McGraw-Hill, New York, 1933), p. 276, 279.
[2] Actually the system must be looked upon as consisting of a number of coupled oscillators representable by a coupled system of linear equations. Such a set can be transformed however to the above form employing normal coordinates.
[3] *Handbuch der Physik* (1928), Vol. XX, p. 496.
[4] M. Born, *Optik* (Julius Springer, Berlin, 1933), p. 478 without assumptions for simplicity.

per cm³. Liquids therefore show the same type of absorption and dispersion as usually identified with gases except that the position of the maximum $\nu_0$ is shifted toward longer waves. Experimentally, such a shift is too small to be observed although there are exceptions.[5] A summation sign is included with each of the above expressions for, at any one frequency, several bands may make contributions to both of these values.

If now one had a band of the above simple form ($n'^2\kappa$ *vs.* $\nu$), it would be desirable to know the characteristic constants of the oscillator which would represent it. The values of $b_0$ and $k$ can be found from the width of the band at half its maximum and the position of the maximum. The other remaining constant $f_0$ can be evaluated in two ways. The first is to set the impressed frequency equal to $\bar{\nu}_0$ and find it from Eq. (5). ($f_0=b_0\bar{\nu}_0/N\epsilon^2 . n'^2\kappa$.) This method although theoretically exact proves of little consequence practically, for the calculation rests upon a single point and even if the band were almost of the above simple form, a large error might result. The better way is to measure the area under the curve given by Eq. (5). This means using a planimeter and graphically evaluating $\int_0^\infty n'^2\kappa d\nu$. If then we let $x=\nu^2$, it will be found that Eq. (5) is directly integrable. If for convenience we let $\gamma=b_0/2\pi m'$, we get when substituting limits and solving for $f_0$ [6]

$$f_0=\frac{2\pi m'/N\epsilon^2 \; (4\bar{\nu}_0^2-\gamma^2)^{\frac{1}{2}}\int_0^\infty n'^2\kappa d\nu}{\pi/2-\tan^{-1}\left[(\gamma^2-2\bar{\nu}_0^2)/\gamma(4\bar{\nu}_0^2-\gamma^2)^{\frac{1}{2}}\right]}. \quad (6)$$

In making the graphical integration, it is assumed that the effect of distant bands is removed by extrapolation so that the summation sign can be eliminated before the above actual integration. If, in addition, the width of the line at half-maximum is small compared with the frequency of the line itself, the above expression will reduce to the more familiar form

$$f_0=\frac{4\bar{\nu}_0 m'}{N\epsilon^2}\int_0^\infty n'^2\kappa d\nu. \quad (7)$$

Assuming $\rho$ to be the density of the liquid, $M'$ the relative molecular weight of the oscillator representing the absorption band ($M'=m'N_1$ where $N_1$ is Avogadro's number), and $M$ the molecular weight of the liquid, and evaluating constant terms, this equation can be reduced to a form more accessible for liquids. If the frequency of the middle of the band is expressed in units of $10^{13}$, the above equation becomes

$$f_0=4.7791\times10^{-16}(MM'/\rho)\bar{\nu}_0\int_0^\infty n'^2\kappa d\nu. \quad (8)$$

If, therefore, one measures the transmission (using Eq. 3 with corrections for losses) and dispersion (using hollow prism or critical angle methods), it is then an easy task to evaluate the oscillator strength of a given band from the above equation. Proceeding as we have in this manner, we have stayed very close to Eq. (5) and have made a minimum of restrictions (assumed the magnetic permeability equal to unity in arriving at Eq. (2) and that the width at half-maximum is small compared to the frequency of the line). If still more rigor is desired, Eq. (6) can be used.

In a similar manner one should expect that the value of $f_0$ could be found from dispersion data using Eq. (4), and such is the case. Herzfeld[7] using this equation as a starting point found an expression for $f_0$ for the case of weak absorption. The equation here developed is applicable for the cases of both weak and strong absorption and does not make it necessary to follow the dispersion through the band as was necessary in the previously cited equation.

In any set of refractive index measurements, the total refractive index can be looked upon as being made up of two parts, that contribution made by the band itself and that part made by the contribution of more distant bands. If these more distant contributions are grouped into a term $n_0$ (also a function of the frequency) and the substitutions $A=N\epsilon^2 f_0/\pi m'$ and $\gamma=b_0/2\pi n'$

[5] *Handbuch der Physik*, Vol. XX, p. 514; Cl. Schaeffer and F. Matossi, *Das Ultra Rote Spektrum* (Julius Springer, Berlin, 1930), p. 242; J. R. Collins, Phys. Rev. **55**, 470 (1939); J. J. Fox and A. E. Martin, Proc. Roy. Soc. **167A**, 257 (1938).

[6] The total refractive index must be used in all these calculations for it is this which determines the velocity of propagation of the wave in the frequency range of the absorption and not that in which the effect of more distant bands has been removed by extrapolation.

[7] K. F. Herzfeld, J. Opt. Soc. Am. **29**, 355 (1939).

are made for simplicity, Eq. (4) may be written (neglecting $\kappa^2$ which is of the order of $10^{-8}$ for liquids)

$$n'^2 = n_0^2 + \frac{A(\bar{\nu}_0^2 - \nu^2)}{(\bar{\nu}_0^2 - \nu^2)^2 + \gamma^2\nu^2}. \tag{9}$$

If this expression is solved for $\gamma^2$ and a change to wave-length units is made, it may be written in the form

$$\gamma^2 = \frac{A(\lambda^2 - \lambda_0^2)}{\lambda_0^2(n'^2 - n_0^2)} - \frac{c^2(\lambda^2 - \lambda_0^2)}{\lambda_0^4\lambda^2}, \tag{10}$$

where $c$ is the velocity of light in vacuum. Even in the case of an ideal set of bands, $\gamma$ would be difficult to evaluate particularly in the presence of a large gradient in the background dispersion. If however $n'$ and $n_0$ are determined for two different sets of wave-lengths in the vicinity of the band, two equations of the above form will be obtained which may be equated and the necessity for knowing $\gamma$ will be eliminated. If these two sets of values are designated by $n_1'$, $n_1^0$, $\lambda_1$, and $n_2'$, $n_2^0$, $\lambda_2$, the resulting equation when solving for $A$ is

$$A = \frac{c^2(\lambda_1^4\lambda_2^2 + \lambda_2^2\lambda_0^4 - \lambda_2^4\lambda_1^2 - \lambda_0^4\lambda_1^2)}{\lambda_0^2\lambda_1^2\lambda_2^2\left\{\dfrac{\lambda_1^2 - \lambda_0^2}{n_1'^2 - n_1^{02}} - \dfrac{\lambda_2^2 - \lambda_0^2}{n_2'^2 - n_2^{02}}\right\}}. \tag{11}$$

If the term outside the brackets in the denominator is included in the numerator and $A$ is replaced by its equivalent value, $f_0$ assumes the value

$$f_0 = \frac{\pi m' c^2}{N\epsilon^2} \cdot \frac{(\lambda_1^2 - \lambda_2^2)(1/\lambda_0^2 - \lambda_0^2/\lambda_1^2\lambda_2^2)}{\dfrac{\lambda_1^2 - \lambda_0^2}{n_1'^2 - n_1^{02}} - \dfrac{\lambda_2^2 - \lambda_0^2}{n_2'^2 - n_2^{02}}}. \tag{12}$$

When the suggested substitutions made in Eq. (8) are included and the constant coefficients evaluated, the equation becomes (if the wave-length is expressed in microns)

$$f_0 = 3.3782\frac{MM'}{\rho} \cdot \frac{(\lambda_1^2 - \lambda_2^2)(1/\lambda_0^2 - \lambda_0^2/\lambda_1^2\lambda_2^2)}{\dfrac{\lambda_1^2 - \lambda_0^2}{n_1'^2 - n_1^{02}} - \dfrac{\lambda_2^2 - \lambda_0^2}{n_2'^2 - n_2^{02}}}. \tag{13}$$

If, therefore, the dispersion curve under observation follows that of the linear harmonic oscillator (follows Eq. (4)), the oscillator strength can be evaluated from the above equation. The positions of $\lambda_1$ and $\lambda_2$ are unspecified so that the equation has the additional theoretical advantage that the oscillator strength can be evaluated from measurements far removed from the band center if the background dispersion can be extrapolated out.

Formally, therefore, there is no difficulty in evaluating the $f_0$'s from either the real or imaginary parts of the complex refractive index if the nature of the oscillator $m'$ is known. In many cases, however, there is no way of finding the value of $\epsilon$, and since $f_0$ can have no definite value without knowing $\epsilon$, it is always assumed identical with the charge of the electron. When once the oscillator strength is known, it requires but a simple calculation to evaluate[8] the transition probabilities so that the characteristics of the oscillator representing the absorption can be completely determined if it behaves like a harmonic oscillator with the simple type of damping assumed in Eq. (1).

Frequently as suggested earlier, one is confronted with bands which do not have the simple form discussed in the above equations. In this case the same experimental procedure of evaluating $n'$ and $n'\kappa$ can be followed and the values of $n'^2\kappa$ as a function of the frequency plotted. The total area under the curve (designated by $T$) can then be resolved into a series of areas of the above suggested form so that one can write

$$\int_T n'^2\kappa d\nu = \int_1 n'^2\kappa d\nu + \int_2 n'^2\kappa d\nu + \cdots. \tag{14}$$

If now these integrals are replaced by their equivalents (Eq. (7)), it can be seen that

$$f_T = {}_n\Sigma f_n \tag{15}$$

only if all the $m$'s and $\bar{\nu}_0$'s are identical. If, therefore, the line is not too broad, an oscillator strength can be evaluated and associated with the band in the same manner as with the more simple form discussed above. If the band is very broad, the same procedure can still be followed, but in this case the individual $f_0$'s must be multiplied by a term which is the ratio of the frequency

[8] A. Einstein, Physik. Zeits. **18**, 121 (1917).

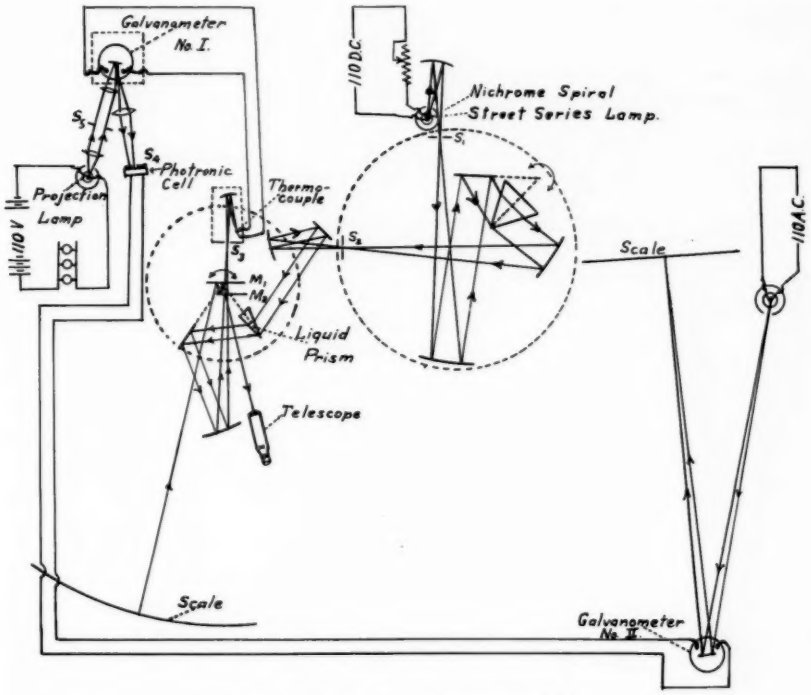


FIG. 1. Infra-red dispersion spectrograph.

of the maximum position of the large band to that of the component band considered. Equation (13) will not, in general, lend itself to bands which have shapes other than that predicted by the above Eq. (4), for plainly the $f_0$ is entirely dependent upon the choice of the refractive index at two points. If the band is not of this simple form, the value of $f_0$ will depend upon the choice of the wave-length at which the calculations are made instead of being a characteristic constant for the entire band. This method then yields at best an approximation and depends upon how nearly the actual conditions approach the above suggested form.[9]

[9] Theoretically, the better way to proceed is to work with areas as in the absorption case for then a given experimental curve might conceivably be built up by a series of curves of the above form. Such an integration of Eq. (9) involves the evaluation of

$$f_0=\frac{\int_{\nu_1}^{\nu_2} n'^2 d\nu-\int_{\nu_1}^{\nu_2} n_0^2 d\nu}{\int_0^{\infty}\frac{Ne^2/\pi m'\cdot(\bar{\nu}_0^2-\nu^2)d\nu}{(\bar{\nu}_0^2-\nu^2)^2+\gamma^2\nu^2}}$$

($\nu_1$ and $\nu_2$ being outside the region of absorption). The upper two integrals can be evaluated graphically, but the lower, although integrable, is somewhat tedious to handle.

## EXPERIMENTAL

### (a) Dispersion

In accordance then with the previously discussed theory, one would always expect an anomaly in the refractive index for a liquid in the vicinity of each absorption band, and such is found to be the case.[10] Furthermore, it is generally the case that the stronger the band the larger the anomaly and vice versa. The difficulties in following the dispersion through a band are well known,[11] for these measurements require small prism angles and sensitive receivers. Little, however, has been done on the dispersion of liquids in the infra-red region because of the additional opacity of liquids to wave-lengths in this region. The first successful measurements beyond Ruben's limit of 2.4 microns were those of Marvin[10] who, using hollow prism methods

[10] Handbuch der Physik, Vol. XX (1928); T. Wetterblad, Dissertation, Upsala (1924); H. H. Marvin, Phys. Rev. [1] **34**, 161 (1912); A. H. Pfund, J. Opt. Soc. Am. **25**, 351, (1935); M. A. Pittman, J. Opt. Soc. Am. **29**, 358 (1939); Landolt-Bornstein, *Physical Chemistry Tables*, Vol. 2 p. 912.

[11] Handbuch der Physik, Vol. XX, p. 499.

TABLE I. *Dispersion of* $CH_2Cl_2$.

| WAVE-LENGTH | REFRACTIVE INDEX | WAVE-LENGTH | REFRACTIVE INDEX | WAVE-LENGTH | REFRACTIVE INDEX |
|---|---|---|---|---|---|
| 0.5893 | 1.41883 | 1.53 | 1.40848 | 3.85 | 1.40480 |
| .72 | 1.41478 | 1.578 | 1.40831 | 3.92 | 1.40463 |
| .73 | 1.41468 | 1.625 | 1.40819 | 4.00 | 1.40447 |
| .74 | 1.41422 | 1.668 | 1.40805 | 4.08 | 1.40437 |
| .75 | 1.41392 | 1.71 | 1.40797 | 4.16 | 1.40425 |
| .76 | 1.41371 | 1.75 | 1.40787 | 4.23 | 1.40433 |
| .77 | 1.41348 | 1.80 | 1.40769 | 4.29 | 1.40455 |
| .78 | 1.41320 | 1.85 | 1.40756 | 4.35 | 1.40439 |
| .79 | 1.41294 | 1.90 | 1.40740 | 4.42 | 1.40419 |
| .80 | 1.41269 | 1.95 | 1.40727 | 4.49 | 1.40396 |
| .815 | 1.41243 | 2.00 | 1.40712 | 4.56 | 1.40377 |
| .825 | 1.41217 | 2.05 | 1.40695 | 4.63 | 1.40365 |
| .83 | 1.41206 | 2.10 | 1.40679 | 4.70 | 1.40348 |
| .84 | 1.41190 | 2.17 | 1.40674 | 4.76 | 1.40336 |
| .85 | 1.41176 | 2.24 | 1.40666 | 4.81 | 1.40318 |
| .86 | 1.41163 | 2.30 | 1.40658 | 4.87 | 1.40303 |
| .87 | 1.41150 | 2.35 | 1.40648 | 4.94 | 1.40286 |
| .88 | 1.41136 | 2.41 | 1.40637 | 5.00 | 1.40270 |
| .89 | 1.41123 | 2.47 | 1.40626 | 5.07 | 1.40253 |
| .90 | 1.41110 | 2.54 | 1.40612 | 5.14 | 1.40240 |
| .915 | 1.41094 | 2.61 | 1.40584 | 5.20 | 1.40224 |
| .930 | 1.41083 | 2.70 | 1.40570 | 5.26 | 1.40204 |
| .950 | 1.41068 | 2.78 | 1.40535 | 5.32 | 1.40183 |
| .975 | 1.41056 | 2.89 | 1.40532 | 5.38 | 1.40166 |
| 1.00 | 1.41041 | 3.00 | 1.40385 | 5.44 | 1.40147 |
| 1.025 | 1.41029 | 3.044 | 1.40380 | 5.49 | 1.40129 |
| 1.05 | 1.41013 | 3.088 | 1.40455 | 5.54 | 1.40108 |
| 1.08 | 1.41001 | 3.132 | 1.40538 | 5.59 | 1.40087 |
| 1.12 | 1.40988 | 3.176 | 1.40698 | 5.65 | 1.40068 |
| 1.14 | 1.40976 | 3.22 | 1.40744 | 5.70 | 1.40045 |
| 1.17 | 1.40964 | 3.264 | 1.40645 | 5.76 | 1.40029 |
| 1.215 | 1.40952 | 3.308 | 1.40624 | 5.82 | 1.40001 |
| 1.235 | 1.40936 | 3.352 | 1.40575 | 5.87 | 1.39988 |
| 1.275 | 1.40925 | 3.396 | 1.40599 | 5.93 | 1.39955 |
| 1.318 | 1.40908 | 3.44 | 1.40576 | 5.98 | 1.39928 |
| 1.36 | 1.40895 | 3.53 | 1.40565 | 6.02 | 1.39907 |
| 1.403 | 1.40884 | 3.62 | 1.40537 | 6.07 | 1.39884 |
| 1.445 | 1.40868 | 3.70 | 1.40518 | 6.12 | 1.39856 |
| 1.488 | 1.40861 | 3.78 | 1.40503 | 6.17 | 1.39829 |

and a Nichol's radiometer as a receiver, measured the dispersion of eight chlorides out to about 14 microns. His measurements showed anomalous dispersion for $CCl_4$, but because of opacity, the dispersion could not be followed through the band. Pfund and Pittman[10] pursued the matter further and Pittman, using amplification methods, was able to follow the dispersion through the region of the C—H absorption band near 3.3 microns in $CHCl_3$ and $CHBr_3$. It is with a further development of these dispersion measurements that we shall be concerned here.

The method employed here for measuring the dispersion of the liquids studied was that of the hollow prism. Since the apparatus has already, to a degree, been described in the paper by Pittman, only the essential parts will be discussed here. Two spectrometers were used in series (each of the Wadsworth mirror type) the first serving as a monochromator for the second (see associated diagram of apparatus). The source was either a street series lamp (used in short wave-length region) or a Nichrome spiral. The first spectrometer had a rocksalt prism and mirrors forty cm in focal length, and the second contained the hollow prism into which the liquids for study were inserted and likewise had mirrors of the same focal length. The Wadsworth mountings[12] in both spectrometers were independently set for minimum deviation for the sodium lines and this procedure was always repeated whenever either prism or liquid were changed in the second spectrometer. The ther-

TABLE II. *Dispersion of* $CH_2Br_2$.

| WAVE-LENGTH | REFRACTIVE INDEX | WAVE-LENGTH | REFRACTIVE INDEX | WAVE-LENGTH | REFRACTIVE INDEX |
|---|---|---|---|---|---|
| 0.5893 | 1.53668 | 1.85 | 1.51799 | 4.70 | 1.51459 |
| .72 | 1.52938 | 1.90 | 1.51783 | 4.76 | 1.51439 |
| .75 | 1.52809 | 1.95 | 1.51768 | 4.81 | 1.51421 |
| .76 | 1.52770 | 2.00 | 1.51751 | 4.87 | 1.51404 |
| .77 | 1.52723 | 2.05 | 1.51734 | 4.94 | 1.51392 |
| .78 | 1.52683 | 2.10 | 1.51714 | 5.00 | 1.51377 |
| .79 | 1.52642 | 2.17 | 1.51712 | 5.07 | 1.51363 |
| .80 | 1.52601 | 2.23 | 1.51711 | 5.14 | 1.51348 |
| .815 | 1.52557 | 2.29 | 1.51699 | 5.20 | 1.51337 |
| .825 | 1.52517 | 2.35 | 1.51682 | 5.26 | 1.51316 |
| .83 | 1.52495 | 2.41 | 1.51678 | 5.32 | 1.51299 |
| .84 | 1.52476 | 2.47 | 1.51660 | 5.38 | 1.51285 |
| .85 | 1.52455 | 2.54 | 1.51642 | 5.44 | 1.51264 |
| .86 | 1.52434 | 2.61 | 1.51616 | 5.49 | 1.51248 |
| .87 | 1.52413 | 2.70 | 1.51598 | 5.54 | 1.51236 |
| .88 | 1.52393 | 2.78 | 1.51517 | 5.59 | 1.51218 |
| .89 | 1.52371 | 2.89 | 1.51555 | 5.65 | 1.51201 |
| .90 | 1.52349 | 3.00 | 1.51324 | 5.70 | 1.51185 |
| .915 | 1.52327 | 3.044 | 1.51317 | 5.76 | 1.51165 |
| .93 | 1.52305 | 3.088 | 1.51434 | 5.82 | 1.51153 |
| .95 | 1.52287 | 3.132 | 1.51564 | 5.87 | 1.51137 |
| .975 | 1.52265 | 3.176 | 1.51816 | 5.93 | 1.51127 |
| 1.00 | 1.52245 | 3.22 | 1.51888 | 5.98 | 1.51113 |
| 1.025 | 1.52225 | 3.26 | 1.51733 | 6.02 | 1.51091 |
| 1.05 | 1.52202 | 3.308 | 1.51699 | 6.07 | 1.51069 |
| 1.08 | 1.52179 | 3.352 | 1.51623 | 6.12 | 1.51056 |
| 1.12 | 1.52158 | 3.396 | 1.51662 | 6.17 | 1.51049 |
| 1.14 | 1.52139 | 3.44 | 1.51625 | 6.22 | 1.51019 |
| 1.17 | 1.52121 | 3.53 | 1.51623 | 6.27 | 1.51011 |
| 1.215 | 1.52099 | 3.62 | 1.51599 | 6.32 | 1.50992 |
| 1.235 | 1.52079 | 3.70 | 1.51577 | 6.37 | 1.50971 |
| 1.275 | 1.52059 | 3.78 | 1.51555 | 6.41 | 1.50956 |
| 1.318 | 1.52039 | 3.85 | 1.51547 | 6.45 | 1.50940 |
| 1.36 | 1.52022 | 3.92 | 1.51542 | 6.50 | 1.50915 |
| 1.403 | 1.51998 | 4.00 | 1.51522 | 6.56 | 1.50897 |
| 1.445 | 1.51978 | 4.08 | 1.51505 | 6.59 | 1.50872 |
| 1.488 | 1.51957 | 4.16 | 1.51489 | 6.64 | 1.50842 |
| 1.53 | 1.51937 | 4.23 | 1.51472 | 6.68 | 1.50820 |
| 1.578 | 1.51916 | 4.29 | 1.51467 | 6.73 | 1.50795 |
| 1.625 | 1.51874 | 4.35 | 1.51455 | 6.77 | 1.50771 |
| 1.668 | 1.51871 | 4.42 | 1.51442 | 6.82 | 1.50751 |
| 1.71 | 1.51857 | 4.49 | 1.51464 | 6.87 | |
| 1.75 | 1.51842 | 4.56 | 1.51486 | | |
| 1.80 | 1.51822 | 4.63 | 1.51475 | | |

[12] F. L. O. Wadsworth, Phil. Mag. p. 348 (1894).

mocouple was mounted behind the exit slit $S_3$ of spectrometer II and received the energy from a short focal length concave mirror which reduced the size of the image to at least equal to or smaller than the receiving surface of the thermocouple itself. The thermocouple was one of the vacuum type suggested by Pfund[13] and was evacuated to quite low pressures using an oil pump and a charcoal trap. Proceeding in this manner gave an increase in sensitivity of from five to ten times.

Since for any given liquid in spectrometer II the energy finally reaching the thermocouple in the region of an absorption band is very small, two further means of amplification were utilized. The deflections of the first galvanometer fastened to the thermocouple were amplified making use of a modification of the Moll relay.[14] The deflections of the second galvanometer were then observed on a scale at a distance of about three meters. It was found that, at one setting of the amplification apparatus, a deflection of one mm of galvanometer I, measured on the photronic cell surface (at about one meter), gave much over a meter on the scale of the second galvanometer. This amplification was changed over quite wide regions by changing the voltage on the projection lamp (see diagram of apparatus, Fig. 1) and with sufficient voltage the Brownian motions of the first galvanometer could be seen on the scale of the second.

Using such high amplifications necessitated other precautions. The first galvanometer had to be mounted on a vibration-free support[15] and enclosed in an air-tight chamber so that disturbances due either to air currents or mechanical disturbances would be reduced to a minimum. In front of the chamber there was, of course, a window to admit the light on its path to and from the galvanometer mirror. It was also found necessary to take further precautions so that stray air currents in the vicinity of the thermocouple and e.m.f.'s along the wires from the thermocouple were not magnified many times. The wires leading to galvanometer I were wrapped and the final slit $S_3$, mirror and thermocouple were packed in an air-tight box. All light sources and rheostats were water cooled. During any set of readings the room was made air- and light-tight so that an equilibrium was established and then readings were taken as rapidly as possible for such states of zero drift were difficult to obtain and retain.

[13] A. H. Pfund, Rev. Sci. Inst. **8**, 417 (1937).
[14] R. B. Barnes and F. Matossi, Zeits. f. Physik **76**, 24 (1932).
[15] A. H. Pfund, not in print.

TABLE III. *Dispersion of* $CH_2I_2$.

| Wave-Length | Refractive Index | Wave-Length | Refractive Index | Wave-Length | Refractive Index |
|---|---|---|---|---|---|
| 0.5983 | 1.75501 | 2.05 | 1.69068 | 4.76 | 1.68669 |
| .815 | 1.70746 | 2.10 | 1.69043 | 4.81 | 1.68686 |
| .825 | 1.70654 | 2.17 | 1.69025 | 4.87 | 1.68746 |
| .83 | 1.70605 | 2.24 | 1.69006 | 4.94 | 1.68711 |
| .84 | 1.70561 | 2.30 | 1.68988 | 5.00 | 1.68694 |
| .85 | 1.70508 | 2.35 | 1.68972 | 5.07 | 1.68669 |
| .86 | 1.70470 | 2.41 | 1.68965 | 5.14 | 1.68650 |
| .87 | 1.70424 | 2.47 | 1.68951 | 5.20 | 1.68631 |
| .88 | 1.70375 | 2.54 | 1.68925 | 5.26 | 1.68615 |
| .89 | 1.70329 | 2.61 | 1.68909 | 5.32 | 1.68596 |
| .90 | 1.70284 | 2.70 | 1.68863 | 5.38 | 1.68577 |
| .915 | 1.70236 | 2.78 | 1.68841 | 5.44 | 1.68565 |
| .930 | 1.70193 | 2.89 | 1.68807 | 5.49 | 1.68552 |
| .95 | 1.70145 | 3.00 | 1.68484 | 5.54 | 1.68535 |
| .975 | 1.70102 | 3.044 | 1.68474 | 5.59 | 1.68520 |
| 1.00 | 1.70072 | 3.088 | 1.68642 | 5.65 | 1.68501 |
| 1.025 | 1.70020 | 3.132 | 1.68828 | 5.70 | 1.68492 |
| 1.05 | 1.69965 | 3.176 | 1.69190 | 5.76 | 1.68478 |
| 1.08 | 1.69923 | 3.22 | 1.69292 | 5.82 | 1.68485 |
| 1.12 | 1.69880 | 3.264 | 1.69071 | 5.87 | 1.68492 |
| 1.14 | 1.69834 | 3.308 | 1.69022 | 5.93 | 1.68477 |
| 1.17 | 1.69792 | 3.352 | 1.68913 | 5.98 | 1.68468 |
| 1.215 | 1.69754 | 3.396 | 1.68968 | 6.02 | 1.68453 |
| 1.235 | 1.69713 | 3.44 | 1.68916 | 6.07 | 1.68444 |
| 1.275 | 1.69666 | 3.53 | 1.68909 | 6.12 | 1.68425 |
| 1.318 | 1.69618 | 3.62 | 1.68871 | 6.17 | 1.68411 |
| 1.36 | 1.69584 | 3.70 | 1.68839 | 6.22 | 1.68394 |
| 1.403 | 1.69543 | 3.78 | 1.68814 | 6.27 | 1.68371 |
| 1.445 | 1.69502 | 3.85 | 1.68791 | 6.32 | 1.68354 |
| 1.488 | 1.69463 | 3.92 | 1.68774 | 6.37 | 1.68340 |
| 1.53 | 1.69426 | 4.00 | 1.68758 | 6.41 | 1.68321 |
| 1.578 | 1.69384 | 4.08 | 1.68749 | 6.45 | 1.68302 |
| 1.625 | 1.69349 | 4.16 | 1.68746 | 6.50 | 1.68276 |
| 1.668 | 1.69314 | 4.23 | 1.68746 | 6.56 | 1.68260 |
| 1.71 | 1.69283 | 4.29 | 1.68721 | 6.59 | 1.68216 |
| 1.75 | 1.69240 | 4.35 | 1.68697 | 6.64 | 1.68197 |
| 1.80 | 1.69213 | 4.42 | 1.68678 | 6.68 | 1.68184 |
| 1.85 | 1.69181 | 4.49 | 1.68668 | 6.73 | 1.68163 |
| 1.90 | 1.69151 | 4.56 | 1.68669 | 6.77 | 1.68137 |
| 1.95 | 1.69121 | 4.63 | 1.68674 | 6.82 | 1.68117 |
| 2.00 | 1.69093 | 4.70 | 1.68674 | 6.87 | 1.68079 |

To calculate the refractive index of the liquid, it was necessary to have some means of measuring the angles of rotation of the hollow prism within the limits of the resolving power of the instrument itself. This was accomplished by a system of two plane mirrors $M_1$ and $M_2$ (see Fig. 1) and a telescope in which light from a well-illuminated scale (484 cm distant) was allowed to fall first on $M_1$ rotating with the prism mounting, then to pass to $M_2$ and back to $M_1$ and finally into the telescope which was

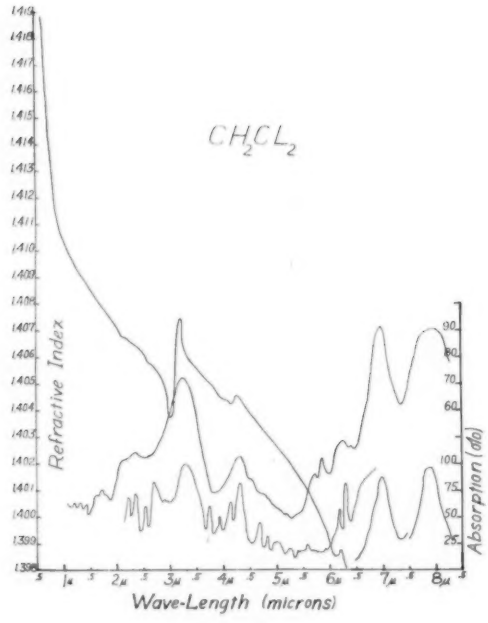


FIG. 2.

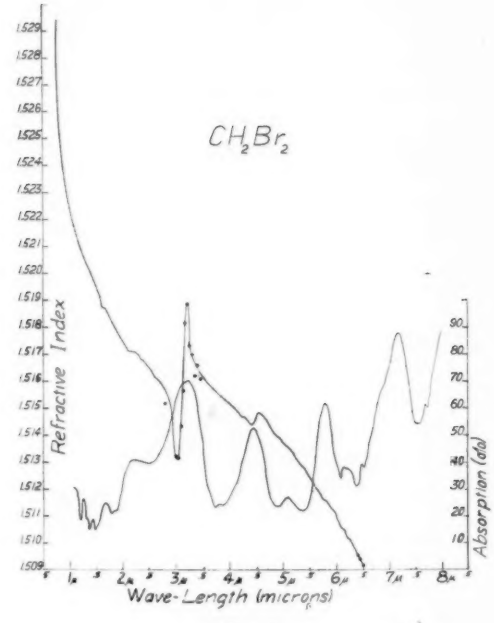


FIG. 3.

focused on the scale. Such an arrangement resulted in 21.3 seconds of arc corresponding to one mm on the scale, and since the readings at best were repeatable to 0.3 mm, the upper limit of the resolving power was utilized.

Because of energy limitations, three hollow prisms of different angles were used in the measurements. The largest was one of angle 59°52′40″ (average of fifteen readings) with plane parallel nonprismatic glass plates glued onto a brass frame. This angle was measured in the conventional manner by observing the reflected light off the surfaces when it was placed on the table of a good spectrometer (R. Fuess, Berlin). Knowing the angle, it was then possible to find the refractive indices for each liquid for the sodium lines by measuring the angles of minimum deviation. The two rocksalt prisms were each made from one piece of rocksalt polished to as near planarity as possible on both sides and then split down the middle. The two resulting pieces were then folded back over the apex of the prism so that any dispersion due to one was at least partially annulled by the other. Since, in general, if the sides were prismatic it would not be safe to use reflection methods to find the prism angle, the usual procedure was reversed and a liquid placed in the prism whose refractive index was known and the angle of minimum deviation measured. Knowing this angle, the ordinary prism formula for the refractive index could be reversed and the angle of the prism found. In this manner the large rocksalt prism was found to have an angle of 32°25′54″ and the smaller an angle of 13°18′58″ (average of ten readings each). To correct for the small remaining prismatic effect, calculations were made for the refractive index in the usual prism manner and the obtained dispersion curve was then compared with that of the large glass prism in their overlapping regions. A small correction could then be added or subtracted until the two curves agreed in position in the shorter wave-length infra-red. For each of the prisms this effect was so small that, in these overlapping regions, the refractive index always agreed exactly to the third place.

All measurements of the angle of minimum deviation on the hollow prism were measured from the position of the sodium lines. It was first established by observation that the angle of deviation for longer wave-lengths lay at smaller values than for the sodium lines. In

determining the angle of deviation, then, for a wave-length $\lambda$, (angle in seconds) the formula derived for the instrument was

$$D_\lambda = D_{Na} - 2(S_{Na} - S_\lambda)424.8/4,$$

where $D_{Na}$ is the angle of deviation for the sodium lines (known from spectrometer measurements), $S_{Na}$ the scale reading in cm when the sodium lines are in focus on the slit $S_3$, and $S_\lambda$ the scale reading when wave-length $\lambda$ is on the same slit. The 424.8 is the number of seconds corresponding to one cm on the circumference of the curved scale 4.84 meters distant. The $\frac{1}{4}$ is necessary because of the double reflection from the moving mirror $M_1$ and the 2 appears because of the fact that in rotating a Wadsworth mounting through an angle $\theta$, the beam is rotated through $2\theta$.[12] If then each value of $D_\lambda$ from the above is inserted in the ordinary prism formula for the refractive index, the dispersion of any unknown liquid can be measured.

The position $S_{Na}$ was observed visually when first the prism was rotated clockwise and then counterclockwise (several readings) and the average taken as its value. $S_\lambda$ was determined in like manner except that the positions chosen corresponded to a maximum in deflection of galvanometer II. Such a procedure then made allowance for the backlash in the rotating mechanism of the prism mounting. Only two readings were taken for wave-lengths other than the sodium lines for it was soon established that, in the region of higher energy, the instrument would repeat to within 0.3 mm while in the region of longer waves this dropped off to 0.5 mm. A slit width of 0.25 mm was used out to about four microns and beyond this it was gradually increased until at seven microns it reached a value of 0.5 mm. The readings were not extended beyond this point for it soon became apparent that these bands could not be traversed with the smallest prism, so readings were not continued on the other sides of the bands.

The liquids chosen for measurement were $CH_2Cl_2$, $CH_2Br_2$, and $CH_2I_2$ in sequence to those measured by Pittman ($CHCl_3$ and $CHBr_3$). They were obtained from the Eastman Kodak Company and their purity was checked by refractive index measurements for the sodium lines using both the Abbe refractometer and the hollow prism. Both values agreed as far as the Abbe could be read with certainty and when corrections were made for temperature, the values obtained agreed very favorably with those quoted in the tables (*International Critical Tables*, Landolt and Bornstein). All refractive index measurements were made at temperatures between 27° and 27½°.

The values obtained are then recorded in Tables I, II, and III and a graphical plot of the dispersion as a function of the wave-length is given in Figs. 2, 3, and 4.

If one considers all the errors which are due to the lack of repeatability of the measurements (after making small correction for prismatic effect of salt plates) the following errors in the values obtained were found: For the large prism the error is found to be not greater than one unit in the fourth place; for the 32° salt prism three units in the fourth place; for the 13° prism six units in the fourth place. In figuring these errors, the upper limit of the deviations from the mean values of the terms involved was used so as to compensate partly for any instrumental errors (resolving power, quality of image, etc.) which

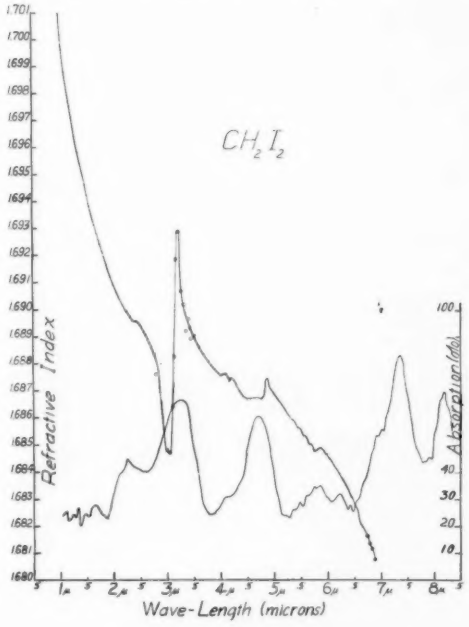


FIG. 4.

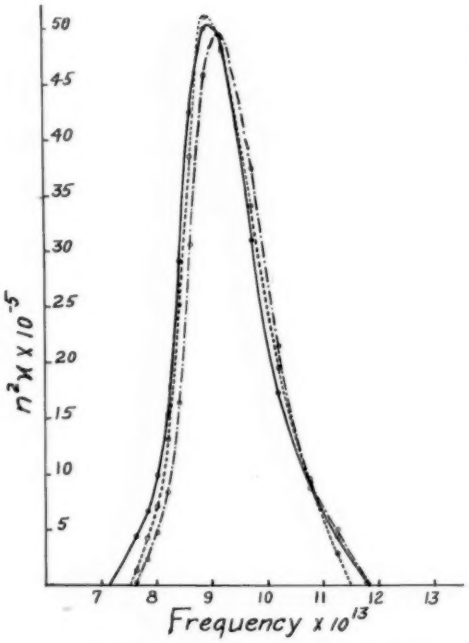


FIG. 5. Absorption $n^2\kappa$ *vs.* frequency. ——$CH_2Cl_2$; —·—$CH_2Br_2$; ····$CH_2I_2$.

we have no good way of determining. In making all calculations on the machine, seven significant figures were carried so that no accumulative errors resulted. Since, in the application of theory to measurement, we are concerned primarily with refractive index differences (see Eq. (13)), the values in the tables are extended to five places; for it is easy to show, with these same existing errors, that although the absolute values are in error in the fourth place, the differences are exact to the fourth place with approximations entering in the fifth.

### (b) Absorption

In order, then, to have an experimental correlation between absorption and dispersion and to supply an additional method for calculating the oscillator strengths, the absorption spectra of these compounds were also measured. Of the three liquid studies, only one has been completed in detail, so far as the author is aware.[16] Lecomte and Ellis[17] have studied the absorption of all three compounds from 7–16 microns and 0.5–2.5 microns, respectively, and Sutherland's measurements on $CH_2Cl_2$ (lower curve in Fig. 2) completed the region within these two limits for this one compound. These measurements are included to show the relative magnitudes of the resolving powers of the two spectrometers, his being the greater because of amplification.

Due to the instability of the amplification apparatus for measuring absolute deflections and the small deflections of the monochromator without amplification, the absorption spectra were measured with a second spectrometer with a higher aperture $f/2$. The prism was mounted on the usual Wadsworth mounting and the concave mirrors were mounted on the axis as suggested by Pfund[18] to minimize astigmatism. Working then with such a spectrometer, the slits could be narrowed until approximately the same wave-length range was incident upon the thermocouple and still larger deflections would result. Although the theoretical resolving powers of neither instrument could be approached because of the lack of sensitivity of the receiver, their values were calculated and compared in the vicinity of three microns and were not found to be appreciably different (0.014 and 0.012 micron).

The calibration of the spectrometer was determined in the usual manner by noting positions corresponding to well-known atmospheric bands, absorption bands of liquids[19] and emission bands of gases. A Pfund thermocouple (unevacuated) was again used to record the transmitted energy. The slit width used throughout these measurements was 0.15 mm.

The absorption cell used throughout these measurements was 0.79 mm in thickness. For any given liquid this cell was placed on a rotating arm and alternately inserted and withdrawn from its position in front of the entrance slit and the corresponding galvanometer deflections recorded. One minus this ratio represents the fraction absorbed and this is the ordinate of the curves plotted in Figs. 2, 3 and 4. Since we are interested in obtaining absolute values of absorption, a second curve was run using the

[16] G. B. B. M. Sutherland, Proc. Roy. Soc. **165**, 43 (1938).
[17] J. Lecomte and J. W. Ellis, *Traite de Chimie Organique*, Grignard II, pp. 196, 197 (1936).
[18] A. H. Pfund, J. Opt. Soc. Am. **14**, 337–338 (1927).
[19] P. E. Shearin and E. K. Plyler, J. Opt. Soc. Am. **28**, 61 (1938).

empty cell and again alternately inserting it and withdrawing it and recording deflections. If one then knows the ratio of the deflections for these two cases, it is easy to show that the fraction of the energy transmitted by the liquid is given by

$$e^{-4\pi\nu n'\kappa x/c}=\frac{s_1(\nu)^2T_1(\nu)^2}{s_2(\nu)^2T_2(\nu)^2}\cdot(I_3'/I_0)/(I_3''/I_0),$$

where $(I_3'/I_0)$ is the ratio of the deflections with cell in and out containing the liquid and $(I_3''/I_0)$ the same ratio with the cell empty. $T_1(\nu)$ and $s_1(\nu)$ are the fractions of the energy transmitted after ordinary specular reflection and scattering take place at salt-air interfaces on inside of the cell, and the same terms with the subscript 2 are identical in definition but apply to the salt-liquid surfaces. $s_1$ and $s_2$ can be made nearly unity by using well-polished salt plates and $T_1$ and $T_2$ calculated using Fresnel's equations for the refractive indices are known from the previous data. An evaluation of $T_1$ and $T_2$ in the vicinity of the three-micron bands for the three liquids showed that $T_1$ is the only one of importance in these calculations. If, with these conditions, one solves the above expression for the extinction coefficient $\kappa$, it becomes

$$\kappa=-\frac{c}{4\pi\nu x n'}\log_e\frac{T_1(\nu)^2(I_3'/I_0)}{(I_3''/I_0)}.$$

TABLE IV. *Values are in units of $10^{-5}$.*

| Wave-Length Microns | Frequency $\times10^{13}$ | Extinction Coefficient $CH_2Cl_2$ | Extinction Coefficient $CH_2Br_2$ | Extinction Coefficient $CH_2I_2$ |
|---|---|---|---|---|
| 3.92 | 7.65 | 4.89 | 2.45 | 2.74 |
| 3.82 | 7.85 | 5.09 | 2.97 | 2.39 |
| 3.73 | 8.04 | 14.12 | 2.60 | 3.36 |
| 3.65 | 8.22 | 10.10 | 3.66 | 4.59 |
| 3.55 | 8.45 | 14.76 | 7.10 | 8.81 |
| 3.46 | 8.67 | 21.52 | 13.33 | 13.49 |
| 3.36 | 8.93 | 25.28 | 19.91 | 17.87 |
| 3.24 | 9.26 | 24.36 | 21.37 | 16.75 |
| 3.07 | 9.77 | 15.70 | 16.32 | 12.00 |
| 2.93 | 10.24 | 8.74 | 9.31 | 6.49 |
| 2.78 | 10.79 | 4.44 | 4.12 | 3.28 |
| 2.66 | 11.28 | 3.55 | 2.67 | 2.03 |
| 2.54 | 11.81 | 3.17 | 2.35 | 2.29 |
| 2.45 | 12.25 | 3.70 | 2.65 | 2.72 |
| 2.35 | 12.77 | 4.39 | 3.09 | 3.12 |
| 2.26 | 13.27 | 3.82 | 3.17 | 3.69 |
| 2.18 | 13.76 | 3.48 | 3.23 | 2.74 |
| 2.10 | 14.29 | 3.35 | 2.43 | 2.33 |
| 2.02 | 14.85 | 2.36 | 1.86 | 1.54 |
| 1.97 | 15.23 | 1.81 | 1.09 | 0.97 |
| 1.92 | 15.63 | 0.85 | 0.38 | 0.58 |

TABLE V.

| Frequency $\times10^{13}$ | $n'^2\kappa$ $CH_2Cl_2$ $\times10^{-5}$ | $n'^2\kappa$ $CH_2Br_2$ $\times10^{-5}$ | $n'^2\kappa$ $CH_2I_2$ $\times10^{-5}$ |
|---|---|---|---|
| 7.15 | 0 | 0 | 0 |
| 7.65 | 4.44 | 0.23 | 1.34 |
| 7.85 | 6.71 | 2.30 | 4.27 |
| 8.04 | 9187 | 4.73 | 7.13 |
| 8.22 | 15.36 | 8.41 | 13.09 |
| 8.45 | 29.16 | 16.32 | 25.13 |
| 8.67 | 42.53 | 30.65 | 38.49 |
| 8.93 | 49.97 | 45.78 | 50.99 |
| 9.26 | 48.20 | 49.25 | 47.94 |
| 9.77 | 30.95 | 37.40 | 34.10 |
| 10.24 | 17.24 | 21.36 | 18.47 |
| 10.79 | 8.77 | 9.46 | 9.35 |
| 11.28 | 4.41 | 4.96 | 2.85 |
| 11.81 | 0.24 | 0.28 | 0 |

The values of $n'$ were then taken from the tables and $T_1$ calculated using a value of $n'$ for rocksalt in this region of 1.523. The values obtained are listed in Table IV. If, now, these are plotted as a function of the frequency, the contributions due to adjacent bands can be eliminated so that $\kappa$ for the three-micron band alone in each compound can be found. Since the refractive indices are known, the values of $n'^2\kappa$ can be calculated as a function of frequency for each of the compounds. These values are then recorded in Table V. The data recorded in Table V were then plotted graphically and the areas under the curves measured with a planimeter in the units of the graph. The resulting curves are indicated in Fig. 5 and the areas as seen from the figure are $CH_2Cl_2$—$98.20\times10^8$, $CH_2Br_2$—$87.65\times10^8$, $CH_2I_2$—$89.35\times10^8$.

## RESULTS

Before the values of $f_0$ can be found from either equation, the nature of $M'$ must first be considered. In a molecule of the form $CH_2X_2$ one would expect nine internal degrees of freedom. These have been formulated by Kohlrausch[20] as five deformation and four valence vibrations. Two of these valence vibrations are closely associated with the $CH_2$ group and may, with sufficient approximation, be thought of as being due to this part of the molecule alone.[21] These

[20] K. W. F. Kohlrausch, Zeits. f. physik. Chemie **B28**, 340 (1935).

[21] Cl. Schaeffer and F. Matossi, reference 5, p. 266; Con. Corin and G. B. B. M. Sutherland, Proc. Roy. Soc. **165**, 48 (1938); J. J. Fox and A. E. Martin, Proc. Roy. Soc. **167A**, 257 (1938).

two vibrations are responsible for the band near 3.3 microns. This band has been resolved into its two components by Sutherland[16] for $CH_2Cl_2$ using high amplification and small slits. Since the binding between the hydrogen atoms is weaker than between the carbon and hydrogens (deformation frequency near seven microns), this group can be looked upon as two C−H groups with the carbon atom in common. Since, in addition, the mass of the hydrogen atom is so much less than the carbon, $M'$ may for the purposes of this calculation be associated with the mass of the hydrogen atom.

Using this value for $M'$ in the absorption Eq. (8) and the data obtained from Fig. 5, the values of the $f_0$'s were found to be

$$f_0 = 2.35 \times 10^{-3} \ (CH_2Cl_2),$$
$$f_0 = 2.47 \times 10^{-3} \ (CH_2Br_2),$$
$$f_0 = 2.85 \times 10^{-3} \ (CH_2I_2).$$

In a similar way the oscillator strengths were obtained from the dispersion data. In evaluating the results, it was necessary to extrapolate the background dispersion through this region, and one of these extrapolations is shown in Fig. 6. The positions of $\lambda_1$ and $\lambda_2$ were chosen at the turning points and the values of the refractive indices taken off the curve as indicated. Using this data and Eq. (13), the oscillator strengths were again found to have the values

$$f_0 = 6.81 \times 10^{-3} \ (CH_2Cl_2),$$
$$f_0 = 20.42 \times 10^{-3} \ (CH_2Br_2),$$
$$f_0 = 39.78 \times 10^{-3} \ (CH_2I_2).$$

The results, therefore, obtained from the two methods show the same trend but apparently have quite large discrepancies in their absolute values. Of the two methods as stated earlier, more confidence should be placed in the absorption calculations than those obtained from the dispersion data. To check whether or not $f_0$ was a constant for the entire band as measured in dispersion, different choices of $\lambda_1$ and $\lambda_2$ were made in Eq. (13). It was found that, in general, as one proceeded further from the band center, the value of $f_0$ decreased indicating therefore that Eq. (1) does not strictly describe the data given here. This, with reservations, is expected to be the case, for in reality the band is double.[16] There are also two additional experimental limitations

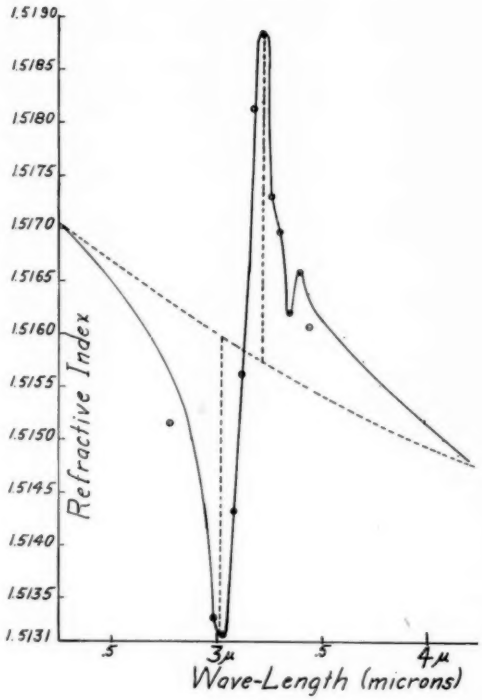


FIG. 6.

which effectively reduce our hope in actually obtaining the exact shape of the dispersion in this region. The first is the relatively large opacity of liquids in this region which forces the use of rather large wave-length intervals in the exit slit of the monochromator and the second is that as one decreases the prism angle to compensate for this, the resolving power of the second spectrometer decreases. The difficulties of resolving power are also present in the absorption method, but not to the same degree, for one can decrease the cell thickness and narrow the slit down to compensate more effectively for the high opacity. A more careful consideration of the effects of these limitations on the dispersion curve can be shown to result in a spreading out in the region of absorption.

Having completed the calculations from the dispersion data, it was next possible to get a

quantitative idea as to how the $f_0$'s changed as the number of hydrogen atoms in a given molecule was increased. Pittman earlier had taken some similar measurements on practically the same instrument on $CHCl_3$ and $CHBr_3$ so his data were used in the region of the three-micron band here calculated.[10] Substitution of his data in Eq. (13) gave the following values:

$$f_0 = 2.61 \times 10^{-3} \ (CHCl_3),$$
$$f_0 = 6.65 \times 10^{-3} \ (CHBr_3).$$

These values are, then, less than those for the similar molecules containing one more hydrogen atom. Such a calculation agrees in direction with measurements of earlier workers[22] who have found that, for a given homologous series, as the number of oscillating particles participating the vibration is increased, the value of the absorption and extinction coefficients increases.

In conclusion, the author would like to acknowledge the generous help and encouragement given by Dr. A. H. Pfund, under whose supervision the experimental part of this work was carried out. The author is also indebted to Dr. K. F. Herzfeld, of Catholic University, whose theoretical interest in the problem was largely responsible for this undertaking. The theoretical part of this paper was discussed with Dr. Herzfeld. Several helpful suggestions were also obtained from additional discussion with Dr. H. M. O'Bryan of Georgetown University and Dr. G. H. Dieke of Johns Hopkins University.

[22] J. Lecomte, Thesis, Paris, 1924; G. B. Bonino, Gazz. Chim. Ital. **53**, 555 (1923); Con. Corin, Comptes rendus **202**, 747–749 (1936); J. W. Ellis, Phys. Rev. **23**, 48 (1924).

# Spectrochemical Analysis in Agricultural Research*

LEWIS H. ROGERS
*University of Florida Agricultural Experiment Station, Gainesville, Florida*

THE importance which the trace elements have assumed in agriculture, particularly in the South, is well known. The classical list of ten elements considered essential for life and growth of living organisms has been extended to include certain other elements, particularly boron, copper, manganese and zinc. Still others have been detected in plant and animal organisms from time to time, and up to the present, 57 of the 92 elements[1] have been found in plants. For convenience, the classical ten elements are here designated as the macroelements, the others as micro or trace elements. In Fig. 1 is shown a periodic table (cf. Steinberg)[2] illustrating some of these relationships.

The addition of copper, boron, manganese or zinc to fertilizer materials is now recommended under certain conditions. Of the other trace elements which have been detected in plants, it has not been established in most cases whether their occurrence is purely adventitious or whether it is indicative of a physiological role.

Certain animal and plant disorders occurring in many regions, including Florida, have made the study of this phase of plant and animal nutrition particularly important. Reviews of this field are to be found in the various issues of *Annual Review of Biochemistry*[3] and a comprehensive bibliography by Willis[4] has been published.

In Florida, copper, boron, manganese, zinc and cobalt responses have been obtained with plants or animals.[5] However, other problems of a similar nature remain unsolved. The study of the occurrence of, and requirements for, the trace elements requires the careful analysis of a large number of materials, including soils, fertilizers, plant and animal tissues. Because of the minute proportions involved, and since microchemical analyses are frequently time consuming, in 1932, through a cooperation between the Physics Department and the Agricultural Experiment Station at the University of Florida, work was initiated in the application of spectrography to this field. In 1934, a Littrow spectrograph with interchangeable quartz and glass optics, and a nonrecording microphotometer were purchased.

Most of the work mentioned below has been done with the d.c. arc, using graphite electrodes and dry ashed material. Two types of analysis are involved, namely: (1) a rough estimate or semiquantitative procedure and (2) a precision procedure. The rough estimate procedure is useful for rapid analysis for a large number of elements where a general idea of the composition of a material and a crude estimate of the proportions present is desirable. This procedure has been used for survey analysis of soils, fertilizers, plant and animal tissues and other agricultural materials, as a guide for later work, and for rough comparisons.

For the rough estimate procedure, three standards are employed, each containing 30 trace elements in different proportions in a base mixture approximating the composition of the material being analyzed. These are spectrographed on either side of and between duplicate exposures of the unknown, and estimations of the proportions of the elements are made visually with a small hand magnifier. This will be superseded wherever possible by the precision procedure which involves the use of the microphotometer and internal standards. This is being used only for copper, zinc and molybdenum at present, but the extension to include other elements is being made as rapidly as possible.

---

* Presented at the Eighth Summer Conference on Spectroscopy and Its Applications at Massachusetts Institute of Technology, July, 1940, and published with the permission of the Director of the Florida Agricultural Experiment Station.

[1] W. O. Robinson, "Agricultural significance of minor elements," Am. Fertilizer **89**, No. 8, 5–8, 24, 26 (1938).

[2] R. A. Steinberg, "Correlation between biological essentiality and atomic structure of the chemical elements," J. Ag. Research **57**, 851–858 (1938).

[3] *Annual Review of Biochemistry* (Stanford University Press, 1932–1940), Vol. I–IX.

[4] L. G. Willis, *Bibliography of References to the Literature on the Minor Elements*, third edition (Chilean Nitrate Educational Bureau, New York, 1939).

[5] L. H. Rogers, "A list of trace element publications by the University of Florida Agricultural Experiment Station." Mimeographed. Florida Agricultural Experiment Station (1940).

The problems being studied may be discussed according to the nature of the materials, namely: (1) soils and waters; (2) fertilizers, soil amendment materials, spray materials and mineral supplements for animals; (3) plant tissues and (4) animal tissues. The analysis of these materials *per se* is not of primary interest, but rather their interrelationship, the presence and availability of the trace elements in soils, their assimilation by plants, and in turn by animals and man.

(1) The purpose in analyzing soils and irrigation waters is to determine the distribution and availability of the trace elements in these materials for purposes of evaluating them with regard to the essential (as well as other) trace elements, and also to determine possible toxicities. A useful by-product of such a study is in connection with a survey of the geologic resources of the state. A study of the distribution of some macro- and microelements in some Florida soils recently has been completed[6] in which it was found that in general the poorly drained soils of peninsular Florida contain greater proportions and a greater variety of both macro- and microelements than do the well-drained soils. Strontium, barium, chromium, manganese, zirconium, titanium, copper, boron and zinc were detected in most of the samples examined, while nickel, silver, vanadium and lead were detected occasionally.

(2) In the analysis of fertilizers, soil amendments and other materials in common use for soil improvement, the possibility of toxic as well as stimulatory effects of the trace elements, contained adventitiously, on plants and animals, is of interest. In a survey conducted several years ago on fertilizer materials,[7] it was found that of the four general types studied (liming, phosphatic potassic and nitrogenous) the phosphatic group contained a greater variety and larger proportions of the trace elements than did the other classes. Barium, strontium, copper, manganese, chromium and boron were detected very extensively in these materials, while bismuth, arsenic, antimony, cadmium, tin and silver were detected in only a few samples. Titanium, nickel, cobalt, vanadium, lead and zinc were only occasionally detected.

In the examination of certain mineral supplement materials used in cattle feeding experiments, a spectrographic analysis of two limonite samples from New Zealand showed the presence of cobalt in one ore but not in the other.[8] The ore containing cobalt was known to be effective in the

H
He
Li Be
B C N O F Ne
Na Mg
Al Si P S Cl A
K Ca Sc Ti V Cr Mn Fe Co Ni Cu Zn Ga Ge As Se Br Kr
Rb Sr Y Zr Cb Mo 43 Ru Rh Pd Ag Cd In Sn Sb Te I Xe
Cs Ba La Hf Ta W Re Os Ir Pt Au Hg Tl Pb Bi Po 85 Rn
87 Ra Ac Th Pa U

FIG. 1. The biologically essential elements (adapted in part from Steinberg, reference 2). Heavy solid blocks enclose elements long known to be essential. Heavy broken blocks enclose elements whose essentiality is fairly well established. Light solid blocks enclose elements frequently detected in biological materials, but whose essentiality as yet remains unproved.

treatment of "bush-sickness," while the other was ineffective. Subsequently, it was found by workers in the Animal Husbandry Department of the Florida Experiment Station that cobalt was effective in the treatment of a certain type of cattle deficiency disease known in Florida as "hill-sickness." Similar results had been obtained previously in New Zealand and elsewhere.

(3) In the analysis of plant tissues, the determination of the essential trace elements for normal plant growth, the investigation of the functions of these trace elements, tolerances, effects of excesses, and differences in requirements by different species as well as by different organs in any one plant species are of interest. Such studies will involve very painstaking solution culture techniques, carefully controlling all factors involved and utilization of spectrographic control of the trace element content of the solutions.

Spectrographic analyses of the ash of citrus fruit juices[9] has shown appreciable amounts of

[6] L. H. Rogers, O. E. Gall, L. W. Gaddum and R. M. Barnette, "Distribution of macro and micro elements in some soils of peninsular Florida," Univ. Fla. Ag. Exp. Sta. Bull. 341 (1939).

[7] L. W. Gaddum and L. H. Rogers, "A study of some trace elements in fertilizer materials," Univ. of Fla. Ag. Exp. Sta. Bull. 290 (1936).

[8] R. B. Becker and L. W. Gaddum, "The composition of limonites effective and ineffective in correcting 'bush-sickness' in cattle," J. Dairy Sci. 20, 737–9 (1937).

[9] J. A. Roberts and L. W. Gaddum, "Composition of citrus fruit juices," Ind. Eng. Chem. 29, 574–575 (1937).

manganese and copper, which are of considerable nutritional value, in addition to strontium, barium, aluminum, chromium and zinc. Titanium, lead, tin, nickel and silver were found occasionally.

In another study of plant tissues[10] it was shown that tung and citrus leaves from trees suffering from zinc deficiency, as judged by external appearance, contained less zinc than did leaves from normal trees.

(4) The problems with animals involve, as in the plant studies, determination of (1) normal requirements (2) tolerances and (3) functions of the trace elements. This will require carefully controlled animal feeding experiments.

[10] L. W. Gaddum, A. F. Camp and W. Reuther, "Spectrographic studies of the composition of tissues and corresponding soils of normal and physiologically diseased horticultural crops," Univ. of Fla. Ag. Exp. Sta. Annual Report, p. 82 (1936).

Analyses of newborn rats[11] to determine the normal trace element content invariably showed aluminum, barium, copper, manganese, strontium, tin and zinc while lead, silver, chromium, nickel and molybdenum were found occasionally.

## Summary

Emission spectrography is a powerful tool for the investigation of agricultural problems involving the trace elements. The technique is especially useful for studying the interrelationships of the trace element content of fertilizers and soils with that of plants and animals. Brief summaries of some investigations on each of these classes of materials are given.

[11] L. L. Rusoff and L. W. Gaddum, "The trace element content of the newborn rat," J. Nutrition **15**, 169 (1938).

# Prism and Sector Photoelectric Photometers for Determination of Concentrations in Gaseous or Liquid Systems*

LOUIS HARRIS, JACK A. KYGER** AND C. NORMAN SJOGREN†
*Research Laboratory of Physical Chemistry, Massachusetts Institute of Technology, Cambridge, Massachusetts*

WE describe here two photometers suitable for the accurate determination of concentrations from transmission measurements. Each of the photometers utilizes a filtered line from an atomic spectral source.

## METHOD OF MEASUREMENT

We divide the original monochromatic light beam into two beams, which are eventually incident upon two photo-tubes. One beam, called the reference beam, is incident upon one photo-tube; the other beam, called the measuring beam, passes through a photometer and the absorption cell containing the substance under investigation before reaching the second photo-tube. The photometer is adjusted until the two "photo-tube currents" are equal, as indicated by a galvanometer in an amplifier circuit.

## SOURCE OF RADIATION

The sources of light are Cooper-Hewitt a.c. Uviarcs, types UA29A2 and UA32A2.[1]

The following filter system is used to isolate the mercury green line:

| | | | |
|---|---|---|---|
| Didymium | 5.0 mm | 512 | Corning |
| Dark blue green | 4.01 mm | 430 | Corning |
| H.R. yellow | 3.01 mm | 351 | Corning |

and a 3.5-cm cell filled with a saturated solution of neodymium ammonium nitrate. The glass filters are cemented to the 3.5-cm cell with Canada balsam. The transmission of this filter is shown in Fig. 1. (The photo-tube current resulting from radiation in the region 5950 to 6350A is at most 0.2 percent of the total photo-tube current.)

The intensity distribution from these lamps changes during the first fifteen minutes of operation. After the lamp has come to a steady state the luminous area consists of a thin vertical column along the axis of the lamp. The cooler gas surrounding this luminous area causes self-reversal of the green line. The effect is very strikingly shown with a 35-foot grating. We have photographed the emission spectrum and found the central component of the 5461A line "missing," and that the two outer components have a maximum intensity at 5460.93 and 5460.58A. Most of the radiation is confined to about 0.57A.

A stop with a 6-mm hole at the center, placed 5 cm from the lamp, acts as a "point source" from which the light is directed by lenses and mirrors into a nearly parallel beam. The aperture of the beam is less than that of any of the parts through which it passes.

## PHOTOMETERS

### Polarizing prisms for measuring light intensity

The light beam after passing through the filters is divided into two beams of mutually perpendicular polarized light by a Wollaston prism. One of these beams is directed to the reference photo-tube; the other beam passes

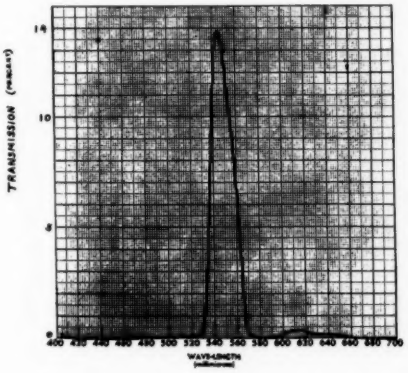


FIG. 1.

* Presented at the Eighth Summer Conference on Spectroscopy and Its Applications at Massachusetts Institute of Technology, July, 1940. Contribution No. 461 from the Research Laboratory of Physical Chemistry, Massachusetts Institute of Technology.

** Present address, Mallinckrodt Laboratories, St. Louis, Missouri.

† Present address, Union Oil Company of California, Los Angeles, California.

[1] L. B. Johnson and S. B. Webster, Rev. Sci. Inst. **9**, 325 (1938).

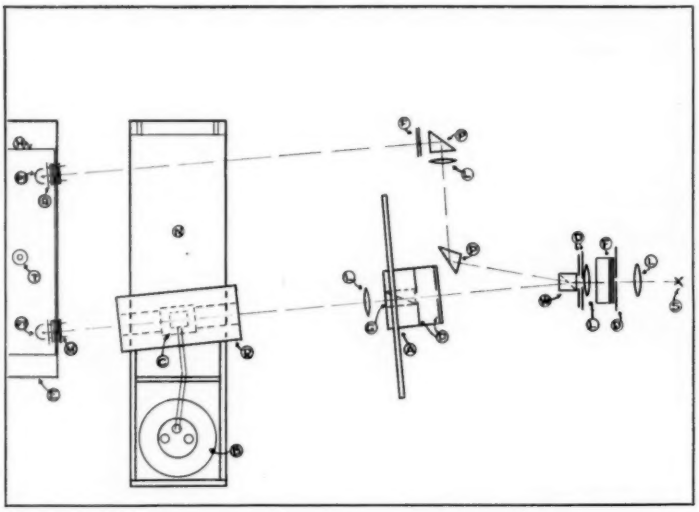

FIG. 2. Prism photoelectric photometer. *S*—light source, *L*—double convex lens, *D*—stops, *F*—filters, *F'*—gray filter, *W*—Wollaston prism, *P*—right angled prisms, *A*—analyzer, *G*—Glan Thompson prism, *N*—mechanical shuttle, *R*—furnace for absorption cell, *C*—absorption cell, *B*—cryostat, *H*—copper box containing photo-tubes, amplifier tube, shorting switch, etc., *PT*—photo-tubes, *T*—FP54 d.c. amplifying tube, *E*—sheet iron box.

through a Glan-Thompson prism and the sample under investigation and is then incident upon the second photo-tube. (The Wollaston prism was 1.8×1.8×1.7 cm with a total refraction angle of 11° 25′. The Glan-Thompson prism was 1.5 ×1.5×4 cm, aperture angle 17°. Both prisms were obtained from Bernard Halle, Berlin.)

The unit by which the Glan-Thompson prism is adjusted and a trace of the light paths are illustrated in Figs. 2 and 3. All metal parts of the apparatus are of cast brass except the steel leveling screws and the bronze cone-shaped bearing. The 11″ diameter silvered scale is graduated every 10′ of arc. Two verniers, each with 60 divisions, are provided. A micrometer screw permitted close adjustment. The verniers were tested against one another at every 10° of arc and found to check within 10″ of arc. The extinction angle was determined visually.

The transmission of a sample measured with this apparatus is given by: transmission

$$I/I_0 = (\sin\theta_2/\sin\theta_1)^2$$

where $\theta_2$ is the angle away from extinction (of the Glan-Thompson prism) when the beam is clear, $\theta_1$, is the angle when the sample is placed in the analyzing beam, to produce balance of photoelectric currents. An additional measurement, the transmission of the empty cell, is necessary when the sample is confined in an absorption cell.

**Rotating-sector for measuring light intensity**

Mercury lamp UA32A2, operating at 3.1 amperes and 184 volts d.c. provides the radiation for these measurements. The filtered light beam is divided into two nearly parallel beams by a semi-transparent mirror and a totally reflecting mirror. The reflected beam is incident on the reference photo-tube; the transmitted beam, reduced in intensity by the rotating sector and the sample, is incident on the second photo-tube.

The rotating sector is a modification of one described by Kortüm.[2] It consists of two superimposed disks, each being solid in two opposite quadrants and open in the other two quadrants. The fraction of light transmitted by the sector may be adjusted while it is in motion. The sector is driven by a motor belt at a velocity of 900 r.p.m. Measurements with such a sector are considerably facilitated by use of a stroboscopic device which permits scale readings while the sector is in motion.[3] The sector scale of 1000 divisions is on the periphery of one of the 12″ disks. Two vernier scales are on the other disk.

SHUTTLES

Since it is necessary to know the relative intensity of the transmitted and of the incident beam for a transmission measurement, a means,

[2] G. Kortüm, Zeits. f. Instrumentenk. **10**, 373 (1934).
[3] L. Harris and J. A. Kyger, J. Opt. Soc. Am. **30**, 505 (1940).

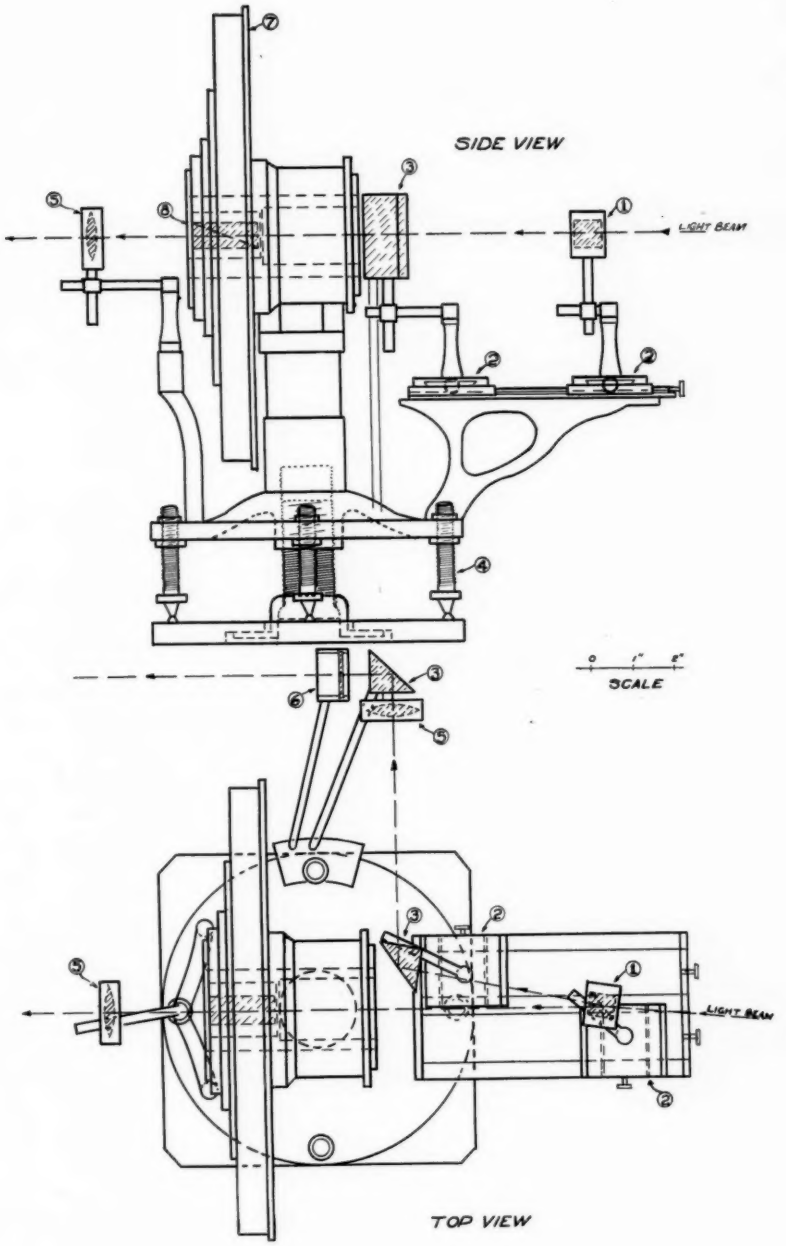


FIG. 3. Polarizer. 1. Wollaston prism; 2. two-way adjustable slide; 3. right angled prisms; 4. leveling screws; 5. lens; 6. gray filter; 7. silver scale; 8. Glan Thompson prism.

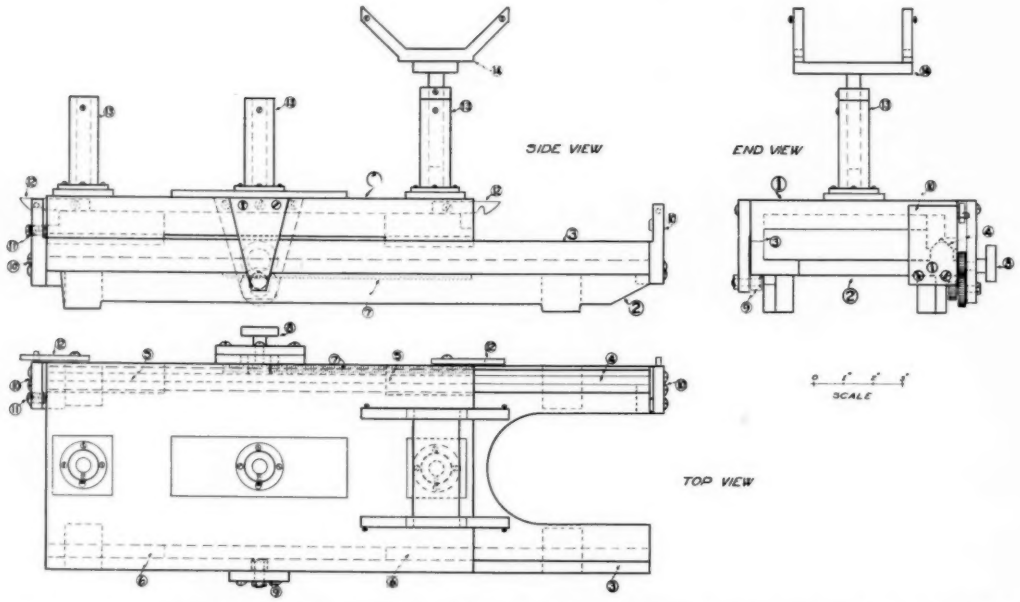


FIG. 4. Mechanical shuttle. 1. Slide of cast bronze; 2. lathe bed of cast bronze; 3. flat track; 4. beveled track; 5. beveled skid; 6. flat skid; 7. ratchet; 8. hand wheel; 9. wheel to prevent tipping; 10. hardened steel stops; 11. adjustable stop head; 12. brass stops to lock top in either of its two limiting positions; 13. support; 14. cradles for cells and furnaces.

either of inserting and removing the sample from the measuring beam, or for shuttling the measuring beam into and around the sample, is required. Apparatus for carrying out both types of operations was built and tested.

The mechanical shuttle was used to move the absorption cell and its connections in and out of the light path. The shuttle is built like a lathe. The bed and the cell-holder-slide are shown in Fig. 4. The hardened steel stops assured reproducible alignment of the slide. A framework (not shown) supporting a heavy cryostat was bolted to the slide and moved with it, the framework rolling along an optical bench.

The optical shuttle was used to pass the incident light beam around the absorption cell. The shuttle consists of two identical elements, each of which supports two silvered mirrors (1″×1″) mounted over one another. The upper mirror in each element is fixed at an angle of 45° to and above the measuring beam; the lower mirrors are hinged in position so that they may be raised out of the measuring beam for a transmission measurement, or lowered parallel to the upper mirror for a measurement with the absorption cell out of the light path.

The optical shuttle has the advantage of permitting more rapid operation than the mechanical shuttle, yet both shuttles gave quite reproducible results (0.1 percent or better over-all reproducibility).

## PHOTO-TUBES

The balanced photo-tube method used here[4] reduces the magnitude of the galvanometer fluctuations caused by variations of the light source intensity. The accuracy of the transmission measurements obtained is independent of the linearity-of-response characteristics of the two photo-tubes used, but requires that the two photo-tubes have approximately the same sensitivity, small "dark-currents" and small variations of the "dark-current" with changes in room temperature.

G.E. PJ22 tubes (a vacuum type caesium oxide tube) proved to be satisfactory from the

[4] See G. Kortüm and H. v. Halban (Zeits. f. physik. Chemie **A170**, 212 (1934) for details of the method.

standpoint of sensitivity. We tested eight of these tubes (selected through the courtesy of the Schenectady laboratories), among which we found two pairs to be quite suitable. However, even the best of these tubes showed "dark-currents" of $1.5\times10^{-10}$ to $3\times10^{-11}$ ampere. We reduced the "dark-currents" to $\sim10^{-12}$ ampere, by the use of suitable "guard rings" on the photo-tubes. The guard rings were made by painting a thin strip of Aquadag between the two "dummy" prongs of a tube and extending the strip to the glass envelope in both directions. Copper foil wound around the tube base was held in contact with the Aquadag strips by wire which was connected to ground.

### Detection of Photo-Tube Current Balance

The "reference" and "measuring" photo-tubes were connected electrically opposed across a resistance of $2\times10^{10}$ ohms to an FP54 tube in a DuBridge and Brown[5] circuit. Balance was indicated by a type R, L and N galvanometer. The operating sensitivity of the amplifiers used was $2\text{–}4\times10^{-15}$ ampere/mm of scale reading. We found that the use of a remote controlled shorting-switch and of a potentiometer in the grid-resistance circuit was indispensable for operation and control of the apparatus.

[5] L. A. DuBridge and H. Brown, Rev. Sci. Inst. **4**, 532 (1933).

### Test of the Photometers

The over-all operation of the photometers was tested by determining the transmission of a Jena BG14 filter, 2.0 mm thick, supplied by the National Bureau of Standards.

### Results

Transmission of Jena filter to mercury green line.

*Photometer No. 1 (polarizing prisms).*—0.6708 $\pm0.0003$[22]. Small area in center of filter, thoroughly cleansed. (Transmission the same in each quadrant of analyzer.)

*Photometer No. 2 (rotating sector).*—0.6680 $\pm0.0014$[30]. (One setting of filter and no *special* precautions taken in cleansing.)

*National Bureau of Standards calibration.*—

$$0.6680\pm0.003.$$

The accuracy of the transmission measurements approaches the reproducibility; namely, 0.1 percent for the prism photometer and 0.2 percent for the sector photometer.

Transmission measurements of the system $NO_2(gas)\leftrightarrows N_2O_4(gas)$ have been made with the object of determining the equilibrium constants of the reaction. The measurements obtained with both photometers will be presented at another time.

We are indebted to Mr. Knut Wilhelmson for the excellent instrument work.

# A Hydrogen Arc of High Intensity for Continuous Ultraviolet Radiation*

ALEXANDER J. ALLEN
*University of Pittsburgh, Pittsburgh, Pennsylvania*

RECENTLY we[1] described a hydrogen arc which provides a convenient source of continuous ultraviolet radiation and is satisfactory for ordinary absorption spectroscopy. There is, however, considerable demand for a more intense source of this type and the arc here to be described is more intense by a factor of approximately ten.

Figure 1 is a drawing showing the construction details of the lamp. The filament *F* of the cathode assembly *A* is made from a rectangular piece of nickel screen (40 mesh) 1″×5″. It is folded to form a ribbon $\frac{1}{3}$″×5″ and then bent into a corrugated form about 1″ long. It is spot-welded onto suitable nickel leads, dipped into oxide coating material and allowed to dry. The filament is mounted in a copper cylinder which is supported and water cooled by means of $\frac{3}{16}$″ standard copper tubing, the tubing being hard soldered to the cylinder for good thermal contact. One terminal is connected to the base of the cylinder with a set screw. The base is removable to facilitate the installation of a new filament. The supporting copper tube is hard soldered into the envelope cap. The other terminal is insulated from the cylinder with a quartz bushing and then passes through a vacuum-tight insulator[2] to form a terminal on the outside of the lamp. Copper cooling fins prevent the heat of the filament from melting the soft solder seals. The arrangement is such that the filament can be easily replaced. *C* is a water-cooled copper anode, and is insulated from the brass envelope in the same manner as the filament lead. Electrons are pulled from the filament through a hole (No. 27 drill) in the copper cylinder toward the anode. An extension on the anode provides a probe for better pulling out of the electron and insures easier starting of the arc. The arc is established from the cathode to the anode and the resultant radiation passes out through a hole in the anode (No. 24 drill),

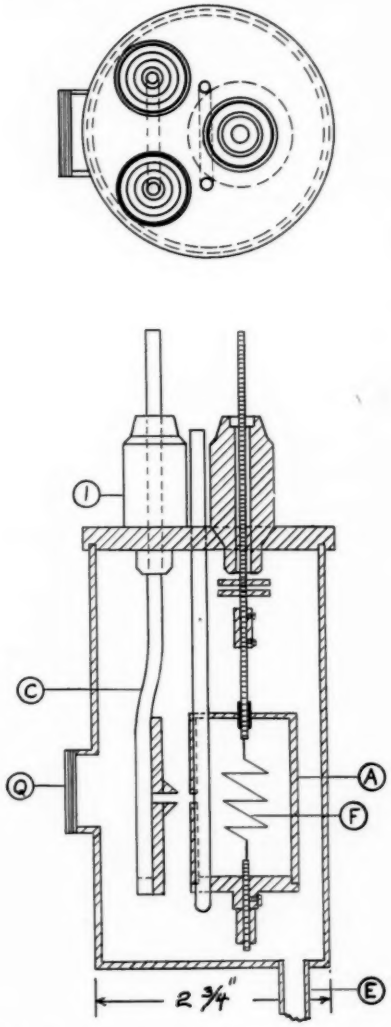


FIG. 1. Drawing of a hydrogen arc having a metal envelope and giving high intensity of continuous ultraviolet radiation. *F*, Oxide-coated nickel screen filament. *C*, Water-cooled copper anode. *A*, Water-cooled copper cathode assembly. *Q*, Quartz window sealed onto brass envelope with Glyptal. *I*, Porcelain insulator. *E*, Evacuating tube and lamp support.

* Presented at the Eighth Summer Conference on Spectroscopy and Its Applications at Massachusetts Institute of Technology, July, 1940.

[1] A. J. Allen and R. G. Franklin, J. Opt. Soc. Am. **29**, 1 (1939).

[2] These are porcelain to glass to Kovar insulators obtained from the Stupakoff Laboratories, Inc., 6627 Hamilton Avenue, Pittsburgh, Pennsylvania. The Kovar ends are soft soldered to the brass cap and to the filament lead to form a vacuum-tight insulating seal.

then out through a quartz window $Q$. The quartz window is sealed on the brass envelope with Glyptal lacquer. The anode and cathode are completely assembled before inserting into the envelope. If Picein or Apiezon wax is used to make the final seal, the lamp can be easily reopened for repair. The envelope is made from standard brass tubing and plate which has been sealed with hard solder.[3] A heavy brass evacuating tube $E$ serves as a support. The final seal may be made by carefully tinning the inside of the brass tube and inserting a close fitting constricted Pyrex tube, which can be sealed with a flame in the usual manner of sealing of glass apparatus. Before filling the lamp with hydrogen it is advisable to make sure the lamp will maintain a good vacuum.

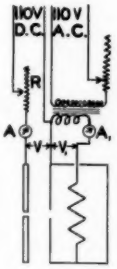


FIG. 2. Schematic drawing showing electrical connection for hydrogen arc. $A$, 10-amp., maximum safe continuous current. $A_1$, approximately 40 amp. $V$, approximately 60 v, d.c. $V_1$, approximately 2 to 2.5 v.

The electrical characteristics are indicated in Fig. 2. The filament carries a current of approximately 40 amperes at 2 to 2.5 volts and should operate at a dull red heat. As soon as the arc is started the filament may be turned off. This is especially important when the arc current is high.

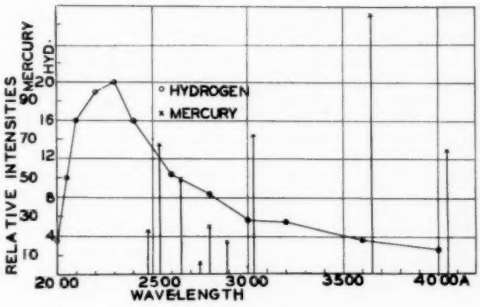


FIG. 4. Spectral energy distribution of metal hydrogen arc operating at 10 amperes plate current. Uviarc arc operating at 2.4 amperes and 60 watts. Data given as transmitted by B and L monochromator with 0.025-mm entrance and exit slits. Energies measured with calibrated sodium cell.

The arc will operate on either alternating or direct current, though direct current is much more satisfactory. The arc voltage $V_2$ is approximately 60 volts and is regulated with a variable resistance $R$. The arc current $A$ should not exceed 10 amperes for continuous running or 15 amperes for short intervals.

For filling the lamp ordinary tank hydrogen is usually satisfactory. Initially the lamp is thoroughly evacuated and the filament maintained at a red heat for fifteen minutes. It is then filled to a pressure of 2 to 3 mm and run for a short time at a current of one ampere then evacuated, refilled and run again. This procedure is repeated five or six times, increasing the current each time until the current reaches 12 amperes. After running at this current for twenty minutes the lamp is refilled to a pressure of 6 mm and sealed off. The

| | | | | | | | | |
|---|---|---|---|---|---|---|---|---|
| 1. | Range | 2450–3300A | 7.5 | amp. | 15 | sec. | exposure | H-arc |
| 2. | " | " | " | " | 30 | " | " | " |
| 3. | " | " | " | " | 60 | " | " | " |
| 4. | " | 2100–2500A | " | " | 60 | " | " | " |
| 5. | " | " | " | " | 120 | " | " | " |
| 6. | " | " | " | " | 240 | " | " | " |
| 7. | " | " | 15.0 | " | 60 | " | " | " |
| 8. | " | " | 6.0 | " | 60 | " | " | Iron-arc |

FIG. 3. Spectrograms obtained with Hilger E-1 quartz spectrograph and unsensitized Eastman process plates.

[3] Easy-Flo solder obtainable from the Air Reduction Company is excellent for this purpose.

lamp is kept cool by circulating tap water through the copper cooling pipes.

Some continuous spectra produced by these arcs are shown in Fig. 3 and are much the same as those shown in Figs. 2 and 3 of our previous paper.[1] These pictures were taken with a Hilger *E*-1 Littrow type spectrograph using unsensitized Eastman process plates.

In Fig. 4 are curves showing the relative wavelength intensity distribution of one of the lamps.[4] It may be noted that at 2537A the intensity of the hydrogen arc is approximately $\frac{1}{5}$ that of a mercury Uviarc operating at 2.4 amp. and rises to a maximum intensity at 2300A.

The intensity of the arc increases almost linearly with increase in current up to 10 amperes where a transition in the arc occurs. Further increase does not appreciably increase the intensity of the radiation emitted. At the transition point the copper lines begin to show up strongly in the continuous background. This is shown in spectrum 7, Fig. 3.

Assistance from the Spang Fund of the Medical School of the University of Pittsburgh is gratefully acknowledged.

[4] The curves were supplied through the courtesy of Professor L. A. DuBridge and Mr. Le Roy Apker of the University of Rochester.

# Far Ultraviolet Spectrophotometric Studies of Fatty Acids by Photoelectric and Spectrographic Methods*†

D. M. KERNS, R. BELKENGREN, HAROLD CLARK AND ELMER S. MILLER
*Department of Botany, University of Minnesota, Minneapolis, Minnesota*

## INTRODUCTION

THIS paper may be considered a progress report of a study concerning the application of spectroscopy to problems of lipid metabolism. For some time[1] it has been known that organisms cannot synthesize either linolic or linolenic acids. In 1929, Burr and Burr[2(a, b)] observed that, in order to maintain normal metabolism, certain fatty acids are indispensable for most animal organisms. The careful exclusion of fat from the diet of rats leads[2(c)] to: (1) development of scaly skin; (2) marked retardation of growth; (3) kidney lesions and hematuria; and (4) early death. The outward symptom of vitamin $B_6$ deficiency is a lesion called acrodynia. However, recent studies[3(a)] show that acrodynia cannot be produced on high-fat diets, and that the curative value of different oils is proportional to the linoleic content.[3(b)]

In 1935, Van der Hulst[4] published the absorption spectra of stearolic acid, ethyl oleate, ethyl linoleate, Δ2–3 oleic acid, and Δ9–11 linolic acid (Fig. 1). These data suggested that if the butter fat samples investigated by Booth *et al.*[5] (Fig. 2) contained only 1 to 2 percent conjugated linolic acid, the $E^{1\%}_{1\text{ cm}}$ would be increased by the amount that these workers observed. This possibility was not recognized by Booth *et al.*, although later studies[6] have shown that this is actually the case. It is now accepted that conjugated fatty acids‡ are universally present in grasses, hence the marked increase in absorption coefficient of butter fat simultaneously with the admission of cows to pasture. Dann and Moore[7] discovered that by prolonged saponification of certain oils and fats, the absorption coefficient ($E^{1\%}_{1\text{ cm}}$) at wave-length 2325A may be increased from 3 to 100. This will henceforth be referred to as the "Moore phenomenon," which is not an oxidation process but merely a rearrangement of the molecule.

Van der Hulst[4] and Dingwall and Thompson[8] have measured the absorption spectra of alpha- and beta-eleostearic acids (Fig. 3). The maxima of the absorption bands characteristic of alpha-eleostearic acid are shifted approximately 30A towards the lower frequencies with reference to the position of the corresponding bands of beta-eleostearic acid. These eleostearic acids have the same chromophore whose space configuration (properly designated as stereo—but commonly called geometric position isomerism) can be determined quantitatively by refractive index measurements and absorption spectra (Table I). Carr and Stücklen[9] have studied (in gas phase) the absorption spectra of *cis*- and *trans*-isomers of butene-2 and pentene-2, and these data are presented in Fig. 4. On the basis of electron diffraction measurements,[10] the higher boiling isomer of butene-2 was identified as the *cis*-form. A similar relationship was observed for pentene-2. Curves 4a and 4b in Fig. 4 show that the average breadth of the sharp bands in *cis*-butene-2 is approximately 90 $cm^{-1}$ whereas in *trans*-butene-2, the breadth is approximately 40 $cm^{-1}$. Although the bands are more diffuse in the heavier pentene molecule, the differences in the respective absorption spectra of the *cis*- and *trans*-geometric isomers are sufficient to serve as a basis for identification and estimation of these forms.

The absorption spectra of *trans*- and *cis*-stilbene in ethanol[11] are illustrated in Fig. 5. (data in Fig. 5 are of a qualitative nature).

Figure 6 presents Van der Hulst's absorption curves of the *trans*-geometric isomer of oleic acid

---

* Presented at the Eighth Summer Conference on Spectroscopy and Its Applications at Massachusetts Institute of Technology, July, 1940.

† This work was supported by grants to the University of Minnesota from the Graduate School of the University of Minnesota, the Hormel Foundation, and the Rockefeller Foundation. Assistance in the preparation of these materials was furnished by the personnel of Works Projects Administration, Official Project No. 65-1-71-140, subproject number 331.

‡ If an oil containing nonconjugated fat acids is fed to the cow, conjugated forms appear in butter fat. (See reference 5.)

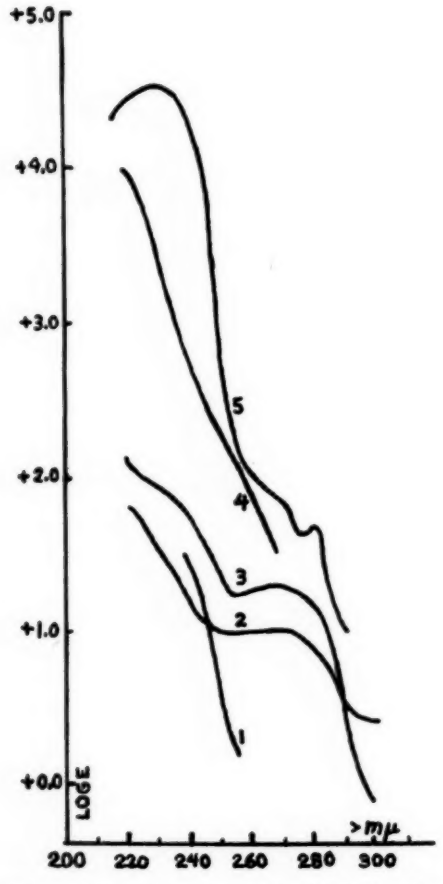


FIG. 1. Absorption spectra of conjugated and non-conjugated acids and esters. (Hulst.[4]) (1) Ethyl oleate; (2) stearolic acid; (3) ethyl linolate; (4) 2–3 oleic acid; (5) 9–11 linolic acid.

(curve 5). This form is known as eladic acid* and melts at 54°C. The absorption curve of the common and *cis*-form is represented by curve 4 and melts at 16°C. Obviously, since the absorption curves are calculated on a molecular basis, the fact that one form is a free acid and the other form the ethyl ester is immaterial. No spectral data are available regarding either double bond position isomers of oleic acid, namely: Δ6 : 7 and Δ12 : 13 octadecenoic acids. Figure 1 contains the absorption curve of Δ2–3 oleic acid. These data have been confirmed by the authors (Fig. 10).

* These data support recent theoretical considerations by Mulliken.

Linoleic acid can exist in four forms, as *trans, trans; trans, cis; cis, trans;* and *cis, cis.* Linolenic (with three double bonds) acid can exist in eight forms. If the double bonds shift along the hydrocarbon chain (as they do in tissue metabolism) giving rise to additional position isomers, the total number of forms becomes correspondingly greater.

It is important to point out at this time that different isomers of fatty acids are metabolized not only at varying rates but that the utilization depends on different enzymatic processes in the respective tissues.

In analytical procedures, conjugation in the hydrocarbon chain may be measured by molecular refraction and absorption spectra. The values for the common chromophores are presented in Table I.

## APPARATUS AND METHODS[14]

Because of spectrographic difficulties encountered below λ2300A, certain apparatus will now be described in detail.

The spectrograph employed is a 1.5-M Gaertner Littrow with crystalline quartz optics. The optical train is shown diagrammatically in Fig. 7.[15] A modified Urey hydrogen discharge tube operated at 0.8 ampere and 4000 volts is a satisfactory light source.

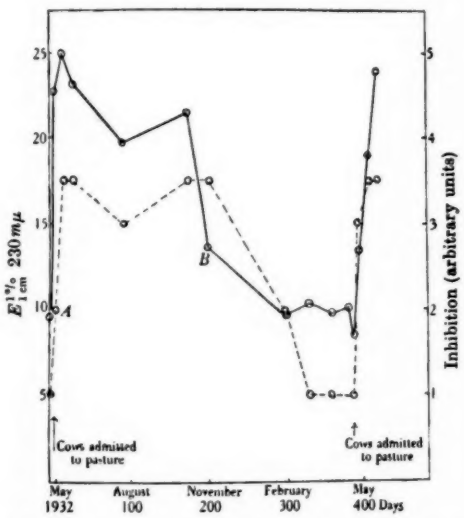


FIG. 2. Inhibitory power of butter fat. Absorptive power of ' acids of butter fat. (Data from Booth *et al.*[6])

CALIBRATION OF SPECTROGRAPHIC APPARATUS

Between λ3500 and 2000A adjacent to the cadmium, bismuth, and zinc emission lines, the "background" on the plate within 0.1A of the edge of the line was less than 3 percent. The center of the collimator lens and prism is covered with a 10-mm bar. The background is not detected when measurements are made 1.0A on either side of the emission line.

The position of the light source was determined according to the method suggested by Meggers. This consists of placing a clear Mazda bulb at *F* as close as possible to the plateholder. This position should be in the green to red position of the spectrum. A cone of rays will emerge at *S* and be reflected 90° by $P_1$. If the light source at *OS* is placed in the center of this beam, it will be on the optic axis of the spectrograph. Test plates of different arcs giving line spectra show that when the image is in proper focus the intensity of ghost images and "scattered radiation" in the vicinity of emission lines (±0.2A on either side) is less than 2 percent of the intensity of spectral light between λ3000 and 2375A.

In lining up the hydrogen tube, the situation is somewhat complicated because it is mounted in a cooling tank and has no definite point source. For convenience, a Mazda bulb is placed at the far end of the hydrogen tube (Fig. 7(c)). The filament is placed at the center of the hydrogen tube capillary. If the image of the filament is emerging from *S* as shown in Fig. 7(b), the hydrogen tube will be properly lined up; thus fulfilling the conditions specified

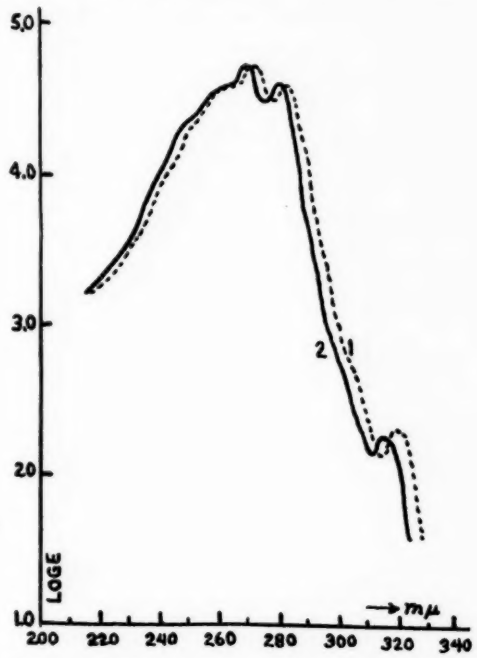


FIG. 3. Absorption spectra of alpha- and beta-eleostearic acids. (Hulst.[4]) (1) α-eleostearic acid; (2) β-eleostearic acid.

TABLE I. *Influence of conjugation on refraction and absorption coefficients.*‡

| CHROMOPHORE | ε AND POSITION OF FIRST BAND. | | $E\Sigma_{r-a}$ |
|---|---|---|---|
| $-CH=CH-$ | <100 | λ1800 | 0.33 |
| $-CH=CH-CH=CH-$ | 33,000<br>52,000 | λ2325 | 1.90 |
| $-CH=CH-CH=CH-CH=CH-$ | 62,000 | λ2700 | 4.20 |
| $-RCH=CH-\overset{O}{\overset{\|\|}{C}}OR$ | 30,000 | λ2040 | —— |
| $-\overset{O}{\overset{\|\|}{C}}-\overset{O}{\overset{\|\|}{C}}-$ | 50<br>1000 | λ2500<br>λ2000 | —— |
| $-\overset{O}{\overset{\|\|}{C}}-CH-\overset{O}{\overset{\|\|}{C}}-$ | 100 | λ2775 | Ca 0.155 |
| $-CH=CH-CH=CH-\overset{O}{\overset{\|\|}{C}}-OR$ | 55,000 | λ2650 | 2.40 |

‡ The molecular refraction data are taken from *Organic Chemistry*, edited by Henry Gilman. Table 15, p. 1741, compiled by Wallace R. Brode and John A. Leermakers.

in Fig. 7. The rotating sector is placed between $L_1$ and $L_2$.

If the hydrogen discharge tube is properly focused, there appear in the spectrum the lines characteristic of neutral silicon atoms. These emission lines are sharp and intense and can readily be identified. They serve as a convenient internal reference standard for calibrating the plates with respect to frequency. Furthermore, they serve as a reliable means not only of determining the spectral purity, but also the position of the plate emulsion with respect to slit image from spectrogram to spectrogram on the same plate.

When Eastman I−O ultraviolet sensitized plates[16] are employed, 2- to 40-second exposures at 0.02-mm slit width; and 45- to 120-second exposures at 0.05-mm slit widths are employed for λ2350 and 2050A, respectively.

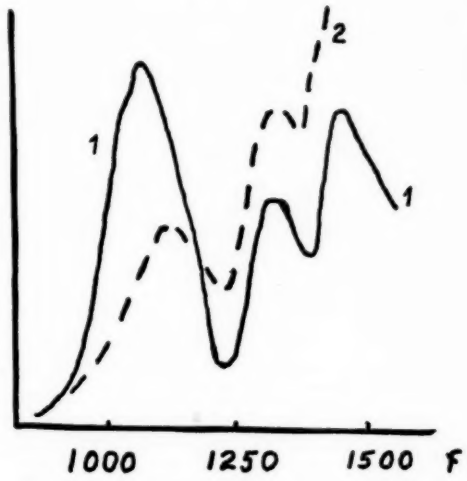


FIG. 5. Absorption spectra of (1) *trans*- and (2) *cis*-stilbene in ethanol. (Data from Smakula et al.[11])

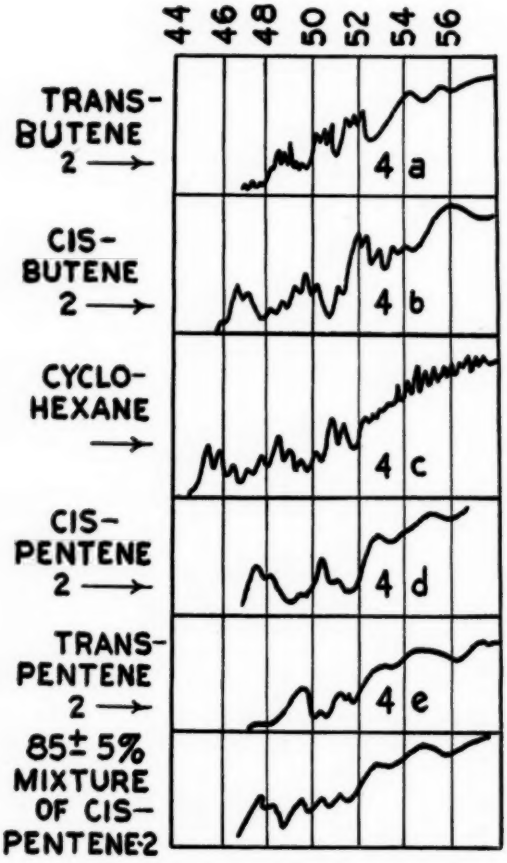


FIG. 4. *Cis-trans* isomers of butene-2 and pentene-2. (Carr *et al.*[9])

## PHOTOELECTRIC METHODS

The photoelectric spectrophotometer is similar in design to the apparatus described by Hogness, Zscheile, and Sidewell.[18]

The spectral region is isolated from the continuous spectrum by a Zeiss fixed arm spectroscope (deviation 90°), used as a monochromator. Referring to wave-length 4861A, the effective aperture is $f/6.4$ for the entire instrument. The error of the wave-length drum is less than 1A at 2150A and 3A at 7800A. Although this instrument is equipped with achromatic lenses, a slight adjustment is necessary to correct for chromatic errors.

A Barth circuit is employed to amplify the photoelectric current. In this circuit an F.P.54 vacuum tube (General Electric) is employed for the amplification of the current. The photoelectric current is passed through a high resistance *Rg* ($1\times10^{11}$ ohms), and the potential across this resistance is impressed on the grid of the amplification tube. The amplified current is measured by a galvanometer (Leeds Northrup Company: 2500-b, period 6 sec.). The sensitivity of the galvanometer is controlled by an Ayrton

shunt. The photo-tube is a cesium oxide gas-filled type, fitted with internal and external guard rings.

With proper electromagnetic shielding, a stable voltage sensitivity of 225,000 mm per volt and a current sensitivity of $1\times10^{-16}$ amp. per mm may be attained. These sensitivities are for 4 meter scale-galvanometer distance with a galvanometer sensitivity of 0.6. The galvanometer drift is less than 0.5 cm per hour with oscillations 1 mm. Usually 40–50 seconds are sufficient for the measurement of two absorption coefficients. The cell carriage which holds three absorption cells is placed behind slit No. 2. Thus, from four transmission measurements, two absorption coefficients may be calculated.

The over-all error for the apparatus, including fluctuations in light source, amplification tube, photoelectric cell, and galvanometer, is less than $\pm0.25$ percent for the visible region and less than $\pm0.35$ percent for the ultraviolet region. The larger error for the ultraviolet region is due to fluctuations in the light source.

Calibration: The following tests were made to standardize the apparatus.

A. Known voltages were impressed on the grid of the amplification tube and the deflections of the galvanometer were observed. Direct proportionality was usually found.

B. The proportionality between the response of the galvanometer and the intensity of the incident light on the photoelectric cell was determined by the interposition of a series of calibrated screens. These screens were calibrated by a thermopile. The transmission values obtained by the photoelectric apparatus agreed (error $\pm0.5$ percent) with those obtained by the thermopile.

C. Calibrated Pyrex filter: Through the courtesy of the National Bureau of Standards a calibrated filter was obtained as an additional check in the ultraviolet. The transmission values obtained by the apparatus are compared with those obtained by the Bureau in Table II.

## Quantitative Absorption Spectra Measurements

### Results

As a test case, the absorption spectrum of crotonic acid was measured for comparison with curves reported by Hausser[13] and Henri.[17] Our data for crotonic acid is in good agreement with that reported by Henri (Fig. 8) in that we observed a band at λ2420 and the second band just above λ2000A. Our absorption curves are lower than those reported by Henri[17] and Hausser, and Smakula.[13]

Morton[19] obtained a molecular absorption curve equal to that which we found (curve 3, Fig. 9), providing we assumed $P=1$. Details of his experimental procedures are not given, but it appears that this factor was neglected.

We have determined that in the case of crotonic acid the error involved in neglecting the

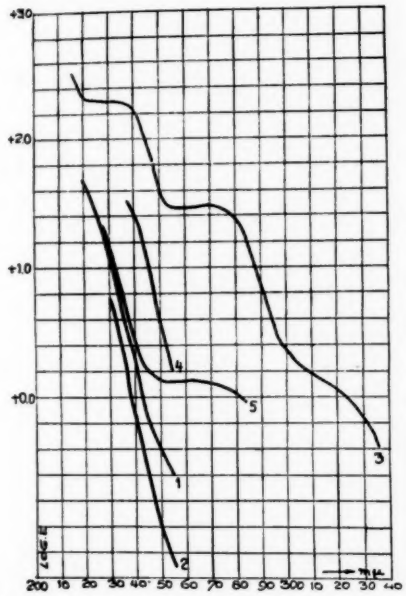


FIG. 6. Absorption spectra of (1) acetic acid, (2) methyl acetate, (3) ethyl oleate (chemically pure), (4) ethyl oleate (optically pure, (5) elaidinic acid. (From Hulst.[4])

"Schwarzschild" constant ($P$) is between 7 and 8 percent. This was determined by the use of accurately calibrated screens so that for equivalent exposures the blackening was the same for solvent and solution. Since the "Schwarzschild" constant is a function of both time and intensity (reciprocity law failure), it cannot be neglected in quantitative studies.

In accurate work the "Schwarzschild" constant must be determined for each individual

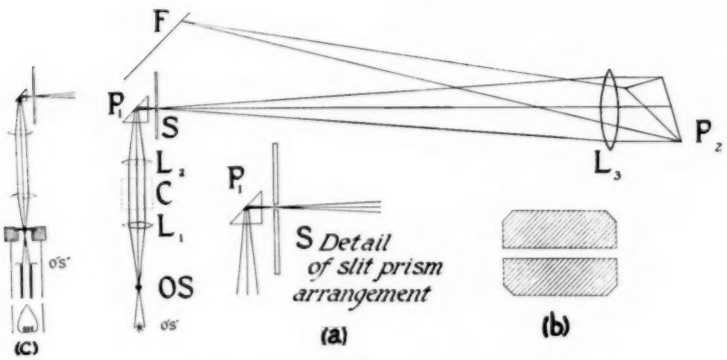


FIG. 7. Optical train of quartz spectrograph.[15]

plate; this can be accomplished by photographing the spectrogram of a calibrated screen on the plate. For routine measurements a single determination may be sufficient. In a paper by Beck,[16] the factors influencing $P$ have been reported, as well as characteristic properties of different emulsions under various conditions of development. Among things to be considered are gamma (the slope of the $d-\log_{10} E$ curve), and the plate inertia. The effects of a rotating sector have also been determined.

The absorption curves for Δ2–3 acids* (same chromophore as crotonic acid) are presented in Fig. 9. These data confirm the published values reported by Van der Hulst. Quantitatively these absorption curves should be similar to those presented in Fig. 8. Only curve 2 (Fig. 8) has a band at λ2100A with an $\epsilon=(ca.)$ 30,000. This suggests that the samples of crotonic acid employed in this study and by Morton[19] may be considered as being "associated." Accepting this tentative explanation for the differences in $\epsilon$, it indicates the sample in Fig. 8, curve 1, was much less associated. Additional evidence of this phenomenon has been reported by Hirst (reference 17, p. 56) for ascorbic acid. This investigator reports $\log_{10} \epsilon=3.97$ to 3.98 for $l$- and $d$-ascorbic acid dissolved in water and alcohol.

The absorption spectra of Δ10–12 linolic (solid), Δ9–11 linolic acid (solid) and Δ10–12 methyl linoleate liquid are presented in Fig. 10. Only the curve for solid Δ10–12 linolic acid attained an $E^{1\%}_{1\text{ cm}}=(1160\pm20)$ as large as that reported by Van der Hulst (Fig. 1, curve 5). In no case is the minimum at λ2150A as low ($E^{1\%}_{1\text{ cm}}=750$) for the solid conjugated linolic acids as that observed for Δ10–12 liquid methyl linoleate.

Data presented in Fig. 11 are absorption spectra for conjugated and nonconjugated linoleyl alcohol.[20] The nonconjugated linoleyl alcohol has an $E^{1\%}_{1\text{ cm}}=1.5$ at λ2325, a minimum at λ2150 and an inflection at λ2000A—this band is due to C−C resonance. The Δ10–12 linoleyl alcohol has a maximum also at λ2324, but $E^{1\%}_{1\text{ cm}}$ is 1200. Apparently at the minima at λ2150, $E^{1\%}_{1\text{ cm}}$ is between 400 and 520. The lower values obtained by the photoelectric spectrophotometer, was undoubtedly caused by scattered radiation.

Curve 5 in Fig. 1 has been employed as a reference standard in the quantitative determina-

* Samples 1 and 2 in Fig. 10 were prepared by Professor W. Lauer and students, Department of Organic Chemistry, University of Minnesota, Minneapolis, Minnesota.

TABLE II. *Transmission values of a Pyrex filter as measured by the thermopile (National Bureau of Standards) and the photoelectric apparatus.*

| | Wave-Lengths in A | | |
|---|---|---|---|
| Method of measurement | 3020 % | 3130 % | 3340 % |
| Thermopile | 29.5 | 54.5 | 86.0 |
| Photoelectric | 29.9±0.2 | 54.6±0.2 | 85.9±0.1 |

tion of conjugated methyl esters of corn oil for tracer studies, such as rates of fat absorption in the intestine and rates of transport to and from the liver.[21,22] Carefully prepared liver lipids from a fasted rat possess an absorption curve that qualitatively is similar to the curves in Fig. 9. Using this curve as the reference spectrum, we have observed that about ten percent of this acid is present in the acetone soluble fraction. This new fatty acid is not present in sufficient amounts to be measured in normal animals.

The absorption spectra of these unsaturated acids and alcohols are now being extended below 2000A.

Since the samples used for absorption spectra studies in Fig. 11 were highly purified, it necessarily follows that the lower absorption coefficients for Δ10–12 liquid methyl linoleate and Δ9–11 solid linolic acid must be due to a difference in space configuration. By extending these curves below λ2000A it is hoped that one will be able to detect a sufficient difference between the four linolic acids[20] so as to assign to the respective isomer the proper geometric formula. Chemical analysis permits the grouping of these isomers into pairs, and quantitative absorption spectra studies of these isomers are now in progress.

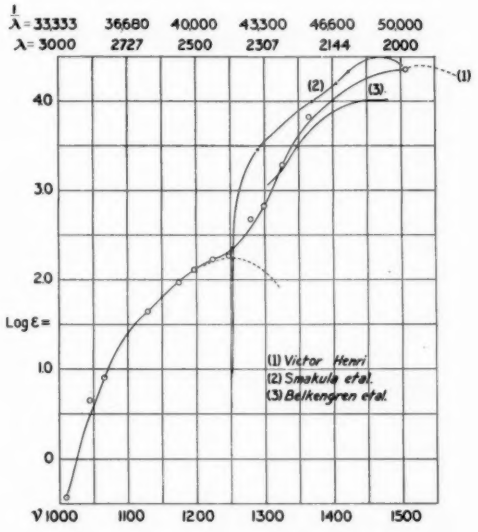


FIG. 8. Absorption curves of crotonic acid.

Figure 12 presents the absorption spectra of Δ1–3-pentadiene[9] and Δ10–12 linoleyl alcohol. The shift of the first band in curve 2 is of the magnitude that Carr *et al.*[9] observed when a hydrogen was replaced by a larger hydrocarbon radical. As to be expected, the absorption due to C=C−C=C in both Δ1–3-pentadiene and Δ10–12 linoleyl alcohol should be very similar for certain space configurations.

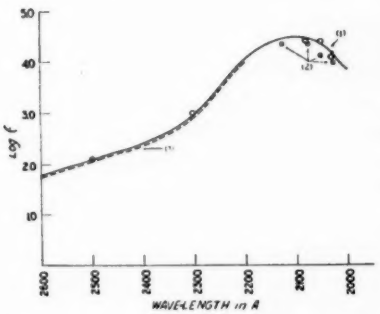


FIG. 9. Absorption spectra of Δ2–3 unsaturated fatty acids.

(1) $CH_3 \cdot (CH_2)_{13} \cdot CH=CH \cdot COOH$(II–11);
(2) $CH_3(CH_2)_{11} \cdot CH=CH \cdot COOH$(8b);
(3) $CH_3(CH_2)_{14}CH=CH \cdot COOH$.

(From Van der Hulst.)

## DISCUSSION OF RESULTS

Data presented in Fig. 11 for comparison of absorption spectra by spectrographic and photoelectric methods show that below λ2300A the absorption coefficients determined by the photoelectric method are lower than those for the photographic method. This difference is due to scattered radiation striking the cathode of the photo-tube. This source of error may possibly explain the minima reported by Hausser *et al.* at λ1900A for crotonic acid. Data presented in Fig. 10 and Fig. 11 show the quantitative absorption spectra for conjugated and nonconjugated alcohols, acids, and esters between λ2800 and λ2000A. In these studies of the absorption by conjugated fatty acids, the samples were purified just previous to measuring the absorption studies. Oxidation may, in many cases, introduce a 10-percent error, even though the samples are sealed in an evacuated ampoule.

## Summary

(1) Calibration details for the use of a Littrow spectrograph between λ2800 and λ2000A are given. Particular tests were made to eliminate or correct the effects of scattered radiation. (2) The importance of stray light in absorption spectral studies with reference to discrepancies reported in the literature is discussed. (3) Quantitative absorption spectra are given for conjugated and nonconjugated alcohols, acids, and esters between λ2800 and λ2000A. (4) Quantitative absorption curves serve as a practical reference standard for the quantitative estimation of that component in unknowns. (5) By quantitative absorption spectral analysis, at least one new fatty acid has been detected in liver lipids.


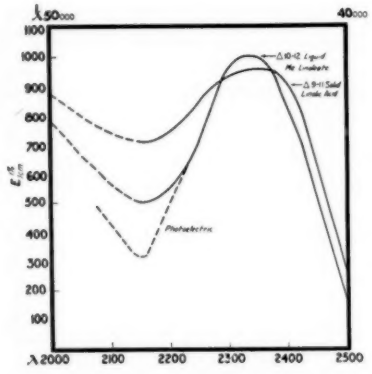


FIG. 10. Absorption spectra of Δ10–12 liquid methyl linoleate and Δ9–11 solid linoleic acid.

## Bibliography


1. W. E. Anderson and H. H. Williams, Oil and Soap **12**, No. 12, 282 (1935).
2. (a) G. O. Burr and M. M. Burr, J. Biol. Chem. **82**, 345 (1929); (b) **86**, 587 (1930); (c) G. O. Burr *et al.*, Proc. Soc. Exp. Biol. Med. **44**, 242 (May, 1940).
3. (a) H. Schneider *et al.*, J. Biol. Chem. **139**, 539 (1940); (b) J. Nutr. **18**, 99 (1939).
4. L. J. N. Van der Hulst, Rec. Trav. Chem. **54**, 639 (1935).
5. R. G. Booth *et al.*, Biochem. J. **29**, 133, (1935).
6. Elmer S. Miller *et al.*, unpublished data.
7. William John Dann and Thomas Moore, Biochem. J. **29**, 138 (1935).
8. A. Dingwall and J. C. Thompson, J. Am. Chem. Soc. **56**, 899 (1939).


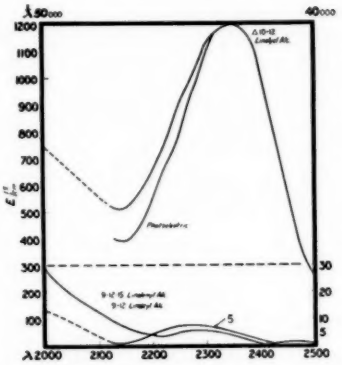


FIG. 11. Absorption spectra of conjugated and nonconjugated alcohols.


9. Emma P. Carr and Hildegard Stücklen, J. Am. Chem. Soc. **59**, 2138 (1937).
10. L. O. Brockway and Paul C. Cross, J. Am. Chem. Soc. **58**, 2407 (1936).
11. A. Smakula and A. Wasserman, Zeits. f. physik. Chemie **A155**, 355 (1931).
12. R. Kuhn, J. Chem. Soc. (May, 1938).
13. K. W. Hausser *et al.*, Zeits. f. physik. Chemie **B29**, 371 (1925).
14. R. Belkengren *et al.*, in press.


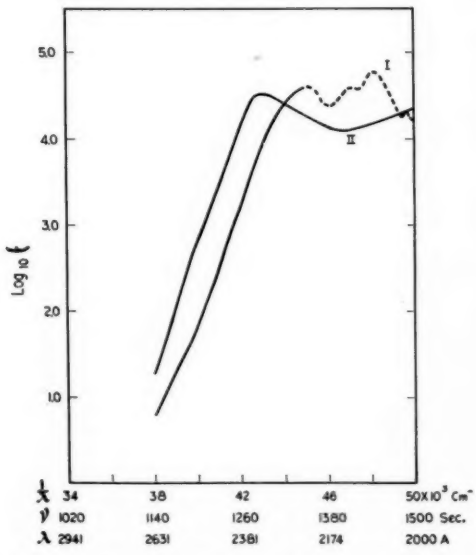


FIG. 12. Far ultraviolet absorption spectra of the >C=C−C=C< chromophore in pentadiene and linoleyl alcohol in ethanol (95 percent). The shift of the first band in curve II is due to damping of resonance by replacing of *H* with *R*. I = Δ1–3 pentadiene (Carr); II = Δ10–12 linoleyl alcohol.

15. Wallace R. Brode, *Chemical Spectroscopy* (John Wiley and Sons, New York, 1939).
16. R. G. Beck *et al.*, "Characteristics of spectrographic plates in the ultraviolet region between 2300 and 2000A," J. Opt. Soc. Am. (In press).
17. Victor Henri, *Études Photochimies* (Gauthier-Villars, Paris, 1919).
18. T. R. Hogness, J. Phys. Chem. **41**, 379 (1937).
19. R. A. Morton, *Absorption Spectra of Vitamins and Hormones* (Adam Hilger, Ltd., London, England, 1932).
20. Elmer S. Miller, unpublished data.
21. Elmer S. Miller *et al.*, Proc. Soc. Exp. Biol. Med. **41**, 485 (1939).
22. Richard H. Barnes *et al.*, Proc. Soc. Exp. Biol. Med. **42**, 45 (1939).

## Radiation from Fluorescent Lamps

THE new fluorescent lamps, now coming into extensive use, are made up of a glass tube lined with a thin film of a substance that is excited to fluorescence by the ultraviolet rays emitted when an electric discharge is passed through mercury vapor within the tube.

If the lamp were made of clear quartz or of certain kinds of glass, the radiation from the electric arc discharge through mercury vapor, being very strong in the spectral region 2537A to 2804A, might cause conjunctivitis, and would have a highly germicidal effect.

In response to repeated inquiries concerning the ultraviolet emission from these lamps, the Radiometry Section of the National Bureau of Standards has examined several makes and colors, including daylight (white), red, gold, green, blue and pink, as well as a lamp having one-half of the tube lined with blue fluorescent material while the other half was of clear glass. The lamps were all of the 115-volt, 15-watt type.

It was found that all the tubes were made of a kind of glass that is highly opaque to short ultraviolet wave-lengths; moreover, the fluorescent lining (especially in the red, gold and pink colored lamps) increased the opacity of the glass to ultraviolet radiation of wave-lengths shorter than about 3000A.

The shortest observable wave-length emitted by any of the lamps was found to be the mercury line at 3132A. This emission line was weak in the daylight, green, blue and pink lamps, and in the clear tube, and was not observed at all in the red and in the gold colored lamps. The ultraviolet emission line of mercury at 3663A was present, but weak, in all the lamps except the gold one. These ultraviolet emission lines are of wave-lengths that occur in sunlight, and appear to be harmless in the fluorescent lamps, as used.

By means of a tantalum photoelectric cell, having a maximum sensitivity at 2537A, check measurements were made against a "cold quartz" mercury arc, which is regularly used as a standard of germicidal ultraviolet radiation. In comparison with the standard lamp, it was estimated that, to 1 part in 50,000, no radiation of wave-length 2537A could be detected at a distance of 10 cm (4 inches) from the fluorescent lamps.

From these observations it appears that no ultraviolet radiation of wave-lengths shorter than 3000A (not in sunlight) emanates in appreciable amounts from fluorescent lamps as used for illumination.—Reprinted by permission from *Technical News Bulletin of the National Bureau of Standards*.

---

## Spectrographic Analysis Conference

A SECOND Midwest Conference on Spectrographic Analysis will be held in the Kent Chemical Laboratory at the University of Chicago on Saturday, March 29. Because of the growing importance of absorption spectroscopy, this year's conference will be held in two divisions, one dealing with emission spectra, the other with absorption spectra. The former is being organized by W. C. Pierce, The University of Chicago, and the latter by Elmer Miller, University of Minnesota. Further information and copies of the final program may be obtained from either of these.